processes

MDPI

Review

Mixed Ionic-Electronic Conducting Membranes (MIEC) for Their Application in Membrane Reactors: A Review

Alba Arratibel Plazaola [1,2], Aitor Cruellas Labella [1], Yuliang Liu [1], Nerea Badiola Porras [1,2,3], David Alfredo Pacheco Tanaka [2], Martin Van Sint Annaland [1] and Fausto Gallucci [1,*]

1 Inorganic Membranes and Membrane Reactors, Sustainable Process Engineering, Department of Chemical Engineering and Chemistry, Eindhoven University of Technology (TU/e), Den Dolech 2, 5612AD, Eindhoven, The Netherlands; alba.arratibel@tecnalia.com (A.A.P.); A.Cruellas.Labella@tue.nl (A.C.L.); Y.Liu4@tue.nl (Y.L.); n.badiola.porras@tue.nl (N.B.P.); M.v.SintAnnaland@tue.nl (M.V.S.A.)

2 TECNALIA, Energy and Environment Division, Mikeletegi Pasealekua 2, 20009, San Sebastian-Donostia, Spain; alfredo.pacheco@tecnalia.com

3 Chemical Engineering and Environmental Department, University of the Basque Country UPV/EHU, C/Alameda Urquijo s/n, Bilbao, 48013, Spain

* Correspondence: F.Gallucci@tue.nl

Received: 15 January 2019; Accepted: 12 February 2019; Published: 1 March 2019

Abstract: Mixed ionic-electronic conducting membranes have seen significant progress over the last 25 years as efficient ways to obtain oxygen separation from air and for their integration in chemical production systems where pure oxygen in small amounts is needed. Perovskite materials are the most employed materials for membrane preparation. However, they have poor phase stability and are prone to poisoning when subjected to CO_2 and SO_2, which limits their industrial application. To solve this, the so-called dual-phase membranes are attracting greater attention. In this review, recent advances on self-supported and supported oxygen membranes and factors that affect the oxygen permeation and membrane stability are presented. Possible ways for further improvements that can be pursued to increase the oxygen permeation rate are also indicated. Lastly, an overview of the most relevant examples of membrane reactors in which oxygen membranes have been integrated are provided.

Keywords: oxygen separation; membrane; fluorite; perovskite; MIEC; membrane reactor

1. Introduction

Oxygen, which is a key reactant in many industrial processes, is among the top five major chemicals produced worldwide [1]. Industrial oxygen production is performed mainly by cryogenic distillation and pressure swing adsorption (PSA), which both require high investments and operating costs [2–5]. Cryogenic distillation technology provides high purity oxygen (>99%), while, generally, the purity is lower for PSA at around 95% [6]. Recent international policies about energy security and greenhouse gas emissions are challenging the conventional oxygen production systems. Oxygen separation using membrane technology is less energy intensive [7] and can, thus, help reduce greenhouse gas emissions related to the chemical industries. When oxygen selective membranes are coupled with high temperature reactions (e.g., syngas production from natural gas) and even higher benefits can be achieved due to process integration [8]. Actually, companies like "Air Products" or "Praxair" are currently doing big efforts on this field, developing novel oxygen membrane units for both air separation and for their integration into chemical processes [9,10]. In literature, two principal types of ceramic membranes have been pointed as possible oxygen separation devices including pure oxygen conducting membranes and

mixed ionic–electronic conducting membranes (MIEC). In the first case, the oxygen ions are transported by the membrane material while the electrons are transported by an external electron material (electrodes). The oxygen generated is controlled by an electric current applied to the system. In contrast, in MIEC membranes, the membrane material transports both ions and electrons, which can be either a single phase or a dual-phase (where one material phase transports the electrons and the other transports the ions). In the two cases, the driving force for the oxygen permeation is the oxygen chemical potential/partial pressure difference on both sides of the membrane [11,12]. Compared with traditional oxygen separation technologies, membrane technology features improved energy efficiency, superior oxygen selectivity (thus high oxygen purity), and compatibility with many industrial reaction systems, including selective oxidation of ethane (SOE) [13], oxidative coupling of methane (OCM) [14,15], and partial oxidation of methane (POM) [16,17] among other reactions.

The mixed ionic and electronic conduction of solid oxide materials was initially described by Takahashi et al. [18] in 1976. Afterward, Cales and Baumard [19,20] introduced the mixed conducting oxide concept to oxygen transport membranes. However, favorable oxygen permeability was not achieved until Teraoka et al. [21] made a breakthrough on oxygen separation membranes in 1985 by introducing the perovskite membranes. One of the drawbacks of oxygen membranes has always been the thermal stability at the high temperatures required for achieving appreciable oxygen fluxes. Attempts of increasing the thermal stability include doping the perovskite (and MIEC) with different elements, which clearly improved the thermal and chemical stability while resulting in a decrease in the oxygen permeation rate [22,23].

It is generally accepted that materials with superior oxygen ionic conductivity usually have correspondingly lower chemical stability when exposed to reducing atmospheres. This is easily explained by the fact that weak chemical bonding of metal and oxygen could be favorable for the fast oxygen mobility in membranes, but it also increases the chances for metals to be reduced at a high temperature in reducing atmosphere. Therefore, this decreases the chemical stability [24].

There are, however, other ways to increase the oxygen flux. In fact, the oxygen permeation rate in MIEC membranes is controlled by two different mechanisms, such as ionic transport within the membrane and surface membrane exchange. When the permeation process is controlled by bulk diffusion, the oxygen permeate flux will increase when decreasing the thickness of the membrane [25,26]. Membranes with a thickness in the order of 400 to 500 μm is, however, sufficiently small, because the surface exchange rate becomes limiting for smaller membrane thicknesses, as shown in Figure 1 [27].

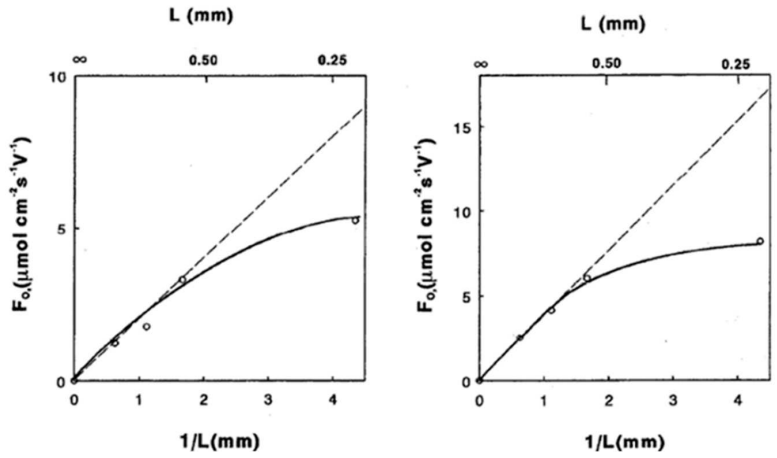

Figure 1. Thickness dependence of oxygen permeation of self-supported (Bi_2O_3)-(Er_2O_3)-Ag membranes at 750 °C (left) and 850 °C (right) [27].

However, thin film membranes of these thicknesses are typically not sufficiently mechanically stable. To develop more stable membranes, research is ongoing to produce asymmetric MIEC membranes with a thin dense layer coated on a thicker porous support, as proposed by Teraoka

et al. [28] in 1989. With supported membranes, high oxygen permeation flux can be achieved without sacrificing the mechanical stability of the membrane. Meanwhile, thinner membranes usually better maintain their chemical stability, because elevated bulk diffusion rates of oxygen can help reduce unwanted chemical reduction on the surface of the membrane [29].

An oxygen selective layer supported onto a porous substrate is the simplest example of an asymmetric membrane structure. Additional layers with specific functions can be added, like a surface activation layer and/or a catalytic layer, to improve and extend the performance of the membranes, which also increases the complexity of the membrane structure (see Figure 2) [26,30]. While several articles have been published on self-supported MIEC oxygen transport membranes, only a limited number of articles were published on the production and testing of asymmetric membranes.

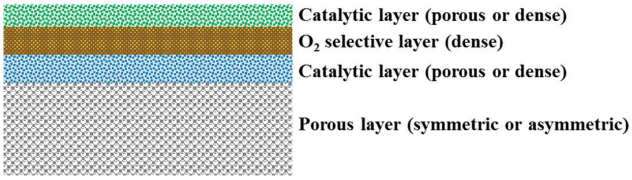

Figure 2. Schematic representation of an asymmetric membrane with several functional layers.

Therefore, this review summarizes recent advances in the material development for both the support and the selective layer(s) of MIEC membranes. In addition, methods to avoid defects and to improve the performance of the membranes are outlined with particular attention to possible problems in the membrane preparation. This extensive description is then linked and discussed for the main applications of such membranes in chemical processes by using membrane reactor technologies. Dong et al. [31] and Deibert et al. [32] described the main applications for chemical processes that MIEC membranes can have. However, this study tries to complete these previous studies by giving indications, based on the description provided in the first part of the review, of which membranes are more suitable and which conditions need to satisfy to ensure a proper reactor operation in each of the studied cases.

2. Oxygen Transport through MIEC Membranes

The oxygen diffusion mechanism through dense ceramic membranes involves several steps. In general, the driving force is the partial pressure difference between the feed and permeate side of the membrane. A schematic representation of oxygen separation is shown in Figure 3.

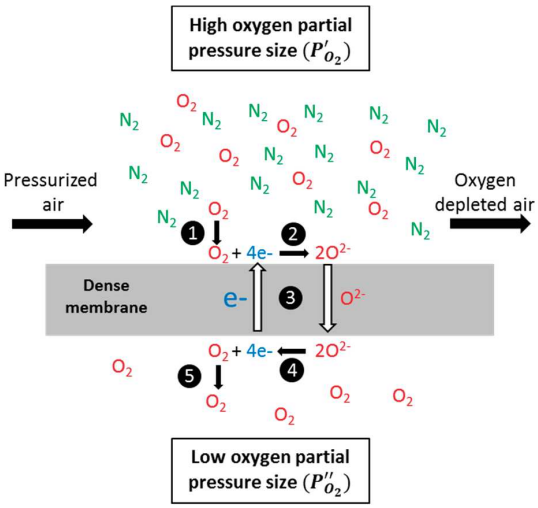

Figure 3. Schematic representation of oxygen permeation through dense ceramic membranes when air is employed as feedstock stream.

Oxygen transport involves five sequential steps [33]:

1. Bulk-to-surface mass transfer of gaseous oxygen (feed side to the membrane surface).
2. Dissociation (surface exchange): The oxygen molecule is adsorbed on the membrane surface and dissociates catalytically in oxygen ions (O^{2-}). On the high oxygen partial pressure side, this can be expressed using the Kröger–Vink notation [34] below.

$$\frac{1}{2}O_2 + 2e^- + V_O'' \rightarrow O_o^x \quad (1)$$

   where V_O'' refers to oxygen vacancies in the ceramic and O_o^x to oxygen ions (O^{2-}) occupying the oxygen lattice.
3. Ionic transport (bulk diffusion): under a pressure gradient between the feed and permeate side, the oxygen ions diffuse through the ceramic crystal lattice (mainly oxygen vacancies, but also other defects). To maintain electrical neutrally, electrons are transported at the same time in the opposite direction.
4. Association (surface exchange): The oxygen ions recombine to form oxygen molecules and desorb from the surface of the membrane. The reaction involved in this step can be represented by the following formula.

$$O_o^x \rightarrow \frac{1}{2}O_2 + V_O'' + 2e^- \quad (2)$$

5. Surface-to-bulk mass transfer of gaseous oxygen (permeate side): Gas transport in the permeate side alone or helped by a sweep gas (helium, CO_2, etc.).

In oxygen separation processes, steps 1 and 5 usually present small mass transfer resistances and can often be neglected [35].

3. Materials and Methods for MIEC Oxygen Membranes

Single-phase ionic transport materials (such as fluorites and perovskites) were studied by many researchers as oxygen permeable membranes. Both types of structures have been well studied with different doping strategies and both as self-supported membranes and supporting selective layers with different thicknesses. Lately, another kind of membrane material has attracted attention known as the dual-phase membranes. The increased interest in dual-phase materials is related to the higher permeation properties combined with improved thermal stability of these membranes. Additionally, dual phase membranes have been obtained via mixing both ceramic-ceramic and metallic-ceramic materials, which gives a high degree of freedom in producing stable and high-flux membranes.

3.1. Single-Phase Ionic Transport Materials

Oxygen permeable ceramic dense membranes can be composed of different structures like perovskites (ABO_3), fluorites (AO_2), brownmillerites ($A_2B_2O_5$), pyrochlores ($A_2B_2O_7$), and Ruddlesden-Popper series ($A_{n+1}B_nO_{3n+1}$). All these materials can conduct oxygen ions through their crystal lattice. Among all materials, perovskites and fluorites are the most studied as oxygen membranes. Perovskites are the most attractive materials since they conduct both oxygen ions and electrons, and are commonly well-known in their extended form as mixed ionic electronic conductors or MIEC [36] (see Figure 4, right). On the other side, fluorites present high ionic conductivity but a low electronic one. Generally, for mixed ionic electronic membranes, the driving force is the gradient on the oxygen chemical potential. In the case of pure oxygen conducting membranes (materials with only ionic conductivity), an external electrical circuit is needed for the conduction of electrons (Figure 4, left) since these materials are very often used in high temperature fuel cell applications [7].

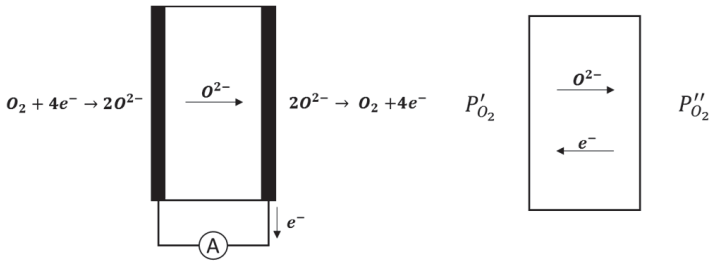

Figure 4. Ceramic membrane types based on the conduction mechanism (Left), Solid electrolyte, and (Right) mixed ionic-electronic single-phase membrane. P'_{O_2} and P''_{O_2} are the oxygen partial pressure in the feed and permeate side, respectively, and $P'_{O_2} > P''_{O_2}$.

3.1.1. Fluorites

Fluorite oxide structures, known as fluorites, are represented by AO_2, where A is the large four valent cation such as Zr^{4+} or Ce^{4+} [37]. These structures exhibit very poor electronic conductivity. Thus, an external electronic conduction to enhance this property is required to function as oxygen transport membranes. The crystal structure of fluorite is shown in Figure 5, where the cations are in the FCC (face-centered cubic) structure, while the oxygen anions are positioned in the interstitial holes forming a simple cubic structure inside the FCC structure of the cations.

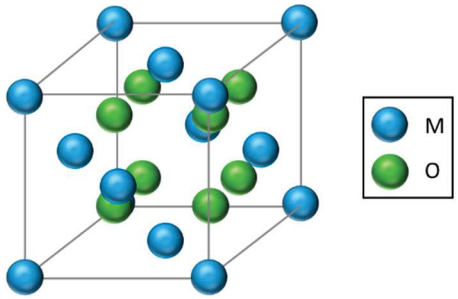

Figure 5. Fluorite-type structure.

Most of the fluorite oxides are widely applied as electrolyte layers in solid oxide fuel cells (SOFC). Typical fluorite oxides used are ZrO_2, CeO_2, and Bi_2O_3 [33,38]. Several oxides such as yttria-stabilized zirconia (YSZ), gadolinium-doped ceria (GDC), or samarium-doped ceria (SDC) present high oxygen ion conduction as well [38]. Employing Gd as a dopant in cerium oxide, the best conductivity was obtained in concentrations of around 10% to 20% [39]. Doped ceria with trivalent elements shows a stable crystal lattice due to the similar size of the host and dopant ions [40]. In case of doping with Pr, the ambi-polar conductivity is enhanced [41].

Bismuth oxide-based materials provide the highest level of oxygen permeability [42]. However, the oxygen flux is too low compared with perovskites since the fluorite oxides have a low electronic conductivity [43].

Zirconium oxide is one of the most studied fluorite type materials. Bulk zirconia is a polymorphic ceramic material, which may exist at different ranges of temperatures and atmospheric pressures: monoclinic (<1000 °C), tetragonal (1100–2370 °C), and cubic (>2370 °C) [44,45]. The cubic structure is stable at temperatures above 2300 °C with a high oxygen ionic conductivity [46]. This phase can be stabilized by doping with rare earth oxides [46] like Y_2O_3, which is the most employed metal oxide for that purpose.

The main benefit of these materials is their small chemical expansion and their phase stability under CO_2 and reducing environments when compared to perovskite materials [47].

3.1.2. Perovskites

Perovskites present a cubic structure with a general formula ABO_3, where the A and B sites are cations occupied by alkali or rare earth elements, respectively. As Figure 6 shows [43], the unit cell is a FCC (face-centered cubic) crystal, where A cations are located in the corners of the cubic lattice and the smaller B cation is located in the body-centered position. Oxygen anions are located at the face-centered positions.

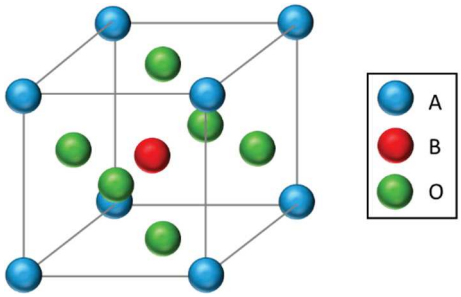

Figure 6. Crystalline structure of perovskite (ABO_3). Alkaline earth metal ions (Ca^{2+}, Ba^{2+}, Sr^{2+}) and/or lanthanide metal ions (La^{3+}, Ga^{3+}, Sm^{3+}, etc.) are usually located at the A-sites [43], while the B-sites are mostly transition metal ions [48].

The conduction of oxygen ions at high temperatures (>700 °C) is related mostly to the number of vacancy sites, which increase with temperature [7]. The oxygen transport rate in a perovskite is governed by the Arrhenius expression (positive activation energy) and is higher when the temperature is increased. The activation energy depends mainly on the bond energy of metal-oxygen in the lattice and the parameter $r_{critical}$, which corresponds to the radius of the opening between the two A site cations and the one B site cation that the mobile anion must pass [49].

Teraoka [21] presented a pioneering work demonstrating that the oxygen vacancy (δ) concentration and, consequently, the ionic diffusion rate is enhanced by doping the cation sites with other cations of different sizes and valences.

The most studied perovskite materials are SCFO ($Sr(Co,Fe)O_{3-\delta}$) and BSCF ($Ba_{0.5}Sr_{0.5}Co_{0.8}Fe_{0.2}O_{3-\delta}$). They exhibit exceptional permeation rates, which are also related to the high surface exchange rates [7,36]. The main problem of these cobalt based membranes is that they are not stable in the presence of some gases, mainly CO_2, which hinders its application in gas separation or membrane reactor processes [43].

In addition, SCFO perovskites are also unstable at low temperatures and when low partial pressures of oxygen are employed. However, the properties of the "standard" perovskites can be tuned by introducing metal cations in the membrane structure [50]. Being more specific, partial substitution of this $Co^{3+/4+}$ and $Fe^{3+/4+}$ with less reducible metal ions (Al^{3+}, Ce^{4+}, Zr^{4+}, etc.) can enhance the membrane stability in the presence of hydrogen such as for their use in the partial oxidation of methane to syngas [51–53].

The substitution of metal ions can also be used to enhance the oxygen permeability. Cheng et al. [54] tested different doped BCFO perovskites. Among all the tested ones, they reported that the Zr-doped, $BaCo_{0.7}Fe_{0.2}Zr_{0.1}O_{3-\delta}$, showed the highest oxygen permeability. On the other hand, $BaCo_{0.7}Fe_{0.2}Ta_{0.1}O_{3-\delta}$ gave the best structural stability. This is in agreement with the findings of Liu et al. [55], which demonstrate an increase of the membrane stability when doping it with Ta. On the other side, the same influence for Zr was also confirmed by Yao et al. [56].

As mentioned above, BSCF is one the perovskites, which shows higher oxygen permeability [57]. Nevertheless, this permeation can be further improved by doping the Fe-ions B-site with Al, Ce, and Ni, as observed by Babakhani et al. [58]. It needs to be considered in any case that, below 850 °C, the cubic perovskite transforms into an orthorhombic phase (brownmillerite), which does not present the same permeation properties [59].

The $La_{1-x}M_xCo_{1-y}Fe_yO_{3-\delta}$ (M = Ba, Sr, and Ca) membranes are another type of perovskite, which have been widely studied. Stevenson et al. [60] investigated the oxygen permeability and the lattice weight loss at a high temperature for A-site substitution of this type of membranes. They observed weight loss when the temperature increases, which they attributed to the lattice oxygen release. This effect would contribute toward increasing the concentration of oxygen vacancies and the ionic conductivity in the membrane, resulting in a growth of the oxygen permeation flux. In particular, Stevenson's group found that, as the Sr content increased in the oxide, the oxygen permeation flux increased significantly, and this was consistent with the thermogravimetric (TGA) results showing a greater oxygen deficiency at higher temperatures.

The same trend was observed by Li et al. [61] for $La_{0.2}M_{0.8}Co_{0.2}Fe_{0.8}O_{3-\delta}$ (M = Ba, Sr and Ca) perovskite membranes. Sr substituted membranes showed the best oxygen permeability. However, the thermal stability is lower than the Ba-substituted oxides, which is attributed to the low average bond energy and high free volume of the Sr substitution compounds.

In order to minimize the thickness of the dense perovskite membrane, which, at the end, would contribute to enhance the oxygen permeation, several researchers have tried to fabricate asymmetric oxygen transport membranes consisting of a dense and a porous layer. To avoid crack formation due to the shrinkage mismatch and thermal expansion coefficient during sintering, similar materials are usually chosen for both layers. For instance, Li et al. [62] produced a supported membrane starting with BSCF powders for the support and the selective layer. An improvement in the oxygen permeability was observed in comparison with self-supported BSCF membranes. More examples of supported membranes will be shown in Section 5.3.

Baumann and co-workers obtained a thin film (70 μm) of BSCF with a permeation rate of 5.04 $\times 10^{-5}$ mol cm^{-2} s^{-1} at 1000 °C under O_2/argon stream at 1 atm of partial pressure of oxygen [63]. In case of an air/argon stream with 0.21 atm oxygen partial pressure at the same temperature, the permeation rate decreased to 9.08 $\times 10^{-6}$ mol cm^{-2} s^{-1}. Recently, Shubnikova et al. reported an O_2 flux of 8 $\times 10^{-6}$ mol cm^{-2} s^{-1} at 950 °C [64] using the 1.5 mm thick molybdenum doped BSCF membrane (air/He), while the un-doped one was 7.48 $\times 10^{-6}$ mol cm^{-2} s^{-1}. Doping B-sites of BSCF with Zn also leads to an improvement in the O_2 permeability. At 850 °C, the O_2 flux of 1 mm-thick membrane increases from 8.56 $\times 10^{-7}$ to 1.08 $\times 10^{-6}$ mol cm^{-2} s^{-1} as a small amount of zinc is added [65].

Perovskites based on $SrCoO_{3-\delta}$ have excellent oxygen conductive properties. Teraoka et al. reported a high oxygen permeation flux of 2.1 $\times 10^{-6}$ mol cm^{-2} s^{-1} for a self-supported $SrCo_{0.8}Fe_{0.2}O_{3-\delta}$ (SCF) membrane [21]. Fan's group [66] fabricated the SCF tubular asymmetric membrane by depositing a dense layer of SCF onto a porous substrate made out of a mixture of SCF and $SrSnO_3$. Their results showed that the two kinds of material were compatible enough to produce the asymmetric membrane. The oxygen flux at 900 °C was 24% higher than that of the SCF symmetric membrane. However, lower chemical and thermal stabilities of SCF oxides were observed in their application processes.

Lastly, another important aspect that would improve the oxygen permeability is the use of micro-channeled membranes. This type of structure greatly increase oxygen separation rates from air compared with conventional dense membranes or supported membranes, as reported by Shao et al. [67]. Gas diffusion through the straight channels have a less tortuous path than the interconnected pores in a convectional supported membrane. In their work, they found that the micro-channeled membrane made of LSCF permeates 1.02 $\times 10^{-6}$ mol cm^{-2} s^{-1} at 1000 °C, which is 50% higher than a self-supported membrane made with the same material and thickness.

3.2. Dual-Phase Ionic-Electronic Transport Materials

Due to the difficulties in identifying a single material that exhibits both a large ionic and a large electronic conductivity, *dual-phase* membranes are attracting increasing interest by several research groups. This is because one can increase the electron conduction by dispersing a metallic or ceramic entity with a high electron conducting property into an ionic conducting phase [7,37]. Mazanec et al. introduced the concept of the dual-phase membrane [68], where YSZ made the transport path for oxygen ions and the palladium network transports the electrons.

Figure 7 represents a dual-phase mixed ionic-electronic membrane, where the white and grey colors refer to the material that conducts the oxygen ions and electrons, respectively.

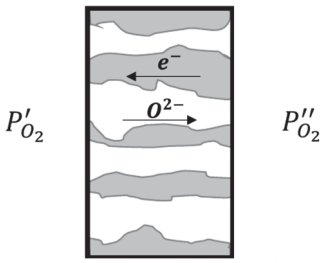

Figure 7. Schematic representation of a dual-phase ceramic membrane. The white colored phase conducts the oxygen ions and the grey colored phase conducts the electrons.

For electronic conductivity, both fluorites and perovskites could be used and mixed with a second phase (metallic or ceramic). An infinitely continuous or percolative network is required to enhance both processes (ionic transport through a ceramic conductive phase and electron conduction through an electronic conductive metallic or ceramic phase) [7]. To maintain electroneutrality in the membrane, a balance between oxygen ions and electrons is required. At the same time, the electronic conductive phase can also promote the association/dissociation for oxygen molecules at the surface [69]. The advantage of dual-phase composites in comparison with singles-phase membranes are their chemical and mechanical stability [70].

Some researchers have prepared dual-phase membranes on porous supports to reduce the bulk diffusion resistance [71,72]. However, surface exchange processes become predominant. Catalysts (noble metal like platinum, palladium, or silver) is required to activate this surface process, which includes oxygen dissociation on the feed side and ion combination at the permeate side [73].

A precise control on the preparation process is necessary to avoid the formation of defects and cracks, since the expansion coefficients between materials would cause leaks and jeopardize complete gas separation [74].

3.2.1. Dual-Phase Based on Ceramic-Metallic Mixtures

Noble metals are preferred for the electronic conduction phase in a dual-phase type membrane, while ceramics like fluorite-based and perovskite-based materials are generally selected as the ionic conductive phase. The oxygen flux measured for some dual-phase membranes based on ceramic-metallic composites are summarized in Table 1.

Table 1. Oxygen permeation flux data of some ceramic-metallic dual-phase membranes.

Membrane	Temperature (°C)	Thickness (μm)	Oxygen Flux (mol cm^{-2} s^{-1})	p'_{O_2} (atm)	p''_{O_2} (atm)	Feed Gas	Sweep Gas	Ea (kJ/mol)	Reference
$(YSZ)_{0.7}$-$(Pd)_{0.3}$	1100	2000	10^{-10}	0.209	$1.4{\cdot}10^{-3}$	Air	He	170	[69]
$(YSZ)_{0.6}$-$(Pd)_{0.4}$	1100	2000	4.3×10^{-8}	0.209	0.014	Air	He	82.6	[69]
$(YSZ)_{0.6}$-$(Pd)_{0.4}$	800	1720	1.6×10^{-8}	0.209	0.026	Air	He	-	[75]
$(YSZ)_{0.5}$-$(Pd)_{0.5}$	1100	800	1.56×10^{-6}	0.209	-	Air	CH_4[a]	-	[68]
$(YSZ)_{0.5}$-$(Pt)_{0.5}$	1100	800	1.34×10^{-6}	0.209	-	Air	CH_4[a]	-	[68]
$(YSZ)_{0.6}$-$(In_{90}Pr_{10})_{0.4}$	1100	800	8.18×10^{-7}	0.209	-	Air	CH_4[a]	-	[68]
$(YSZ)_{0.5}$-$(In_{90}Pr_{10})_{0.5}$	1100	800	1.71×10^{-6}	0.209	-	Air	CH_4[a]	-	[68]
$(YSZ)_{0.5}$-$(In_{90}Pr_{10})_{0.5}$	1100	300	$4.09 \times{\cdot}10^{-6}$	0.209	-	Air	CH_4[a]	-	[68]
$(YSZ)_{0.5}$-$(In_{95}Pr_{2.5}Zr_{2.5})_{0.5}$	1100	300	5.80×10^{-6}	0.209	-	Air	CH_4[a]	-	[68]
$[(Bi_2O_3)(Er_2O_3)]_{0.6}$-$Ag_{0.4}$	800	1600	1.19×10^{-7}	0.209	0.026	Air	He	-	[75]
YSZ-Pd-YSZ	1050	10	2.0×10^{-8}	6×10^{-3}	1×10^{-5}	Air	-	193	[71]
YSZ-Pd-YSZ	1050	10	4.8×10^{-8}	6×10^{-3}	1×10^{-5}	O2	-	193	[71]
$[(Bi_2O_3)_{0.74}(SrO)_{0.26}]_{0.6}$-$Ag_{0.4}$	680	1000	5×10^{-8}	0.209	0.0024	Air	He	185	[76]
$[(Bi_2O_3)_{0.75}(Er_2O_3)_{0.25}]_{0.6}$-$Ag_{0.4}$	852	230	3.08×10^{-7}	0.209	0.046	Air	He	48.9	[27]
$[(Bi_2O_3)_{0.75}(Er_2O_3)_{0.25}]_{0.6}$-$Ag_{0.4}$	680	129	1.79×10^{-7}	1	2×10^{-6}	O_2	Ar	-	[77]
$[(Bi_2O_3)_{0.75}(CaO)_{0.25}]_{0.6}$-$Ag_{0.4}$	680	75	2.95×10^{-8}	1	2×10^{-6}	O_2	Ar	-	[77]
$(Bi_{1.5}Y_{0.3}Sm_{0.2}O_3)_{0.6}$-$Ag_{0.4}$	850	1300	5.80×10^{-7}	0.21	0.009	O_2/N_2	He	87.30	[70]
$(NiFe_2O_4)_{0.4}(Ce_{0.8}Tb_{0.2}O_{2-\delta})_{0.6}$ $[(Ce_{0.8}Ga_{0.2}O_{2-\delta})(La_{0.8}Sr_{0.2}MnO_{2-\delta})]$ +Pd	1000	680[b]	1.26×10^{-7}	0.21	-	Air	Ar	-	[78]
$(NiFe_2O_4)_{0.4}(Ce_{0.8}Tb_{0.2}O_{2-\delta})_{0.6}$ $[(Ce_{0.8}Ga_{0.2}O_{2-\delta})(La_{0.8}Sr_{0.2}MnO_{2-\delta})]$ +Pd	1000	680[b]	1.49×10^{-7}	0.21	-	Air	CO_2	-	[78]

[a] Oxygen membrane directly employed in a syngas production from methane. [b] 30 μm thick layer of $(Ce_{0.8}Ga_{0.2}O_{2-\delta})(La_{0.8}Sr_{0.2}MnO_{2-\delta})$ were deposited in both sides of the disk of $(NiFe_2O_4)_{0.4}(Ce_{0.8}Tb_{0.2}O_{2-\delta})_{0.6}$.

As mentioned before, Mazanec produced and tested the first dual-phase composite membranes consisting of YSZ with Pd, Pt, $In_{90}Pr_{10}$, and $In_{95}Pr_{2.5}Zr_{2.5}$. The oxygen permeation flux was improved when the volume percentage of metal was above the critical value for obtaining a percolative composite, while the best results were obtained with a 50 vol.% of $In_{95}Pr_{2.5}Zr_2$. [68]. It was observed that 30 vol.% of metal is required in the mixture to obtain a percolated network [79].

Chen et al. [69] worked extensively on YSZ/Pd. In their first study, they compare a YSZ fluorite with dual-phase YSZ/Pd with different volume ratios. Since the volume percentage of palladium is around 40%, the oxygen flux through the membrane increases three orders of magnitude compared with YSZ alone. Kim and co-workers [71] prepared a 10-µm thick layer of YSZ/Pd onto a porous alumina support by dip-coating with an extra YSZ thin layer on top of that deposited by CVD. The oxygen permeation through the asymmetric membrane was lower than expected at 1050 °C when using either air or pure oxygen as feed gas. The authors attributed the measured low membrane flux to the YSZ submicron layer deposited on top of the YSZ/Pd to reduce the leakage of the composite, while the electron conductivity is decreased.

In a second study by Chen et al. [75], an erbium-stabilized bismuth oxide-noble metal (Ag and Au) membrane was prepared and compared with a YSZ/Pd membrane. A higher oxygen permeation rate (1.19×10^{-7} mol cm^{-2} s^{-1}) was observed for the self-supported 1.6 mm-thick $(Bi_2O_3)(Er_2O_3)$-Ag (40% in volume) membrane at 800 °C, which is one order of magnitude higher compared with the permeation rate through the 1.72 mm thick membrane of $YSZ_{0.6}Pd_{0.4}$ [75]. The thickness dependency of the erbium-stabilized bismuth oxide-silver composites were studied at different temperatures, which have the best result with self-supported membranes of 230-µm thick at 852 °C (3.08×10^{-7} mol cm^{-2} s^{-1}) [27]. A thicker membrane (1 mm) was tested at a lower temperature (680 °C) and exhibited an O_2 flux of one order of magnitude lower [76].

Capoen et al. [77] observed that when CaO replaces erbium oxide, there is no improvement in the oxygen permeability. The authors also found that addition of Au instead of Ag does not improve the oxygen flux due to the low activity of Au for oxygen dissociation. The higher permeation flux (1.79×10^{-7} mol cm^{-2} s^{-1}) was measured at 680 °C for a composite $(Bi_2O_3)_{0.75}$-$(Er_2O_3)_{0.25}$ with 40 vol.% of silver. Kim et al. prepared a fluorite type $Bi_{1.5}Y_{0.3}Sm_{0.2}O_3$ (BYS) mixed with 40 vol.% silver [70], which showed a larger O_2 flux (5.8×10^{-7} mol cm^{-2} s^{-1}) at a higher temperature (850 °C) for a membrane with a thickness of 1.3 mm. From a practical and industrialization perspective, employment of noble metals is restricted due to their high price [75], unless thinner yet stably-supported membranes are produced. In Table 2, some physical properties of the metals used in the dual-phase oxygen membranes are summarized.

Table 2. Physical properties and price of some metals used as the electronic conductive phase in dual-phase membranes [80]. TEC: thermal expansion coefficient. Tm: melting point.

Element	Z	Tm (°C)	TEC × 10^6 (°C^{-1})	Cp at 25 °C (J g^{-1} K^{-1})	Electrical Resistivity ×10^{-8} (Ω·m)			Price (€ kg^{-1})
					700 °C	800 °C	900 °C	
Zr	40	1855	5.7	0.278	104.2	114.9	123.1	-
Pd	46	1555	11.8	0.246	24.2	27.1	29.4	40000
Ag	47	962	18.9	0.235	4.21	4.91	5.64	470
In	49	156.6	32.1	0.233	-	-	-	-
Pr	59	931	6.7	0.193	-	-	-	-
Pt	78	1768	8.8	0.133	25.4	28.7	32	25500
Au	79	1064	14.2	0.129	5.82	6.81	7.86	37000

3.2.2. Dual-Phase on Mixed Ceramics

Another option to enhance the electronic conductivity without increasing the price as much as with noble metals, is to mix the ionic conducting phase with another ceramic phase that can conduct electrons, such as perovskites and spinel materials. For the case of ceramic-ceramic systems, some other aspects need to be considered including the stability of both phases (temperature, CO_2 tolerance,

etc.) and the thermal-chemical expansion (compatibility between both phases) and this is discussed in the next section.

Perovskite and spinel structures show higher electronic conductivity than other ceramic materials; therefore, they are employed as the electronic phase, whereas structures of the fluorite type are used as the oxygen conductive phase [78]. Furthermore, fluorite structured materials present good phase stability under CO_2 and reduce atmospheres and low thermal expansion coefficients when compared with perovskites [47]. Table 3 summarizes some important parameters of different ceramic-ceramic dual-phase membranes presented in the literature.

Table 3. Oxygen permeation flux data of several ceramic-ceramic dual-phase membranes.

Membrane	Temperature (°C)	Thickness (μm)	Oxygen Flux (mol cm^{-2} s^{-1})	p'_{O_2} (atm)	p''_{O_2} (atm)	Feed Gas	Sweep Gas	Ea (kJ mol^{-1})	Reference
(LSM)(YSZ) two-step sequential tape casting	900	150	3.31×10^{-8}	0.21	0.002	Air	He	145.3	[72]
(LSM)(YSZ) phase-inversion tape-casting	900	150	1.90×10^{-7}	0.21	0.002	Air	He	142.5	[72]
$(PSFO)_{0.4}(CPO)_{0.6}$	950	600	1.34×10^{-7}	-	-	20% O_2 80% N_2	CO_2	-	[81]
$(PSFO)_{0.4}(CPO)_{0.6}$	950	600	1.93×10^{-7}	-	-	20% O_2 80% N_2	He	-	[81]
$(SDC_\delta)_{0.7}(LSFO)_{0.3}$	950	1100	1.59×10^{-7}	-	-	Air	He	115	[82]
$(SDC_\delta)_{0.7}(LSFO)_{0.3}$	950	1100	1.59×10^{-7}	-	-	Air	CO_2	115	[82]
$(SDC_\delta)_{0.7}(LSFO)_{0.3}$	950	1100	8.92×10^{-7}	-	-	Air	CO_2	96.2	[82]
$(SDC_\delta)_{0.7}(LBCO)_{0.3}$	950	600	4.59×10^{-7}	-	-	21% O_2 79% N_2	He	84.8	[83]
$(LSM)_{0.5}(CGO)_{0.5}$	807	1000	1.8×10^{-8}	18	1	O_2	-	-	[84]
$(LSCF)_{0.7}(CGO)_{0.3}$	950	800	1.56×10^{-6}	0.209	-	Air	Ar	95	[85]
$[(LSCF)_{0.7}(CGO)_{0.3}]$+Pt	950	700	2.83×10^{-6}	0.209	-	Air	Ar	71	[85]
$(BSCF)_{0.4}(CGO)_{0.6}$	875	500	8.04×10^{-7}	-	-	Air	He	-	[86]
$(BSCF)_{0.4}(CGO)_{0.6}$	950	500	1.33×10^{-6}	-	-	Air	He	-	[86]
$(BSCF)_{0.4}(CGO)_{0.6}$	875	500	1.93×10^{-7}	-	-	Air	[a]	46.75	[86]
$(BSCF)_{0.4}(CGO)_{0.6}$	950	500	6.32×10^{-7}	-	-	Air	[a]	46.75	[86]
(YCCC) + (SDC)	950	1300	2.1×10^{-6}	-	-	Air	[b]	82-90	[87]

[a] 80 vol.% CO_2 + 20 vol.% He. [b] 50 vol.% CO_2 + 50 vol.% forming gas (3% H_2+97% N_2).

A dual-phase oxygen membrane (600 μm thick) that was chemically stable under a reducing atmosphere and based on 40 wt.% $Pr_{0.6}Sr_{0.4}Fe_2O_{3-\delta}$ (PSFO) and 60 wt.% $Ce_{0.9}Pr_{0.1}O_{2-\delta}$ (CPO) [81] showed at 950 °C an oxygen flux of 1.34×10^{-7} mol cm^{-2} s^{-1} and 1.93×10^{-7} mol cm^{-2} s^{-1} when CO_2 or helium was employed as sweep gas, respectively.

In another study [82], Pr was replaced with La in the electronic conducting phase ($La_{0.9}Sr_{0.1}FeO_{3-\delta}$) and Pr for Sm for the fluorite type oxygen ion conducting phase ($Ce_{0.8}Sm_{0.2}O_{2-\delta}$, SDC). The highest oxygen permeation flux was obtained for $(SDC)_{0.7}$-$(LSFO)_{0.3}$ at 950 °C, 1.59×10^{-7} mol cm^{-2} s^{-1} employing CO_2 or helium as sweep gas for a 1.1 mm thick membrane. In case of CO as sweep gas, the partial oxygen pressure difference became larger and the oxygen permeation flux increased (8.92×10^{-7} mol cm^{-2} s^{-1}) and, at the same time, the activation energy decreased to 96.2 kJ mol^{-1} compared to 115 kJ mol^{-1} obtained when CO_2 or He were employed as sweep gas, which could be related to the enhanced surface exchange rate at the permeate side. In order to accelerate surface reactions for the CGO-LSCF membrane, Pt was deposited as a catalyst in the surface [85]. The oxygen flux was enhanced with the addition of Pt. A thinner membrane (600 μm thick) made by SDC mixed with a 40 vol.% of $LaBaCo_2O_{5+\delta}$ (LBCO) exhibited an oxygen flux of 4.59×10^{-7} mol cm^{-2} s^{-1} at 950 °C [83].

Yoon et al. [87] reported on a highly permeable and stable membrane under an H_2–CO_2 atmosphere, composed by Ca and Co-doped yttrium chromite, $Y_{0.8}Ca_{0.2}Cr_{0.8}Co_{0.2}O_3$ (YCCC) and samaria-doped ceria, $Sm_{0.2}Ce_{0.8}O_{1.9}$ (SDC). An oxygen flux of 2.1×10^{-6} mol cm^{-2} s^{-1} was measured for a 1.3-mm thick membrane at 950 °C. A long-term test was performed at 950 °C with air at the

feed side and 50% CO_2 + 50% forming gas (3% H_2 + 97% N_2) at the permeate side. The initial flux decreased less than 2% after 350 h.

A 1-mm thick CGO-LSM membrane showed no degradation after 100 h of operation at 950 °C, which showed an oxygen flux of ~8 × 10^{-8} mol cm^{-2} s^{-1} [84]. However, after 500 h of operation, the oxygen flux decreased to ~2.2 × 10^{-9} mol cm^{-2} s^{-1}. No phase transformation was found according to XRD analysis. The authors attributed the decay to the possible formation of a new phase between CGO grains due to the diffusion of elements from the perovskite phase, which blocked the ionic conductivity. Employing CGO and replacing LSM [84] for BSCF [86], higher oxygen fluxes were achieved of 8.04 × 10^{-7} and 1.33 × 10^{-6} mol cm^{-2} s^{-1} at 875 and 950 °C, respectively, by using helium as sweep gas.

To conclude with some examples for ceramic-ceramic dual-phase membranes, an YSZ mixed with $La_{0.8}Sr_{0.2}MnO_{3-\delta}$ (LSM) membrane showed a lower permeation rate at 900 °C, when it was prepared by two-step sequential tape casting (3.31 × 10^{-8} mol cm^{-2} s^{-1}) compared to a membrane obtained via phase-inversion tape-casting (1.90 × 10^{-7} mol cm^{-2} s^{-1}). In both cases, the thickness of the selective layer was around 150 μm [72]. In the case that LSM was replaced by BSCF, the O_2 fluxes were observed to be 1 to 2 orders of magnitude higher in the temperature range of 875–950 °C, despite the thicker membrane (500 μm) [86]. As previously explained, the dual phase membranes can be a good option due to the presence of two different phases with different properties for conduction of oxygen ions and electrons. On the other hand, their chemical compatibility and expansion at high temperatures must be considered, as well as their stability in the presence of some gas species.

4. Factors Affecting Permeation and Stability

As already amply discussed, the main issues of oxygen selective materials employed for oxygen membranes are their thermal, phase, and chemical stability. The selection of the materials is a very critical point since many properties need to be fulfilled at the same time.

For MIEC membranes, materials with high ionic and electronic conductivity are required, which have appreciable values only at high temperatures (>800–850 °C). The phase change of perovskites at these temperatures requires special doping strategies to avoid this. In addition, they must be stable under different atmospheres, which depend on the application (oxygen separation from air, partial oxidation of methane, etc.).

Chemical resistance to different gaseous components, like H_2S and CO_2, also play an important role in the material selection. Again, doping strategies have been proposed to increase the chemical resistance.

Membrane preparation involves different steps depending on the selected technology. The sintering step defines the grain size and composition across the membrane. By controlling the sintering temperature and time, the O_2 permeability can also be improved.

4.1. Chemical and Thermal Expansion

Thermal expansion is one of the key factors that may influence performance of MIEC membranes, especially during the sealing process and co-sintering of different layers for the asymmetric membranes. In engineering, the thermal expansion coefficient is usually considered to be linear. However, for some MIEC oxides such as the Fe-containing or Co-containing perovskites, oxygen loss mainly occurs when the temperature is higher than 400 to 600 °C, which results in a higher thermal expansion coefficient at such a temperature range.

Apart from thermal expansion, some MIEC materials such as $La_{1-x}Sr_xCo_{1-y}Fe_yO_{3-\delta}$ (LSCF) also undergo chemical expansion. This term refers to the formation of vacancies during the ionic transport due to the reduction of the metal cation, which leads to lattice expansion primarily due to steric effects of the positively charged oxygen vacancies. This modifies the cation radius [88,89]. Undesired chemical expansion is the result of high temperatures and fluctuations in the partial pressure of oxygen on the feed and the permeate side. As the operating partial pressure of oxygen decreases and the temperature

increases, the number of oxygen vacancies increases considerably, which results in significant chemical expansion and causes stress across the membrane and, eventually, leads to membrane failure [90,91].

The thermal expansion coefficient of some fluorite and perovskite structures are presented in Table 4.

Table 4. Thermal expansion coefficient of some perovskites and fluorites for different temperature ranges and oxygen partial pressures, $P(O_2)$.

Membrane	$p(O_2)$ atm	Temperature Range (°C)	$\alpha \times 10^6$ (K^{-1})	Reference
$SrCo_{0.8}Fe_{0.2}O_{3-\delta}$	1.00 1.00	RT–430 430–1000	18.5 31.1	[92]
	1.00	600–900	31.1	[93]
	0.21 0.21	RT–500 500–1000	17.8 30.3	[92]
	0.21 0.21	27–427 427–827	18.8 ± 0.3 29.4 ± 0.8	[94]
	0.21	Room–1000	17.9	[95]
	10^{-4}	RT–540 540–1000	12.3 19.7	[92]
$Ba_{0.5}Sr_{0.5}Co_{0.8}Fe_{0.2}O_{3-\delta}$	1.00	RT–440 440–1000	12.2 24.5	[92]
	0.21	RT–440 440–1000	13.6 24.1	[92]
	0.21	RT–500 700–1000	13.6 24.8 [a]	[96]
	0.21	Room–1000	11.5	[95]
	10^{-4}	RT–1000	18.2	[92]
$(ZrO_2)_{0.92}$-$(Y_2O_3)_{0.08}$ (YSZ)	0.21	Room–1000	10.7	[92]
$(ZrO_2)_{0.85}$-$(Y_2O_3)_{0.15}$ (YSZ)	0.21	50–1000	10.8	[40]
CeO_2	0.21	50–1000	12.3	[40]
$Ce_{0.9}Gd_{0.1}O_{2-\delta}$	0.21	Room–1000	12.4	[92]
$Ce_{0.8}Gd_{0.2}O_{2-\delta}$	0.21	50–1000	12.5	[40]
$Ce_{0.6}Gd_{0.4}O_{2-\delta}$	0.21	50–1000	12.1	[40]
$Ce_{0.5}Er_{0.5}O_{2-\delta}$	0.21	50–1000	11.4	[40]
$Ce_{0.9}Ca_{0.1}O_{2-\delta}$	0.21	50–1000	12.8	[40]
$Ce_{0.8}Ca_{0.2}O_{2-\delta}$	0.21	50–1000	13.6	[40]

[a] Thermal and chemical expansion.

Reported values for the expansion coefficients for perovskites depend on the temperature. Below 500 to 600 °C, only thermal expansion prevails while a combination of thermal and chemical expansion occurs at higher temperatures (even if most of the reported expansion coefficients are specified as thermal). Choi and co-workers reported on the thermochemical expansion of BSCF perovskites that are often employed in oxygen membrane technology [96]. The thermal expansion was measured for $Ba_{0.5}Sr_{0.5}Co_{0.8}Fe_{0.2}O_{3-\delta}$ at around 13.6×10^{-6} °C^{-1} up to 500 °C, while, from 700 °C to 1000 °C, the total expansion measured was 24.8×10^{-6} °C^{-1} (see Figure 8). This increase is related to the chemical expansion. As the partial pressure of oxygen decreases and the temperature increases, the chemical expansion increases linearly.

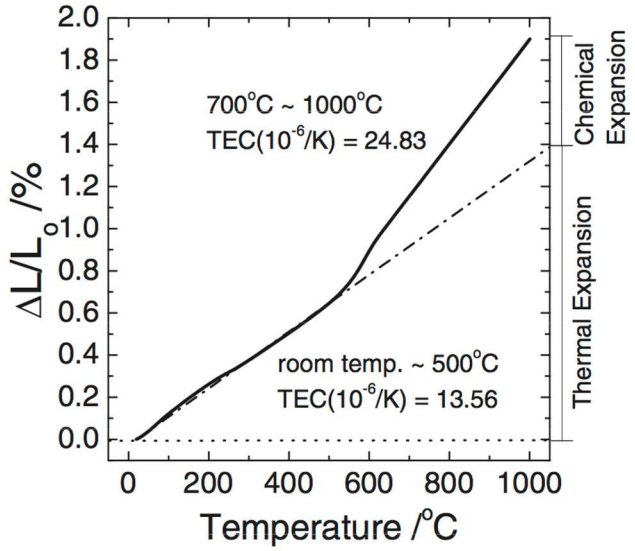

Figure 8. Thermochemical expansion curve for $Ba_{0.5}Sr_{0.5}Co_{0.8}Fe_{0.2}O_{3-\delta}$ in air (pO_2 = 0.21 atm) from room temperature to 1000 °C [96].

A study on the thermo-chemical expansion of LSCF ($La_{0.6}Sr_{0.4}Co_{0.2}Fe_{0.8}O_{3-\delta}$) perovskite type material also revealed an important chemical contribution to the total expansion [97]. Figure 9 shows experimentally measured and predicted results from a mathematic model for the thermo-chemical expansion. Oxygen vacancies, δ, are represented in the right part of the figure.

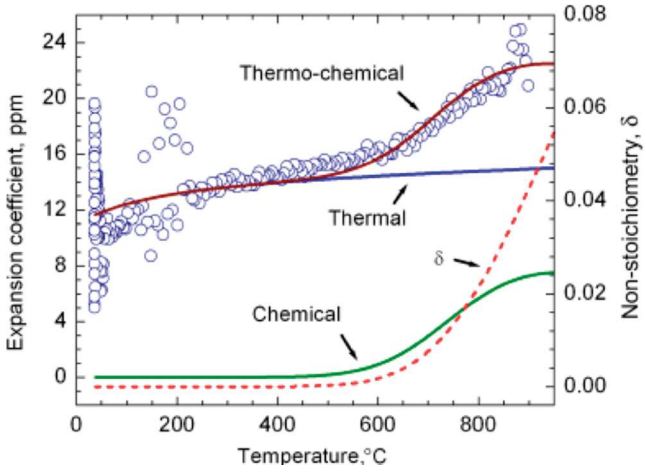

Figure 9. Thermochemical expansion coefficient for LSCF obtained experimentally in air and predicted mathematically [97].

On the other hand, fluorite type structures exhibit lower expansion than perovskites, which represents an advantage in avoiding (or decreasing) stress problems and membrane failure [47].

Bishop and co-workers studied the chemical expansion of gadolinium and un-doped cerium oxide [91]. The study reported a chemical expansion for very low oxygen partial pressures that are less than 10^{-16} atm. Omar et al. studied the expansion effect of doping ceria with different cations [90]. Experimental data were compared with results obtained employing a mathematical model proposed by Hong and Virkar (see Figure 10). As the radius of the trivalent doping increases, the chemical expansion (or chemical elastic strain induced by the non-stoichiometry) of the material increases.

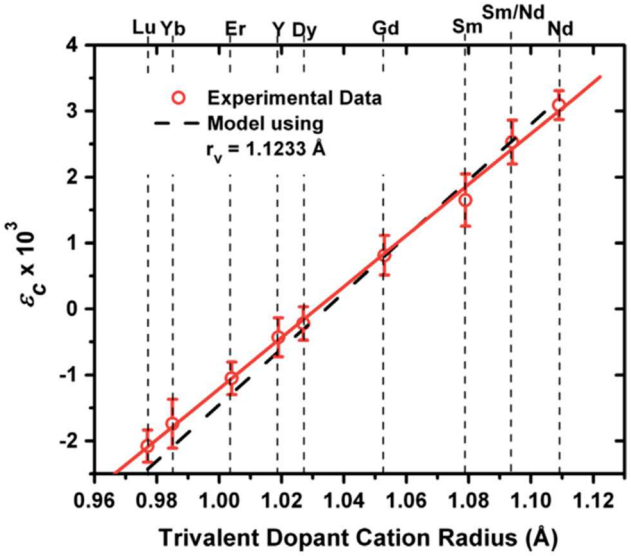

Figure 10. Chemical elastic strains of CeO_2 doped with 10 mol% of rare earth metals at room temperature [90].

The expansion coefficients of ceria and doped-ceria with Gd, Er, and Ca are also presented in Table 4. Their constant expansion coefficient over a large temperature range (50–1000 °C) indicates that their chemical expansion can be considered negligible [40]. Nevertheless, the CeO_2 lattice suffers from expansion when cerium is reduced from Ce^{4+} to Ce^{3+} (the radius of Ce^{3+} is larger than Ce^{4+}). Nonetheless, ceria stabilized with gadolinium and samarium are promising materials since their fluorite structure does not show high chemical expansion compared to perovskites [47].

Ruddlesden-Popper series also showed lower thermal expansion than perovskite type oxides. Un-doped $Pr_2NiO_{4+\delta}$ (PNO) showed a linear TEC of 13.9 × 10^{-6} K^{-1} in the temperature range of 30 to 1000 °C. This value, which decreases to 13.5 × 10^{-6} K^{-1} as B-sites, are substituted with Mo [98].

4.2. Phase Transformation

As previously explained, perovskite materials present relatively high oxygen flux because they are mostly based on alkaline earth compounds. Between all the possible phases that a perovskite can adopt, the cubic perovskite phase is the most favorable structure for the oxygen permeation. An example of this is the $Ba_{0.5}Sr_{0.5}Co_{0.8}Fe_{0.2}O_{3-\delta}$ (BSCF) and $SrCo_{0.8}Fe_{0.2}O_{3-\delta}$ (SCF), which present high permeation rates at high temperatures (>850 °C) due to the relatively stable cubic phase. Below 850 °C, these cubic perovskite transforms into an orthorhombic brownmillerite phase [8,11], with a concomitant dramatic decrease in the oxygen permeation rate. The ordered arrangement of oxygen vacancies in the brownmillerite structure, in which one-sixth of the oxygen sites are vacant, reduces the oxygen flux. In addition, the lattice expansion associated with the phase transition results in mechanical instability issues [99]. In the phase transformation from perovskite (ABO_3) to brownmillerite ($A_2B_2O_5$), a two-phase region exists at lower oxygen partial pressures (<0.1 atm) and at low temperatures [100]. As the oxygen content of the perovskite phase decreases (i.e., increase in the number of oxygen vacancies), a more ordered brownmillerite phase is formed [8], which has lower permeation flux due to the vacancy ordered structure [93]. Nevertheless, the brownmillerite phase can change again into a perovskite phase when the temperature is increased [34,101]. In order to improve the stability of the perovskite material, several strategies have been presented [7].

1. Incorporation of zirconium in the B-site cation of perovskite compounds [53].
2. Introduction of higher valence cations into the A site cation (i.e., La) [102] or (i.e., Ti, Cr, and Ga) [94,103,104] into the B site cation. The phase stability of $SrFeO_3$ can be, thus, improved by introducing metal cations such as Ti, Ni, Mn, Cu, Cr, etc. Moderate amounts of Ti or Cr into the

Co or Fe sub-lattice improves the structural stability, but might decrease the electron conductivity and oxygen permeability [50].

3. Partial substitution of the A site or the B site cation with ions with larger radius. Phase stability could be improved by partial substitution of B-cations with bigger cations, like Nb [105] or Zr [106]. The main advantage of Zr doping is the reduction of the lower temperature limit of the perovskite phase stability range to below 800 °C. As an example, the SCFO cubic phase is stable under an oxygen content higher than 0.1 atm at high temperatures. However, the transformation of the perovskite structure to the brownmillerite phase occurs at an oxygen content below 0.1 atm, where the stoichiometry is around 2.5 (3-δ) at temperatures below 770 °C (when this stoichiometry increases) [107]. Similar results were observed for the phase stability of $SrFeO_{3-\delta}$ [108]. In case of introducing Ba into $SrCo_{0.8}Fe_{0.2}O_{3-\delta}$ by partial substitution of Sr, phase stability is obtained while the conductivity is not affected [109,110]. A single-phase BSFC membrane presented a cubic structure at temperatures over 900 °C for a range of oxygen partial pressures from 10^{-4} to 1 atm [92], whereas un-doped SCF changes from cubic perovskite to orthorhombic brownmillerite are below 677 °C. In this case, the cubic structure is stable at temperatures above 777 °C. Unger et al. [111] studied the effect of Yttrium doped BSCF for different Ytrium concentrations to analyze the partial transformation to Fe-depleted hexagonal phase during long term annealing in ambient air for 240 h for intermediate temperatures as well as cobalt precipitates and anomalies in the morphology. They concluded that the partial B site doped with 10% of Y extended the stability range of the cubic BSCF perovskite phase at lower temperatures. In addition, no secondary phase formation was observed at 800 ºC and, at lower temperatures, the degradation was significantly reduced. Fang et al. [105] investigated the performance and stability of niobium-substituted BSCF. They could demonstrate that the partial substitution of niobium for Co and Fe suppress the phase instability at intermediate temperatures (below 850 ºC). At 800–900 ºC with He as purge gas, the oxygen permeation flux only decreased 10% for the 10% mol Nb-subtituted BSCF compared to pure BSCF, but, over the long term, the test with CO_2 in the purge gas, the Nb present was not enough to stabilize the cubic phase and consequently oxygen flux decreased dramatically. Ravkina et al. [112] extended the research done with Zr-doped BSCF on long-term experiments at an intermediate temperature range and they could conclude that a BSCF membrane with up to 3% (mol) Zr content at an intermediate temperature range (i.e., 773–1123 K) showed improved phase stability compared with pure BSCF. However, for a practical application, the Zr doped BSCF could not maintain a stable oxygen permeation flux and it decreased continuously, which concludes that BSCFZ materials are not an appropriate alternative for intermediate temperature oxygen transporting membranes. Not only the effect of the temperature in the phase transformation, but also the oxygen pressure need to be taken into account to consider the feasibility of perovskite membranes implementation. Ravkina et al. analyzed the phase separation of BSCF perovskite [113] at high and low temperature ranges. The influence of elevated oxygen pressure (from 1 to 50 bar) on the decomposition process of BSCF ceramic with a cubic structure was investigated from 300 to 1300 K. It could be found that, at high pressures, a mixture of cubic phase and a super structure (with double cell parameter) could be found in a single lamella decreasing oxygen permeation.
4. The development of perovskite compounds without cobalt. Cobalt based perovskite type membranes present high oxygen permeability but the stability at intermediate temperatures or under reducing conditions is poor because the cobalt easily reduces and results in big changes in the unit cell dimension. Development of cobalt-free MIEC membranes could be another alternative to solve the long-term stability problems caused by the reaction with gas species like CO_2, SO_2, or water vapor [114]. One of the most studied cobalt-free membranes is the $BaFeO_{3-\delta}$, but it shows low oxygen permeability because it crystalizes in the hexagonal structure, which permeates less than the cubic structure. The partial substitution in the A site with smaller cations like Sr, Ca, La, and Y can lead to the stabilization of the cubic structure. However, since

the volume of the cubic unit cell is reduced, the oxygen flux also decreases. Yet, the partial substitution on the B site with low valence cations like Y, Cu, Ni, and Zr can increase the volume of the cubic unit cell and the oxygen vacancy concentration. Liang et al. [114] studied the influence of the partial substitution of La for Fe on the B-site of $BaFe_{0.95}Zr_{0.05}O_{3-\delta}$. Long-term tests suggest that BFLZ (x = 0.4) exhibits good oxygen permeability. Tan et al. [115] fabricated a cobalt-free $La_{0.7}Sr_{0.3}FeO_{3-\delta}$ hollow fiber membrane and observed that the stability in He and CO_2 atmosphere was higher than for the LSCF ($La_{1-x}Sr_xCo_{1-y}Fe_yO_{3-\delta}$) membrane. However, the LSF membrane still suffered from a reaction with H_2 and CH_4 and porous debris were formed, which resulted in membrane leaking or even a mechanical stability decrease.

For the case of fluorites, most of these do not show phase changes even though ZrO_2 presents a mixed phase and/or phase transition, depending on the operating conditions. This phase transformation vanishes with Y_2O_3 or Bi_2O_3 addition since these are stabilizing the cubic phase [38,46]. High oxygen permeable fluorite, Bi_2O_3, is thermodynamically unstable. At temperatures below 700 °C, a phase transformation to disordered δ-Bi_2O_3 occurs under high oxygen partial pressures, which results in very poor ionic transport [42].

4.3. Cationic Diffusion and Creep

When MIEC membranes are employed for oxygen separation, the oxygen chemical potential gradient across the membranes would result in an inverse cation chemical potential gradient. Cation diffusion is, therefore, expected through the membranes. Although, for most perovskite materials, the activation energy for cation diffusion is several times higher than the oxygen ionic diffusion, and its contribution to the electrical conductivity is also negligible, cation diffusion is still necessary to be studied with regards to the long-term stability of some materials with high cationic diffusion coefficients. At an elevated temperature, cations tend to diffuse from the low oxygen chemical potential side to the high oxygen chemical potential side. Different diffusivities of the cations may result in de-mixing of the material or precipitation of certain elements on the surface of the membrane. For instance, Lein and co-workers [116] observed several secondary phases on the oxidizing side of LSCF membranes after 1 month of operation at 1150 °C, which was attributed to the higher mobility of Fe and Co than that of Sr and La.

Apart from cation diffusion, high oxygen partial pressure also applies stress and sufficient activation energy to provoke a creep deformation of some MIEC membranes. Creep refers to the non-elastic or plastic deformation of some solid materials, influenced by temperature, pressure, time, and the material properties. For MIEC oxides, oxygen partial pressure is also one of the key factors that may cause creep. The steady state creep rate can be described by the equation below [117].

$$\dot{\varepsilon} = K\left(\frac{1}{d}\right)^{p}\left(P_{O_2}\right)^{m}\sigma^{n}e^{-\frac{Ea}{RT}} \quad (3)$$

where K is a constant and d, P_{O2}, σ, and Ea are grain size, oxygen partial pressure, stress, and creep activation energy, respectively. For engineering ceramics, the acceptable strain is reported to be lower than 1% per year [118].

4.4. Gas Poisoning

Membrane surfaces exposed to gases containing small amounts of carbon dioxide (CO_2), sulphur compounds (H_2S and SO_2), or steam (H_2O) are often poisoned (depending on the membrane material), which results in a decrease in the oxygen flux and, in the worst case, in membrane failure. The surface morphology is modified as the material reacts with these gases to create new phases. Thus, the applicability of the perovskites for some applications is limited, since they contain alkaline-earth metals than can react in the presence of gases like CO_2 and steam [48,119,120]. Doping strategies can

again improve the tolerance to these gases. However, in this case, the stability improvement comes at the expense of decreased permeability.

4.4.1. CO_2 and Steam Tolerance

When exposed to CO_2, some MIEC perovskite membranes show a decrease in the O_2 permeation. This variation could be attributed to the absorption of CO_2 on the surface of the membrane or to a carbonation process. For instance, carbonation of some alkaline earth elements (e.g., Ba or/and Sr) can destroy the perovskite structure. On top of it, the formation of a new phase producing a partial or complete loss of oxygen permeation [7] is likely to occur in such conditions. Furthermore, BSCF contains Co, which is not stable at high temperatures due to the volatility of this element [82]. Thus, one can conclude that an uncoated Co-based perovskite-type membrane for natural gas conversion to syngas in a membrane reactor is not feasible [8,121]. The thermal stability can be enhanced by partial substitution of Co and Fe (reducible ions) for less reducible metal ions, such as Ti [50,119], Zr [120], Ce [82,119], Al [122], and more.

Cheng et al. [123] fabricated cobalt-free SDC–BLFZ to study the effect of zirconium replacing iron, on structural characteristics, oxygen permeability, and CO_2 resistance. With the appropriate doping of zirconium, the oxygen permeability is decreased only slightly, but the structural stability and the CO_2 tolerance is improved. A stable oxygen permeation flux of 1.64×10^{-7} mol cm^{-2} s^{-1} was achieved at 925 °C for a 1.0-mm thick membrane with CO_2 as the sweep gas for more than 80 h. This flux value is only 19% lower than that under an air/He gradient, which is much better than the fluxes obtained with most alkaline-metal-containing composite dual-phase membranes.

Arnold et al. [124] reported an immediate decrease in the oxygen flux for a BSCF ($Ba_{1-x}Sr_xCo_{1-y}Fe_yO_{3-\delta}$) membrane when CO_2 was used as sweep gas. Tong's group [53] also found that exposure of BCFZ ($BaCo_{1-x-y}Fe_yZr_xO_{3-\delta}$) membranes to CO_2 could lead to a significant decrease in the oxygen permeability. This process is also associated with the formation of some metal oxides such as the CoO and/or Fe_3O_4 [109,123,124]. Efimov et al. evaluated the stability for carbonates for metals such as Ca, Sr, Ba, and La [125] using the Ellingham diagram (see Figure 11). It can be seen from the diagram that the carbonate of Ba is more stable than $SrCO_3$ and $CaCO_3$, which means $BaCO_3$ is much easier to form. Although Ba^{2+} (large alkaline earth cation) favors a high oxygen conductivity, this cation can also lead to inferior CO_2 tolerance. On the other hand, the smaller cation of Ca^{2+} shows better stability but disfavors the oxygen permeability. Substitution of Fe with Ti also improves the CO_2 tolerance while the O_2 permeability decreases slightly [126]. Moreover, a high cobalt-containing perovskite also presents a low chemical stability in CO_2-containing atmospheres [121]. According to the research of Waindich et al. [127], $Ba_{0.3}Sr_{0.7}Fe_{0.8}Co_{0.2}O_{3-\delta}$ is more stable than $Ba_{0.5}Sr_{0.5}Fe_{0.2}Co_{0.8}O_{3-\delta}$ in the presence of CO_2.

Zeng et al. [128] improved the CO_2 tolerance of SCF ($SrCo_{1-x}Fe_xO_{3-\delta}$) perovskite oxides by introducing Ti into SCF oxides, and they found that the sample with a low Ti content showed a dramatic decrease in the oxygen flux after exposure to CO_2 for 70 h, while higher Ti-substituted samples remained almost stable after 90 h. The author attributed the improved CO_2 tolerance to the stronger chemical bond between Ti and O than the Fe-O and Co-O bonds.

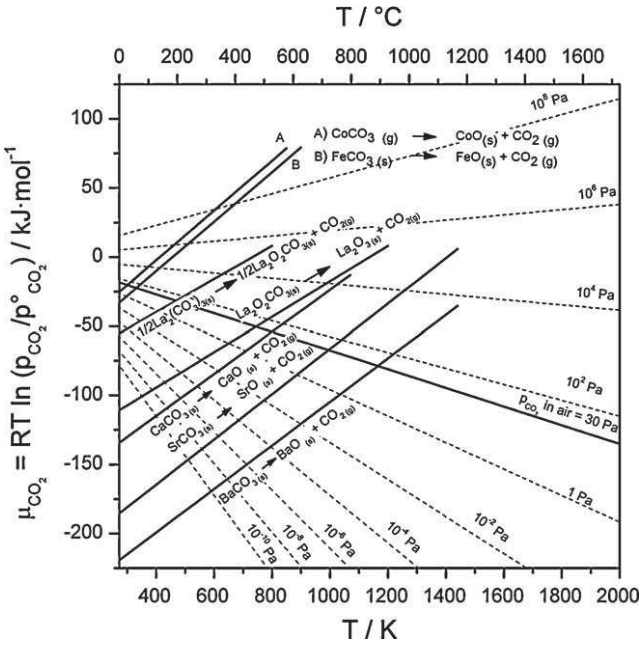

Figure 11. Ellingham diagram for some elements present in MIEC membranes and their carbonate phase stability at different temperatures [125].

Another possibility is doping with highly charged metal B^{5+} like Ta and Nb. The last element has been proven to be a stabilizer with better results for both purposes, viz. O_2 permeability and CO_2 resistance [105,129,130]. Chen et al. [131] found that, when SCF is doped with Ta, the CO_2 erosion is almost negligible. Yi et al. [132] investigated the corrosion of $BaCo_{1-x-y}Fe_xNb_yO_{3-\delta}$ (x = 0.2–0.8, y = 0.1–0.5) in the temperature range of 800 to 1000 °C. The chemical stability was found to be improved when increasing the Nb content while no significant degradation was observed when Co was totally substituted by Fe and Nb. The Ba and/or Co substituted perovskite materials can provide increased chemical stability, but the oxygen permeability may also be decreased. The addition of metals B^{6+} (Mo, W) can stabilize the membrane in a CO_2 environment as well as suppress the polymorphic transition. Popov et al. [133] reported that substitution of Co by W to a BSCF not only improves the CO_2 tolerance, but the O_2 permeability was also enhanced one order of magnitude. The same effect has been reported by Shubnikoba et al. Cobalt was substituted with molybdenum [64].

Another type of perovskite, $La_{0.6}Ca_{0.4}Co_{0.8}Fe_{0.2}O_{3-\delta}$, was studied under a continuous gas flow containing CO_2, which revealed a higher resistance than the one considered from Ellingham diagrams [125]. Un-doped cobalt $La_{0.6}Ca_{0.4}FeO_{3-\delta}$ can resist the presence of CO_2 in the stream. However, the phase transformation was found on the surface of a Ca_2FeO_4 spinel structure at high sintering temperatures.

Lanthanum gallate ($LaGaO_3$) is usually doped with Sr, Ba, or Ca into the lanthanum sub-lattice to increase the ionic conductivity. However, it was reported that it should be preferable to incorporate bivalent cations like Ni and Cu on the Ga sub-lattice [134].

Many fluorite type materials have good phase stability under CO_2 atmospheres [47]. Due to this reason, a dual phase type membrane could help increase the tolerance to CO_2 poisoning. A dual-phase membranes with a composition of 40 wt.% of PSFO ($Pr_{0.6}Sr_{0.4}FeO_{3-\delta}$) and 60 wt.% of CPO ($Ce_{0.9}Pr_{0.1}O_{2-\delta}$) present improved phase stability in an atmosphere containing 50 vol.% CO_2 [81]. The membrane was integrated in a reactor providing oxygen from air for the partial oxidation of methane. A 99% methane conversion was achieved at 950 °C with a measured oxygen flux of 3.27×10^{-6} mol cm^{-2} s^{-1}.

Wang et al. developed a promising dual-phase membrane showing CO and CO_2 stability [82] based on 70 wt.% SDC ($Ce_{0.8}Sm_{0.2}O_{2-\delta}$) and 30 wt.% LSF ($La_{0.9}Sr_{0.1}FeO_{3-\delta}$). Permeation tests after 450

h revealed that the initial permeated oxygen flux was not diminished after exposure to CO_x. Xue et al. developed another membrane with good chemical stability and stable O_2 flux [86] consisting of a dual phase with 40 wt.% of BSCF mixed with 60 wt.% CGO. Their study reveals good stability without flux reduction after 250 h of testing at 950 °C.

A 60 vol.% $NiFe_2O_4$ mixed with 40 vol.% $Ce_{0.8}Tb_{0.2}O_{2-\delta}$ (NFO-CTO) dual phase (thus spinel and fluorite structures) showed a surprisingly higher oxygen permeation flux after 76 h at 900 °C in a pure CO_2 stream [78]. High oxygen fluxes were measured for this spinel-fluorite type membrane. The membrane was exposed to a mixture containing CO_2 with 5% O_2, 1% of SO_2, and 2.5% of H_2O at 800 °C over 6 days and no morphological changes were found, according to the XRD diffractogram.

From another side, materials from Ruddelson-Popper series like PNM ($Pr_2Ni_{0.9}Mo_{0.1}O_{4+\delta}$) can represent a good choice since no alkali-earth metals are present, which as explained before tend to react with CO_2. Recently, the CO_2 tolerance of this type of material in presence of He-CO_2 mixtures (10-50 vol.% CO_2) as sweep gas has been tested [98]. The oxygen permeation flux at 950 °C was ~1×10^{-6} mol cm^{-2} s^{-1} (air at feed side), which decay slightly in the presence of CO_2. Nevertheless, the permeation flux was recovered when CO_2 was removed from the gas stream.

In some cases, ceramic membranes may be operating under harsh conditions with $CO_2/H_2O/O_2$ as feed gas. Some research studies have been devoted for investigating the synergistic effect of H_2O and CO_2 on the chemical degradation of the membranes. Carolan et al. [135] prove that, at 783 °C, the oxygen permeability through the LSCF membrane decreased due to a long time operation in CO_2-containing atmosphere and the permeation flux further decreased when water was added into the feed gas. Yi et al. [136] reported that the co-presence of H_2O and CO_2 in feed gas influences the microstructure and performance of a $Sr_{0.95}Co_{0.8}Fe_{0.2}O_{3-\delta}$ membrane, which attributes this effect to the formation of some bicarbonate. When either H_2O or CO_2 was removed from the feed gas or the operation temperature was increased, the oxygen permeability was improved. Wang et al. [137] applied pure steam as the sweep gas for the test of oxygen permeability through $BaCo_xFe_yZr_zO_{3-\delta}$ (BCFZ) membranes, and the performance is found to be stable after working in the H_2O containing atmosphere for 200 h.

4.4.2. Sulphur Resistance

The CO_2 produced in most of the chemical processes in which MIEC membranes are thought to be applied justifies the efforts done on the development of CO_2-tolerant MIEC membranes [138]. However, the presence of CO_2, which commonly comes from the combustion of light hydrocarbons, is, in many cases, linked to the presence of SO_2 coming from the sulphur containing feedstocks (like coals, natural gas, or biomass). It is proven that this SO_2 can lead to a degradation of the oxygen flux and decrease the mechanical stability of oxygen membranes. Specifically, alkaline and alkaline earth metals compounds, commonly present in MIEC membranes, can form Sulphur compounds. In particular, alkaline earth sulfates are likely to be formed [123].

Most oxygen membranes, both single and dual phase, contain alkaline metals because they provide higher oxygen permeabilities. Sheima and co-workers [139] reported some of the Sulphur compounds that these metals can form in their review for hydrogen membranes. They have collected the heat of formation of binary Sulphur compounds for most of the elements, which is reproduced in Figure 12.

1 IA	2 IIA	3 IIIB	4 IVB	5 VB	6 VIB	7 VIIB	8	9 VIII	10	11 IB	12 IIB	13 IIIA	14 IVA	15 VA	16 VIA	17 VIIA	18 O
H_2S(g) -20.6																	He
Li_2S -447.3	BeS - 234.3				Comp. ΔH°_{298}	Values in kJ/mol						B_2S_3 - 252.3	CS_2(g) 117.7	N_2S_4	SO_2 - 296.8	F_4S - 763.2	Ne
Na_2S -364.8	MgS - 346.0											Al_2S_3 - 724.0	SiS_2 -213.4	P_4S_3 - 155.0	S	Cl_2S -50.0	Ar
K_2S -380.7	CaS - 482.4	Sc_2S_3 -983	TiS_2 - 336.0	V_2S_3 - 953.4	CrS -155.6	MnS -214.2	FeS_2 - 178.2	Co_3S_4 - 478.6	NiS - 82.0	Cu_2S -79.5	ZnS - 206.0	Ga_2S_3 - 516.3	GeS -69.0	As_2S_3 - 169.0	SeS_2	Br_2S_2 -13.0	Kr
Rb_2S -469.4	SrS - 472.4	Y_2S_3 -1260	ZrS_2 - 577.4	NbS_2 - 354.8	Mo_2S_3 -270.3	Te	RuS_2 - 202.0	RhxS	PdS - 75.0	Ag2S -32.6	CdS - 161.9	In_2S_3 - 355.6	SnS -100.0	Sb_2S_3 - 174.9	TeS	I_2S_2	Xe
Cs_2S -483.7	BaS - 460.0	La_2S_3 -1205	Hf_3S_2	TaS_2 - 354.0	WS_2 -201.2	ReS_2 -186.1	OsS_2 - 144.7	IrS_2 - 133.1	PtS - 81.6	Au_2S(g) 230.5	HgS -58.2	Tl_2S -97.1	PbS -100.4	Bi_2S_3 - 143.1	PoS	At	Rn
Fr_2S	RaS	Ac_2S_3															

Figure 12. Heat formation of binary compounds with Sulphur. Units kJ mol^{-1}. Adapted from Reference [139].

BSCF-based membranes exhibit low stability in the presence of Sulphur compounds, since the heat formation of BaS and SrS are very high, −406 kJ mol^{-1} and −472 kJ mol^{-1}, respectively. YSZ is the most sensitive material under Sulphur compound containing atmospheres since yttrium present a high tendency to form the corresponding sulphate with a heat formation of −1260 kJ mol^{-1}. In addition, lanthanum-based perovskites are strongly affected by Sulphur since the corresponding heat formation for La_2S_3 is also large, −1205 kJ mol^{-1} [139]. The influence of SO_2 on the oxygen permeation of LSCF hollow fiber membranes was studied [140] when the membrane was exposed to SO_2. Surface decomposition was observed, which resulted in a significant decrease in the oxygen permeation flux. The XRD analysis showed a peak related to the formation of $SrSO_4$. In another study, an LSCF membrane was exposed to 200 ppm of H_2S for 100 h at 900 °C [141]. Again, strontium sulphate was formed with the corresponding decay in the oxygen flux. The membrane performance was, however, completely recovered when air was fed, which is attributed to the formation of SO_2.

Hence, alkaline earth elements should be avoided to obtain MIEC membranes, which can offer a stable performance under CO_2 and SO_2 containing atmospheres. For this aim, the use of Ni, as well as Co and Cr for single phase and dual phase membranes are an alternative. Nevertheless, this materials present a problem due to their toxicity and high cost [138]. Dual phase hollow fibers made from $(Pr_{0.9}La_{0.1})_2(Ni_{0.74}Cu_{0.21}Ga_{0.05})O_{4-\delta}$ exposed to SO_2 for 170 h at 800 °C showed a decrease in the oxygen flux due to the formation of $Pr_2O_2SO_4$ and $La_2O_2SO_4$ [142]. In agreement, a CO_2 stable NFO-CTO dual-phase membrane also showed Sulphur resistance after exposure to SO_2 for 170 h at 800 °C [78], which makes this membrane very interesting for applications where CO_2 and SO_2 are both present in the feed gas stream. Wei et al. [143] also reported the performance of an alkaline earth metal free of K_2NiF_4 type MIEC membrane based on $(Pr_{0.9}La_{0.1})_2(Ni_{0.74}Cu_{0.21}Ga_{0.05})O_{4-\delta}$. The K_2NiF_4

structure of the PLNCG membrane was destroyed in the presence of SO_2 concentration higher than 383 ppm when the temperature was higher than 800 °C. In this case, the oxygen permeation decreases from 0.75 mL/min cm^2 to 0.1 mL/min cm^2 at 975 °C when SO_2 is added. The results indicate that the PLNCG membrane is sensitive to SO_2 because the Pr and La tend to form the sulphates ($Pr_2O_2SO_4$ and $La_2O_2SO_4$). However, there is a need to use less expensive and toxic material for the development of CO_2 and SO_2 resistant oxygen membranes. Cheng et al. [138] reported ZnO-based dual phase membranes as an alternative to overcome the drawbacks previously underlined. They fabricated 50% (vol) $Al_{0.02}Ga_{0.02}Zn_{0.96}O_{1.02}$-50% (vol) $Gd_{0.1}Ce_{0.9}O_{1.95-\delta}$ (AGZO-CGO55) and the post XRD characterization indicated had mutual enough stability in contact with CO_2 for 120 h at 850 °C and in contact with SO_2 for 2 h at 850 °C.

Garcia et al. [144] prepared a 50% vol $LaCo_{0.2}Ni_{0.4}Fe_{0.4}O_{3-\delta}$ −50% (vol) $Ce_{0.8}Gd_{0.2}O_{2-\delta}$ membrane activated by the deposition of a 30 μm thick porous layer of 50% (vol) $Ce_{0.8}Gd_{0.2}O_{2-\delta}$ -50% (vol) $La_{0.8}Sr_{0.2}MnO_{3-\delta}$ at both sides of the membrane. The oxygen flux permeation under the SO_2 atmosphere for the membrane with the activated layer was higher than without an activated layer, which shows that it works as a protective layer to preserve the surface stability of the membrane and its performance.

It is also worthy to underline that not only the SO_2 coming from the process can affect the membrane performance, but also Sulphur coming from impurities of the raw material in membrane preparation can result in a detrimental effect for the membrane. Wu et al. [145] showed that a dual phase membrane $Ce_{0.9}Gd_{0.1}O_{2-\delta}$-$SrCo_{0.8}Fe_{0.1}Nb_{0.1}O_{3-\delta}$ prepared with low Sulphur content raw materials present a constant permeation rate of 30 mL $min^{-1}cm^{-2}$ in which the permeation is higher than the $Ce_{0.9}Gd_{0.1}O_{2-\delta}$- $SrCo_{0.8}Fe_{0.1}Nb_{0.1}O_{3-\delta}$ prepared with high Sulphur content (because of the impurities in the raw material), which contribute to the sulphate formation in the membrane.

As discussed, many materials can be involved in the preparation of the membranes. However, many other aspects not considered in this section also need to be considered, such as the preparation method (which is not discussed in this review) and sintering conditions and conditions (atmospheres, temperature) to which the membrane will be exposed, depending on the application.

There is still a lot of work to do regarding this problem in order to have more data available about the oxygen permeation performance and the microstructure as well as the phase structure behavior under the SO_2 atmosphere [143].

4.5. Sintering Temperature

An important factor to improve the performance of oxygen membranes is the sintering temperature since it strongly affects the microstructure and the texture of the membrane, viz. grains size, and grain boundaries [43]. These grain boundaries could provide a pathway for oxygen transport in the membrane material. As the sintering temperature increases, the grain size increases, the grain boundary decreases, and the number of final oxygen permeable sites decreases, which results in a lower oxygen flux [146].

Contrary to these authors, Wang and co-workers [95] found higher oxygen permeation when the grain size increases (at higher temperatures), which attributes this behavior to the faster oxygen ion transfer through the grain bulk than along the grain boundary. In particular, BSCF membranes sintered during 5 and 50 h at 1200 °C and 1150 °C, respectively, showed similar permeation fluxes, which were higher than the membranes sintered at 1150 °C for 5 h. Therefore, the sintering temperature is not the only parameter affecting the grain size, but also the sintering time influences the grain size distribution. For instance, Martynczuk et al. [147], for samples calcined at 950 °C, found that the grain size on the surface/bulk changed from around 435/302 μm^2 to 1029/781 μm^2 when the dwell time was increased from 10 to 40 h. Thus, it can be concluded that the grain size tailoring, which affects the oxygen permeation, can be strongly influenced and needs to be carefully controlled both by the sintering time and the sintering temperature of the membrane.

Dual-phase membranes present a more complex mechanism due to the presence of different materials, which respond differently to the sintering conditions. A dual phase membrane composed of $Ce_{0.85}Sm_{0.15}O_{3-\delta}$ and $Sm_{0.6}Sr_{0.4}FeO_{3-\delta}$ (SDC–SSF) was sintered at temperatures ranging from 1400 °C to 1525 °C [148]. At high sintering temperatures, the SSF phase was destroyed adversely, which impacts the electronic transport rate.

5. Oxygen Permeation Improvement

Wagner et al. [149] first described oxygen permeation through MIEC membranes in 1951, with the Wagner equation.

$$J_{O^{2-}} = -\frac{\delta_t t_{e^-} t_{O^{2-}}}{2F} \frac{\partial \mu_{O_2}}{\partial X} \tag{4}$$

where δ_t is the total electron and oxygen ions conductivity, t_{e^-} is the transference number of electrons, $t_{O^{2-}}$ is the transference number of oxygen ions, $\frac{\partial \mu_{O_2}}{\partial X}$ is the chemical potential gradient at a position X far from the membrane wall, and F is the Faraday constant. However, although the permeation of oxygen in MIEC membranes involves at least five steps, this equation accounts for the bulk diffusion. In 1997, Xu and Thomson [35] developed an expression that considers, even if it is simplified, the splitting and recombination of the oxygen steps.

$$J_{O_2} = \frac{D_V K_r \left(P_{O_2}^{'0.5} - P_{O_2}^{''0.5} \right)}{2LK_f \left(P_{O_2}^{'} P_{O_2}^{''} \right)^{0.5} + D_V \left(P_{O_2}^{'0.5} + P_{O_2}^{''0.5} \right)} \tag{5}$$

where D_V is the diffusion coefficient of oxygen vacancies, K_r is the reaction rate constant for the oxygen recombination step, K_f is the reaction rate constant for the oxygen splitting step, and L is the membrane thickness.

This oxygen permeation equation provides a general idea of the permeation values that can be achieved when employing these membranes. However, there are strategies that allow us to modify the 'standard' permeation of a certain membrane.

As stated in the previous equations, the oxygen permeation flux in oxygen selective membranes depends on the following parameters [150].

- Membrane thickness: Oxygen permeation through the membrane is related to the inverse of the thickness following the Wagner equation (Equation (4)). As thickness decreases, the bulk diffusion process become less relevant than the surface exchange.
- Ionic and electronic conduction capacity: Depends on selected materials and operating conditions (temperature, pressure, gases).
- When the limiting step is the surface exchange kinetics, the dissociation and association processes at both sides of the membrane need to be promoted. This could be improved by:
- Deposition of a very thin porous layer on top of a dense selective layer increasing the surface area for the dissociation and recombination of oxygen ions/molecules [151].
- Deposition of catalysts to improve oxygen splitting/recombination.

The combination of both strategies could offer the best solution if the issue of the sintering effect of catalysts at high temperatures is addressed. In the case in which bulk diffusion is the rate limiting step, reduction of the membrane thickness is an appropriate strategy. However, the mechanical stability may decrease dramatically [152], which requires supported membranes.

All these possibilities for improvement of the oxygen permeation are illustrated with some examples in the following subsections.

5.1. Surface Area Modification

Modifying the surface of the membrane can lead to a strong enhancement on the oxygen permeation. As the surface per volume ratio increases in a porous top layer, the adsorption and dissociation of oxygen molecules is promoted [37]. A very thin layer composed of nanoparticles is an interesting approach to obtain a meso-structured layer on top of the oxygen selective layer [153,154]. The layer can be obtained by using nano-filling agents, which are removed during a consecutive calcination/sintering step, such as carbon black or polymeric nanoparticles [155]. The material used for the porous coating can be the same as the selective layer [48,156,157] or a different layer [158], and can possess ionic and/or electronic conductivity. However, a porous coating with a very similar composition as the selective layer is preferred to avoid expansion/compatibility problems.

As an example, the oxygen permeation of a 20 µm-thick LSFT membrane was improved by 50%, when the surface area at the permeate side was increased, as described in Reference [156]. At 1000 °C, the membrane permeation increases from 2.23 × 10^{-6} to 4.31 × 10^{-6} mol cm^{-2} s^{-1} by increasing the roughness of the membrane at the permeate side. On the other hand, the addition of a porous LSC layer (20 µm-thick) on both sides of a SDF-SSF (75wt.% $Ce_{0.85}Sm_{0.15}O_{1.925}$-25 wt.% $Sm_{0.6}Sr_{0.4}FeO_3$) membrane not only increased the oxygen permeation, but also provided a faster steady state permeation obtained (0–8 h) than without the presence of the porous LSC layer (18–40 h) [159]. For the case of a LSTF-coated BSFC membrane, an increase of 20% in the oxygen flux was obtained relative to the flux through a bare BSFC at 950 °C [158], which results in an oxygen flux of 2.23 × 10^{-6} mol cm^{-2} s^{-1} at an atmospheric pressure. The authors reported a reduction in the performance of both membranes after 12 days of testing, but the reduction for the coated membrane was significantly smaller (7.6%) compared to the decrease in performance for the non-coated BSCF (31%).

Hayamizu et al. reported a decrease in the activation energy by addition of a thin porous layer [160]. The activation energy in the temperature range of 725–775 °C decreased from 177.8 kJ mol^{-1} to 102.6 kJ mol^{-1} after a 6.5 µm-thick porous BSCF layer was deposited onto a 120 µm-thick dense BSCF membrane, while the oxygen permeation flux increased by a factor of 3.6 and 1.35 at 700 °C and 850 °C, respectively.

5.2. Deposition of Catalyst

The addition of noble metals, like palladium [71] or platinum [85] onto a porous surface or a thin porous metal oxide layer on a dense membrane increases the catalytic activity for oxygen splitting and oxygen ion recombination, which results in an increase in the oxygen permeability [73,161].

Platinum was added to a micro-channeled LSCF-CGO dual-phase membrane to accelerate the surface reaction kinetics [85]. The oxygen permeation flux was enhanced by a factor of 2.7. Jacobs et al. [162] found that LSCF works as a catalytic layer for a CTF asymmetric membrane and performed better than LSC. The oxygen flux of an uncoated CTF membrane was improved by 88% after a catalytic layer was coated onto this surface. However, the measured oxygen flux at 1000 °C was still quite low, only at 1.26 × 10^{-7} mol cm^{-2} s^{-1}.

The addition of a ceramic catalytic layer of SDC-LSCF onto an asymmetric dual-phase membrane composed of CGO-LSM (30 µm-thick dense layer) resulted in an increase in the oxygen permeation flux from 7.16 × 10^{-8} to 5.32 × 10^{-7} mol cm^{-2} s^{-1} at 950 °C [163]. It was demonstrated that the deposition of an ultra-thin (100 nm) dense $Sm_{0.2}Ce_{0.8}O_{1.9}$ (SDC) layer onto a BSCF membrane led to an increase in the permeation from ~2.38 × 10^{-6} to 2.75 × 10^{-6} mol cm^{-2} s^{-1} at 900 °C [164].

5.3. Thickness Reduction and Supported Thin Film Membranes

Supporting a dense membrane layer onto a porous substrate can help reduce thickness of the functional layer without sacrificing the mechanical strength of the membrane. For successful fabrication of a supported thin-film membrane, certain criteria must be fulfilled [43].

- The thermal and chemical expansion of the selective layer and the support must be as close as possible.
- No reactions should take place between the different materials at high temperatures.
- The dense selective layer should be free of defects, such as cracks and pinholes.

For the selection of the support material, there are two options including using the same material as employed for the selective layer or using a different material, but with good chemical and thermal compatibility. Fluorite type oxides are good candidate materials for the support material due to their good chemical and mechanical stability. When the selected materials differ too much, spallation phenomena (fragments of material at the surface are ejected due to stress suffered by the larger shrinkage of the selective layer) may appear during the heating process due to the mismatch in thermal expansion or due to the larger shrinkage of the dense layer compared to one of the porous supports. For example, porous substrates made of Al_2O_3 are very common in the water purification industry and can be applied as a support for hydrogen separation technologies, which takes advantage of their low cost [165,166]. However, the low thermal expansion coefficient of this material leads to fracture of the selective layer due to the chemical and physical incompatibility with perovskites, which have a much larger chemical and thermal expansion (see Section 4.1) in comparison with aluminum oxide (Al_2O_3: 7.6×10^{-6} °C^{-1}) [167]. For this reason, a thin dense layer is easier to deposit onto a porous support of the same material. Another good support candidate is MgO thanks to its good chemical and mechanical stability at high temperatures and lower cost compared to perovskite and fluorite materials. Since the thermal expansion coefficient of MgO (13.9×10^{-6} °C^{-1}) is close to that of CGO (12.7×10^{-6} °C^{-1}) [26], this material is preferred as support. Ovtar et al. [168] prepared a thin dense layer (10 μm) of CGO-LSF onto MgO. The measured oxygen flux at 850 °C was 1.56×10^{-6} mol cm^{-2} s^{-1}, using N_2 as sweep gas, while this value increased to 1.16×10^{-5} mol cm^{-2} s^{-1} when H_2 was employed as sweep gas. A larger flux (2.97×10^{-6} mol cm^{-2} s^{-1}) was reported under the same conditions by Ramachandran et al. [26] for a 30 μm-thick CGO dense layer deposited onto MgO.

Apart from MgO, CeO_2 may also be a good support candidate for the fabrication of CGO-based membranes because their thermal expansion coefficients closely resemble those of CGO. Yin et al. [169] tested the performance of a CeO_2 supported CGO membrane (10–20 μm-thick), where an oxygen flux of 3.35×10^{-7} mol cm^{-2} s^{-1} was measured at 900 °C.

Metal supports are attractive because of its high mechanical strength and easier integration in the reactor. However, it is usually very hard to find metals with similar thermal expansion coefficients as the ceramic membrane layer material, and there are not many papers on metal-supported oxygen transport membranes. A successful example was given by Sadykov's group, which reported on the deposition of a mixture of LSFN and CGO onto a Ni–Al alloy foam substrate. This shows that the materials are compatible with each other during the sintering process [30]. Stainless steel is a common low-cost metal, but, depending on the steel grade, their use at high temperatures (>500 °C) is hampered by loss of their mechanical properties due to the precipitation of carbides. However, in recent years, some researchers have tried to apply oxygen selective materials onto a stainless steel support using a plasma spray deposition method, which could avoid the problems caused by high-temperature sintering. Fan and Kesler [170] deposited a 55 μm-thick LSCF ($La_{1-x}Sr_xCo_{1-y}Fe_yO_{3-\delta}$) layer onto a stainless steel support using the plasma spray deposition method, which showed a very low gas leakage during testing at high temperatures. Niu's group [171] tried to fabricate an LSCF layer onto a stainless steel support with two plasma spray-based methods, where the plasma spray deposition method performed better by avoiding vertical cracks on the membrane layer.

On the other hand, large oxygen fluxes are required for industrial exploitation of the oxygen perm-selective membranes. One of the best results for supported membranes were reported by Baumann et al. [63], who coated a BSCF layer (70 μm) onto a BSCF substrate that shows an outstanding O_2 flux of 4.62×10^{-5} mol cm^{-2} s^{-1} at 1000 °C using pure oxygen as feed and argon as sweep gas, while, when air was used as feed, a flux of 8.32×10^{-6} mol cm^{-2} s^{-1} was measured. Another membrane showing a high oxygen flux consisted of a micro-channeled CGO-LSF membrane with

a dense 100 µm-thick layer prepared by one-step phase inversion [157]. This membrane showed an oxygen flux of 7.51 × 10^{-6} mol cm^{-2} s^{-1} at 900 °C using CO as sweep gas with air as feed gas. Cao et al. [172] reported a dual-phase supported membrane with a large oxygen flux (2.90 × 10^{-6} mol cm^{-2} s^{-1}), composed of a 40-µm dense layer of SDC-SSAF on top of a porous substrate made of the same material. Meng et al. [25] fabricated asymmetric membranes using the $BaCo_{0.7}Fe_{0.2}Nb_{0.1}O_{3-\delta}$ (BCFN) as material for both the dense layer (20 µm thick) and porous support. At 900 °C, the oxygen flux was 3.35 × 10^{-6} mol cm^{-2} s^{-1}.

In addition, the porosity of the support is another important issue, which was observed by Schulze-Küppers et al. [74]. They observed that, when the porosity of the BSCF support was increased from 26% to 41%, the oxygen flux of the supported dense BSCF layer with a thickness of 20 µm increased by 50% (2.01 × 10^{-6} mol cm^{-2} s^{-1} at 1000 °C). Escribano et al. [173] deposited a layer with the same thickness (20 µm) consisting of NFO-CGO onto an YSZ porous support showing an oxygen flux of ~3.41 × 10^{-7} mol cm^{-2} s^{-1} at 850 °C.

Zhang et al. prepared an YSZ–LSCrF asymmetric composite membrane with a dense layer of thickness ~30 µm and a finger-like porous support with a thickness of ~1 mm by using a phase-inversion tape-casting method. The YSZ-LSCrF composite was subsequently coated with $Sm_{0.2}Ce_{0.8}O_2$ nano-particles on the inner surfaces of the support, and the oxygen permeation flux observed was 1.64 × 10^{-6} mol cm^{-2} s^{-1} at 900 °C [174]. All these results are summarized in Table 5 together with other membranes and supports.

Table 5. Permeation results of supported oxygen permeable membranes.

Material (Membrane/support)	Temperature (°C)	Thickness (µm)	Oxygen Flux (mol cm^{-2} s^{-1})	p'_{O2} (atm)	p''_{O2} (atm)	Feed Gas	Sweep Gas	Reference
BSCF/BSCF	1000	70	4.62×10^{-5}	1	-	O_2	Ar	[63]
CGO-LSF/MgO	850	10	1.12×10^{-5}	0.21	-	Air	H_2	[168]
BSCF/BSCF	1000	70	8.32×10^{-6}	0.21	-	Air	Ar	[63]
CGO-LSF/CGO-LSF	900	100	7.51×10^{-6}	0.209	9.87×10^{-3}	Air	CO	[169]
BCFN/BCFN	900	20	3.35×10^{-6}	0.21	-	Air	He	[25]
CGO/MgO	900	31	2.97×10^{-6}	0.209	2.96×10^{-3}	Air	He	[26]
SDC-SSAF/SDC-SSAF	950	40	2.90×10^{-6}	0.209	4.93×10^{-3}	Air	He	[172]
BSCF/BSCF	1000	20	2.01×10^{-6}	0.209	-	Air	Ar	[74]
BSCF/BSCF	850	40	1.95×10^{-6}	0.21	-	Air	Ar	[175]
YSZ-LSCF-SCO/YSZ-LSCF	900	30	1.64×10^{-6}	0.21	-	Air	CO	[174]
CGO-LSF/MgO	850	10	1.56×10^{-6}	0.21	-	Air	N_2	[142]
CDS-SSF/CDS-SSF	950	160	8.06×10^{-7}	0.209	0.0316	Air	He	[176]
SCFZ/SCFZ	800	20	7.41×10^{-7}	0.209	2.96×10^{-3}	Air	He	[177]
CGO-NFO/YSZ	850	20	3.41×10^{-7}	-	-	Air	Ar	[173]
CGO/CeO_2	900	10-20	$3.35 \cdot \times 10^{-7}$	0.21	-	Air	-	[169]
CTF/CTF	1000	30	3.35×10^{-7}	0.209	-	Air	Ar	[178]
BYS-LSM/ BYS-LSM	850	290	2.56×10^{-7}	1.05	1.05	Air	He	[179]
SCFZ-MgO/SCFZ-MgO	900	200	2.00×10^{-7}	0.209	9.87×10^{-4}	Air	He	[180]
LSM-YSZ/LSM-YSZ/	900	150	1.90×10^{-7}	0.209	0.002	Air	He	[72]
LSCF/LSCF	800	200	1.45×10^{-7}	0.21	$1 \cdot 10^{-3}$	Air	He	[181]
LSCF-YSZ/YSZ	900	60	1.12×10^{-7}	-	-	CO_2	H_2	[182]
LSCF-YSZ/YSZ	900	120	4.46×10^{-8}	0.209	-	Air	CO	[183]
LSCO/CeO_2	900	10	1.17×10^{-8}	0.209	-	Air	He	[184]

5.4. Application of Advanced Membrane Preparation Methods

The fabrication process used for the preparation of MIEC membranes determines their geometry and microstructure, and also influences their performance during the operation process. The dry pressing method is considered the easiest way for planar membrane preparation, which consists of pressing the ceramic powders into 1 to 2 mm discs and sintering at high temperature. Another widely used method for planar membrane fabrication is tape casting. Different from dry pressing, tape casting is a slurry-based method. A ceramic slurry of certain viscosity should be prepared before being casted into a tape with the blade. The thickness of the membrane is controlled by the slurry viscosity and the blade gap. Geffroy et al. [185] proved that this method can result in flat membranes with good microstructure homogeneity. Extrusion is another slurry-based membrane fabrication method. Green membranes are formed by pushing the ceramic slurry through a die orifice with a high pressure, and the dimensions of the die determine the geometry of the membrane. Many tubular membranes such as

the $La_{0.7}Ca_{0.3}Fe_{0.85}Co_{0.15}O_{3-\delta}$ (LCFC) [186] and BSCF [187,188] tubes are successfully fabricated with this method. However, membranes with thick walls are usually obtained with the extrusion method.

The methods mentioned above can be applied for the fabrication of symmetric membranes or membrane supports. However, with the application of some advanced preparation methods, an asymmetric membrane could be prepared in a single step and oxygen permeation resistance could be reduced. The phase inversion method, which was mainly applied for polymer membrane fabrication, has now become an attractive strategy for the fabrication of asymmetric ceramics. A homogeneous mixture with ceramic powders and polymer solvent is prepared before being shaped into the desired geometry and introduced into the coagulation bath. In the coagulation bath, the coagulant exchange with the solvent of the slurry, which result in polymer-lean and polymer-rich phases. The solidified slurry is achieved because of the polymer-rich phase, while finger-like channels are formed from the polymer-lean phase in the green membrane after the drying process. Oxygen transport resistance through the membrane is reduced due to the micro-channelled structure and the channels provide a large surface area, which would promote the oxygen permeability of the membrane by increasing surface kinetics. The phase inversion was mainly adapted for the preparation of hollow fiber membranes [189–192], but, recently, some porous ceramic wagers have been prepared by combining the phase inversion and tape casting processes [72,193,194].

The freeze cast is another promising method for preparing asymmetric membranes with oriented pores and low gas transfer resistance. This method starts with the preparation of a colloidal suspension and this suspension was then freed in a mould. During the sublimation of the solvent, a network of oriented holes is formed inside the membrane, which provides a shorter gas transfer distance than the sponge-like microstructure formed by burning the sacrifice phase. Liu et al. [195] fabricated a $Zr_{0.84}Y_{0.6}O_{1.92}$-$La_{0.8}Sr_{0.2}Cr_{0.5}Fe_{0.5}O_{3-\delta}$ dual-phase asymmetric membrane by the freeze cast process and the oxygen permeability is proven to be better when compared with the fabricated phase-inversion tap-casting strategy.

6. Application of Oxygen Conducting Membranes in Membrane Reactors

The integration of oxygen perm-selective membranes into a membrane reactor has been, together with the solid oxide fuel cells, the main application for MIEC membranes because of the high required operating temperatures. Oxidative coupling of methane, partial oxidation of methane, and oxidative dehydrogenation of ethane are the reaction systems where the application of these membranes have attracted the most interest in the literature. In this section, the most studied processes in which oxygen membranes have been applied are described, paying special attention to the works in which these membranes have improved the performance of these processes.

6.1. OCM (Oxidative Coupling of Methane)

The oxidative coupling of methane (OCM) is a high temperature reaction, which is commonly performed between 750 and 950 °C. This directly produces olefins from natural gas as feedstock. This process consists mainly of three primary reactions. The desired production of ethane Equation (6) and the undesired combustion reactions (Equation (7) and Equation (8)).

$$\mathbf{2}\,\boldsymbol{CH_4} + \boldsymbol{O_2} \rightarrow \boldsymbol{C_2H_6} + \mathbf{2}\,\boldsymbol{H_2O},\ \Delta H_r = -88.3\ \text{kJ/mol} \quad (6)$$

$$\boldsymbol{CH_4} + \mathbf{2}\,\boldsymbol{O_2} \rightarrow \boldsymbol{CO_2} + \mathbf{2}\,\boldsymbol{H_2O},\ \Delta H_r = -803\ \text{kJ/mol} \quad (7)$$

$$\boldsymbol{CH_4} + \boldsymbol{O_2} \rightarrow \boldsymbol{CO} + \boldsymbol{H_2O} + \boldsymbol{H_2},\ \Delta H_r = -277.8\ \text{kJ/mol} \quad (8)$$

The competition between the primary reactions combined with the consecutive reactions that are also involved in the process (for instance, Stansch et al. [196] used 10 reactions to describe the OCM kinetics) makes this process very complex. Because of the importance of the undesired reactions, the conventional OCM process has the common selectivity-conversion problem of consecutive reactions,

which usually results in a poor performance impeding the implementation of this process at industrial scales [197]. The most important OCM membrane reactor studies, including their achieved OCM performances, are listed in Table 6.

Table 6. Different membranes tested in literature for the OCM reaction.

Membrane	Temperature (°C)	Oxygen Flux (mol cm^{-2} s^{-1})	Dilution (%)	Catalyst	CH_4 Conversion	C_{2+} Selectivity	C_{2+} Yield	Reference
$La_{0.6}Sr_{0.4}Co_{0.2}Fe_{0.8}O_{3-\delta}$	975	-	67.5 (He)	$SrTi_{0.9}Li_{0.1}O_3$	0.3	0.7	0.21	[198]
$BaCe_{0.8}Gd_{0.2}O_{3-\delta}$	780	-	96 (He)	$BaCe_{0.8}Gd_{0.2}O_3$	0.26	0.62	0.16	[199]
$BaCo_xFe_yZr_zO_{3-\delta}$	800	-	75 (He)	$MnNa_2WO_4/SiO_2$	0.35	0.5	0.17	[200]
$Ba_{0.5}Sr_{0.5}Co_{0.8}Fe_{0.2}O_{3-\delta}$	850	1.12×10^{-6}	80 (He)	La-Sr/CaO	0.22	0.67	0.15	[201]
$Ba_{0.5}Sr_{0.5}Co_{0.8}Fe_{0.2}O_{3-\delta}$	1000	4.09×10^{-6}	47 (He)	Pt/MgO	0.05	0.5	0.03	[202]
$Ba_{0.5}Sr_{0.5}Co_{0.8}Fe_{0.2}O_{3-\delta}$	900	2.60×10^{-6}	66 (He)	LaSr/CaO	0.25	0.7	0.18	[202]
$Ba_{0.5}Sr_{0.5}Co_{0.8}Fe_{0.2}O_{3-\delta}$	950	1.49×10^{-6}	89 (He)	Sr/La_2O_3	0.25	0.37	0.09	[202]
$Bi_{1.5}Y_{0.3}Sm_{0.2}O_{3-\delta}$	900	4.00×10^{-8}	98 (He)	$Bi_{1.5}Y_{0.3}Sm_{0.2}O_{3-\delta}$	0.648	0.54	0.35	[203]
$Ba_{0.5}Ce_{0.4}Gd_{0.1}Co_{0.8}Fe_{0.2}O_{3-\delta}$	850	1.04×10^{-6}	50 (He)	Na-W-Mn/SiO_2	0.516	0.67	0.35	[204]
$La_{0.6}Sr_{0.4}Co_{0.2}Fe_{0.8}O_{3-\delta}$	900	6.50×10^{-6}	25 (Ar)	$Bi_{1.5}Y_{0.3}Sm_{0.2}O_{3-\delta}$	0.49	0.79	0.39	[205]

Santamaría et al. [206] proposed an alternative to the conventional configuration, in which methane and oxygen are co-fed, to improve the yield of the process. A porous membrane was simulated to distribute the oxygen along the axial length of the reactor. Unlike the co-feeding case, the distribution of oxygen allows us to keep a low oxygen partial pressure in the reactor, which maximizes the formation of ethane among the three main reactions of the process (the oxygen reaction order of Equation (8) is lower than in both complete and incomplete combustion reactions). A C_{2+} yield of 29% was achieved with this concept, which results in an improvement of 20% in comparison with the simulated conventional reactor.

In 1994, Coronas et al. [207] investigated the concept described above experimentally. Li/MgO was used as a catalyst and was placed in the inner part of a porous Al_2O_3 tube that was selected to distribute the oxygen along the packed bed. In comparable cases, the C_{2+} selectivity increased between 10% and 15% when the oxygen was uniformly distributed. Furthermore, the temperature increase in the bed, which is known as a significant issue in OCM (oxidative coupling of methane) reactors because of the highly exothermic behavior of the process, was better controlled by distributing the oxygen and, consequently, the reaction along the bed, which reduces the maximum temperature rise reached in the bed to only 20 °C. Additionally, the distribution of oxygen allows, contrary to the conventional co-fed packed bed reactor concept, to work below the overall explosive limits for the CH_4-O_2 mixtures at lower CH_4/O_2 ratios, which, thereby, increases the overall CH_4 conversion of the process.

Tan et al. [198], in 2007, implemented and compared with the co-feed concept the same concept by placing the catalyst ($SrTi_{0.9}Li_{0.1}O_3$) inside the membranes and feeding oxygen from the outer zone of the membrane. In this study, a dense LSCF membrane was chosen to distribute the oxygen. By using an oxygen-selective membrane, the air separation unit that would be needed to purify the oxygen is avoided, which significantly reduces the costs of the OCM process. Regarding the OCM performance, the maximum C_{2+} yield achieved in this work goes from 12% with the conventional configuration to 21% when the membrane reactor was used. According to the authors, the selection of the catalyst was not optimal and the C_{2+} yield could have been further improved by choosing a more C_{2+} selective catalyst.

Lu et al. [199] prepared a tubular oxygen-selective $BaCe_{0.8}Gd_{0.2}O_3$ and then tested this membrane under OCM conditions. Without the use of any additional catalyst, a 16% C_{2+} yield was reached in a membrane reactor. This study also demonstrated the catalytic activity of some MIEC materials, which results in similar yields to those where a separate catalyst was placed inside the reactor. According to the authors, a significant improvement of the OCM performance could be reached by increasing the activity of the species that catalyze the reaction.

In contrast to the previous study, Czuprat et al. [200], who used a BCFZ membrane, did not observe any methane conversion (below 0.3% in the best case). In a second batch of experiments of the same work, the reactor was packed with $Mn/Na_2WO_4/SiO_2$, which is one of the most often used

catalysts in literature for OCM [208]. A maximum yield of 17.5% was found with these operating conditions, which reached a selectivity towards C_{2+} of 50%. It was also noticed that higher residence times enhance the CH_4 conversion, but at the expense of simultaneously decreasing the C_{2+} selectivity because of the oxidation of the desired products. The main factor hampering the process performance in these experiments was the fast formation of gaseous oxygen from the oxygen ions at the permeate side of the membrane, which accelerates the undesired gas-phase combustion reactions. According to the authors, the deposition of a catalyst on the membrane surface could reduce this effect, which leads to higher OCM performances.

Wang et al. [201] explained the fast recombination of oxygen ions at the permeate side in comparison with the production of methyl radicals from these oxygen ions (which favors the desired path for the production of C_{2+}) to justify their observed poor OCM reactor performance. A maximum C_{2+} yield of 15% was achieved in their study, where La-Sr/CaO was used as a catalyst and BSCF as the oxygen perm-selective membrane.

Olivier et al. [202] coated the surface of a membrane with different active OCM catalysts, which limits the issue of the fast recombination of oxygen ions, as explained above. An oxygen-selective membrane BSCF ($Ba_{1-x}Sr_xCo_{1-y}Fe_yO_{3-\delta}$) disk was coated with three different catalysts, viz. Pt/MgO, LaSr/CaO, and Sr/La_2O_3. It was noticed that the highest C_{2+} yield was obtained with the LaSr/CaO catalyst, reaching values above 18%, while the Pt/MgO catalyst showed the worst results with yields below 3%. This work underlines that a suitable modification of the membrane surface to properly control and tune the catalytic activity of the system is critical in order to obtain the optimal OCM yield even though no strict correlation between oxygen permeability and C_{2+} selectivity was found.

Contrary to the findings of Olivier et al., Haag et al. [209] found a correlation between the oxygen permeation rate and the C_{2+} selectivity. Experiments where a Pt/MgO catalyst was coated onto the membrane surface of different MIEC membranes (BSCF, BSMF, and BBF) were performed in this work. It was found that a proper tuning of the catalytic activity and oxygen flux across the membrane is crucial to achieve good OCM performance. Too high oxygen membrane permeation would lead to a decrease in the C_{2+} selectivity, while too low permeation would make the catalyst inefficient, which is detrimental for the process.

Akin et al. [203] reported promising OCM results in a membrane reactor using the catalytically active $Bi_{1.5}Y_{0.3}Sm_{0.2}O_{3-\delta}$ as an oxygen-selective membrane. With a 98% helium dilution, a maximum C_{2+} yield of 35% with a C_{2+} selectivity of 54% was reached. An increase of 20% in the CH_4 conversion without any loss in the C_{2+} selectivity was observed when the experiments of this study were compared with some literature-fixed bed reactor experiments performed using other typical OCM catalysts.

In agreement with Akin et al., Bhatia et al. [204] showed in their study that a catalyst-coated membrane could be a good solution to significantly increase the C_{2+} yield of the OCM process. A Na-W-Mn/SiO_2 catalyst was coated on the surface of $Ba_{0.5}Ce_{0.4}Gd_{0.1}Co_{0.8}Fe_{0.2}O_{3-\delta}$ supported onto Al_2O_3. A C_{2+} yield of 34.7% was reached (with a C_{2+} selectivity of 67.4% and a CH_4 conversion of 51.6%) with a relatively low dilution (50%) in this study using the described configuration, which is a value that extrapolated to industrial scales, would make the process competitive with other C_2H_4 production technologies. Additionally, in this study, it was emphasized that it is necessary to carefully tune the catalyst-loading and the oxygen permeation rate to hinder the fast formation of gaseous oxygen species at the permeate side of the membrane. The configuration shows a large improvement with respect to the catalytic packed bed reactor, where a maximum C_{2+} yield of only 15.2% was achieved.

Othman et al. [205] found the highest OCM performance reported in literature by using a membrane reactor configuration. A maximum C_{2+} yield of 39% with a 79% C_{2+} selectivity was achieved when the active specie, $Bi_{1.5}Y_{0.3}Sm_{0.2}O_{3-\delta}$ (BYS), was coated onto the surface of the micro-channels of an oxygen selective $La_{0.6}Sr_{0.4}Co_{0.2}Fe_{0.8}O_{3-\delta}$ hollow-fiber membrane (see Figure 13). According to the authors, another parameter that needs to be carefully controlled is the residence time. A compromise between a high CH_4 conversion, achieved with large residence times, and a high C_{2+} selectivity, was

found at low residence times because of the minimization of C_2 consecutive reactions, which has to be found to achieve optimal performance of the system.

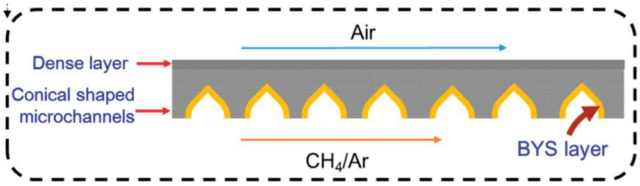

Figure 13. Othman et al. used the scheme of the membrane to perform their experiments [205].

As mentioned by many authors in the literature, it has been demonstrated that a membrane reactor has significant benefits for the OCM process. However, perovskite membranes do not seem to be a good option when looking for a proper membrane for the OCM process because of their poor tolerance to CO_2 atmospheres (which is a by-product of the reaction). Fluorites, despite of their poor O_2 flux, would suit better in long-term experiments because of their better stability under reacting atmospheres. Hence, a fluorite membrane would be, in principle, suitable for its application in an OCM membrane reactor even though a dual-phase one could also be an option. Regarding the shape, a tubular membrane is more promising than the conventional planar because of the higher surface area per reactor volume and because of the better accomplishment of the required oxygen distribution along the axial reactor length. In addition, an extra "catalytic" coating, as it has been already shown by some authors, would also contribute toward increasing the performance of the reaction. Nevertheless, there are still many challenges that need to be solved to make the membrane reactor economically viable at larger scales. The poor stability under OCM conditions, mainly related to the reactivity of CO_2 with MIEC materials, and a better understanding of the membrane-catalyst interaction have been the main challenges discussed in the literature. A solution to these two concerns together with an improvement of the oxygen flux across the membrane would satisfy most of the requirements that currently hinder the implementation of the OCM membrane reactor technology in industrial applications.

6.2. Partial Oxidation of Methane (POM)

The partial oxidation of methane (Equation (9)) is a process used for the production of syngas.

$$\boldsymbol{CH_4} + \boldsymbol{0.5O_2} \rightarrow \boldsymbol{CO} + \boldsymbol{2H_2},\ \Delta H_r = -36\ \text{kJ/mol} \quad (9)$$

This reaction is mildly exothermic, which is, consequently, better thermally balanced than the highly endothermic processes that are widely used for syngas production (steam reforming and dry reforming). It is commonly performed between 700 and 950 °C, and a Ni-based catalyst is used to catalyze this reaction in most of the published research papers. In addition, POM produces syngas with an H_2/CO ratio that is considered optimal for further applications in the chemical industry.

Contrary to OCM, the introduction of oxygen-selective membranes in the reactor designed for the partial oxidation of the methane process does not result in an improvement of its performance in terms of conversion or yield. However, the energy intensive air separation unit used to feed pure oxygen into the reactor (required to avoid N_2 dilution in the high-pressure downstream process units that convert syngas into valuable chemicals) can be circumvented by using an oxygen membrane reactor, which saves a significant amount of energy and, consequently, makes the process more efficient [210]. The POM membrane reactor studies published in the literature are summarized in Table 7.

Table 7. Different membranes tested in the literature for the POM reaction.

Membrane	Temperature (°C)	Oxygen Flux (mol cm^{-2} s^{-1})	Shape	Catalyst	Operating Hours	CH_4 Convulution	CO Selectivity	Reference
$Ba_{0.5}Sr_{0.5}Co_{0.8}Fe_{0.2}O_{3-\delta}$	875	8.56×10^{-6}	planar	$LiLaNiO_x/\gamma$-Al_2O_3	500	0.97	0.96	[110]
$Ba_{0.5}Sr_{0.5}Co_{0.8}Fe_{0.1}Ni_{0.1}O_{3-\delta}$	850	8.93×10^{-6}	planar	Ni	120	0.98	0.97	[211]
$Ba_{0.9}Co_{0.7}Fe_{0.2}Nb_{0.1}O_{3-\delta}$	875	1.19×10^{-5}	planar	Ni	100	0.97	0.75	[212]
$La_{0.4}Ba_{0.6}Fe_{1-x}Zn_xO_{3-\delta}$	900	2.83×10^{-6}	planar	Ni	500	0.99	0.97	[213]
$Ba_{0.9}Co_{0.7}Fe_{0.2}Nb_{0.1}O_{3-\delta}$	875	5.28×10^{-6}	planar	NiO/MgO	400	0.93	0.95	[214]
$La_{0.6}Sr_{0.4}Co_{0.8}Ga_{0.2}O_{3-\delta}$	750	1.86×10^{-6}	hollow fiber	$Ni/LaAlO_3$-Al_2O_3	-	0.97	0.91	[215]
$SrCo_{0.8}Fe_{0.1}Ga_{0.1}O_{3-\delta}$	800	3.08×10^{-6}	hollow fiber	Ni/Al_2O_3	220	1	0.33	[216]
$BaBi_{0.05}Co_{0.8}Nb_{0.15}O_{3-\delta}$	730	1.12×10^{-5}	hollow fiber	Ni phyllosilicate	<5	0.8	0.85	[217]
$BaCo_{0.7}Fe_{0.2}Ta_{0.1}O_{3-\delta}$	875	1.49×10^{-5}	hollow fiber	Ni	83	0.96	0.99	[218]
$(Pr_{0.9}La_{0.1})_2(Ni_{0.74}Cu_{0.21}Ga_{0.05})O_{4+\delta}$	900	7.81×10^{-6}	hollow fiber	Ni	140	0.97	0.99	[219]
$SrFe_{0.8}Nb_{0.2}O_{3-\delta}$	900	1.43×10^{-5}	hollow fiber	Ni/Al_2O_3	120	0.95	0.99	[220]
YSZ-$La_{0.8}Sr_{0.2}Cr_{0.5}Fe_{0.5}O_{3-\delta}$	800	1.30×10^{-6}	planar	Ni/Al_2O_3	-	0.9	0.95	[221]
Ag-$Ce_{0.9}Gd_{0.1}O_{2-x}$	700	1.34×10^{-7}	planar	Ni	-	0.21	0.9	[222]
(0.5 wt.% Nb_2O_5-doped $SrCo_{0.8}Fe_{0.2}O_{3-\delta}$) ($Ba_{0.3}Sr_{0.7}Fe_{0.9}Mo_{0.1}O_{3-\delta}$)	900	1.38×10^{-5}	planar	Ni/Al_2O_3	1500	0.99	0.94	[223]

Balachandran et al. [224] reported in 1995 the first paper in which the POM process was performed in a membrane reactor. Since then, the POM membrane reactor research has been mainly focused on finding membranes with a high oxygen flux together with a high mechanical stability under POM conditions.

As a follow up, several studies have been using planar membranes to test the POM membrane reactor because of their simple production and sealing. Shao et al. [139] reached a stable and relatively high oxygen flux of 8.6×10^{-6} mol cm^{-2} s^{-1} using a BSCF planar membrane. Contrary to many other studies [219] that reported that the BSCF material interacts with the CO_2, the authors could keep a long-term (500 h) experiment without any noticeable change in the POM performance.

Babakhani et al. [211] doped the typical BSCF membrane with Ni ($Ba_{0.5}Sr_{0.5}Co_{0.8}Fe_{0.1}Ni_{0.1}O_{3-\delta}$) to increase its oxygen permeation, where they achieved, in their experiments, a maximum of 8.9×10^{-6} mol cm^{-2} s^{-1}. Although the authors reported that the perovskite structure was unchanged after 120 h of POM tests, they observed the formation of carbonates in the membrane surface.

Song et al. [212] developed a three-layer membrane based on $Ba_{0.9}Co_{0.7}Fe_{0.2}Nb_{0.1}O_{3-\delta}$. The thin dense oxygen-selective layer (120 µm) was placed between two porous layers of the same material. In addition, the porous zone in contact with the reaction side was coated with Ni, which is a typical POM catalyst that improves the catalyst-oxygen contact and, consequently, reduces the amount of catalyst required for the process. A maximum permeation rate of 1.2×10^{-5} mol cm^{-2} s^{-1} was found during the 100 h long-term tests. Afterward less changes in the membrane structure were found as a result of carbonate formation than with the conventional BCFN.

Contrary to many authors focused on improving the oxygen permeation of POM membranes, Gong et al. [213] chose doping elements with stable valences to improve the stability of the POM membrane. Although the maximum permeation in their tests was found to be only 2.8×10^{-6} mol cm^{-2} s^{-1}, the stability of the 1 mm thick $La_{0.4}Ba_{0.6}Fe_{1-x}Zn_xO_{3-\delta}$ was demonstrated. After 500 h of a long-term POM test, an XRD analysis showed that the structure of the membrane remained the same.

Due to the limitations of planar membranes in terms of the surface area to the reactor volume ratio, more effort has been invested in hollow fiber membranes. Their commonly tubular shape provides a higher surface area per reactor volume, while their thinner wall can increase the oxygen permeation rate.

Song et al. [214] modified an A-site deficient $Ba_{0.9}Co_{0.7}Fe_{0.2}Nb_{0.1}O_{3-\delta}$ to increase the number of oxygen vacancies to enhance the oxygen permeation. A value of 5.2×10^{-6} mol cm^{-2} s^{-1} was achieved at 875 °C in a 400-h long-term test without any change in performance even though the authors noticed the growth of Ba-carbonates in the membrane surface.

Kathiraser et al. [215] reported a study on the $La_{0.6}Sr_{0.4}Co_{0.8}Ga_{0.2}O_{3-\delta}$ hollow fiber membrane. The authors introduced the Ga^{3+} cation in the membrane structure to improve its mechanical stability. The maximum permeation rate of 1.9×10^{-6} mol cm^{-2} s^{-1} was achieved at 800 °C. Although the results were stable after a 24-h test, some Sr carbonates were observed in the membrane surface, which limited the membrane operation in a longer-term experiment.

In agreement with Kathiraser et al., Meng et al. [216] also added Ga^{3+} ion to improve the stability of their hollow fiber membranes. The membrane selected by these authors was $SrCo_{0.8}Fe_{0.1}Ga_{0.1}O_{3-\delta}$, and obtained a maximum permeation rate under a 24-h POM test of 3×10^{-6} mol cm^{-2} s^{-1}. In a different test, the membrane showed good stability after 250 h in a 4% H_2 atmosphere, while, under 6% H_2, the membrane was immediately etched due to the reduction of Fe and Co. It is also shown in this study that the amount of oxygen permeating across the membrane has to match the amount of CH_4 fed into the reactor because high oxygen permeation would lead to over-oxidation of the products.

Wang et al. [217] proposed a $BaBi_{0.05}Co_{0.8}Nb_{0.15}O_{3-\delta}$ hollow fiber with a high oxygen permeation rate (1.1×10^{-5} mol cm^{-2} s^{-1}) operating at relatively low temperatures (between 650 and 750 °C). A 100-h long-term POM test was performed, where the membrane showed good stability. Once more, the formation of Ba carbonates in the membranes surface was observed even though the bulk was still conserving the perovskite structure.

Some studies have modified the shape of the commonly straight hollow-fiber membranes giving them a U-shape and gaining mechanical stability during the heating and a consequent expansion process. Using a U-shape hollow fiber $BaCo_{0.7}Fe_{0.2}Ta_{0.1}O_{3-\delta}$, Liao et al. [218] found a maximum flux of 1.5×10^{-5} mol cm^{-2} s^{-1} under POM conditions, even though, after 83 operating hours, the permeation decreased steeply. In the analysis performed afterwards, it was found that the formation of $BaCO_3$ and the reduction and segregation of Co and Fe caused membrane breakage, which results in the described loss of performance.

Wei et al. [219] justified the anticipated carbonates formation and the substitution of the perovskite-type for a CO_2-tolerant K_2NiF_4-type membrane. A $(Pr_{0.9}La_{0.1})_2(Ni_{0.74}Cu_{0.21}Ga_{0.05})O_{4+\delta}$ U-shape hollow fiber membrane was tested in a POM reactor at 900 °C. A stable permeation of 7.8×10^{-6} mol cm^{-2} s^{-1} was reached during a 140-h experiment. The membrane structure was characterized after the test and, contrary to most of the perovskites, the K_2NiF_4 structure remained unchanged. The only remarkable differences were the formation of finger-like structures in the membrane surface, which are beneficial for the oxygen permeation and the presence of some extra Ni in the membrane surface because of its interaction with the Ni-based catalyst even though it was claimed that the membrane bulk structure was not affected.

Zhu et al. [220] modified the widely studied single hollow fiber to a $SrFe_{0.8}Nb_{0.2}O_{3-\delta}$ multichannel hollow-fiber membrane (Figure 14). The robustness and also the oxygen permeation, due to the small thickness of the dense oxygen-selective layer, were enhanced by using these multichannel hollow fiber membranes. A stable oxygen permeation rate of 1.4×10^{-5} mol cm^{-2} s^{-1} was reached during a 120-h experiment. Post characterization showed the formation of impurities at the surface, even though the perovskite structure remained intact.

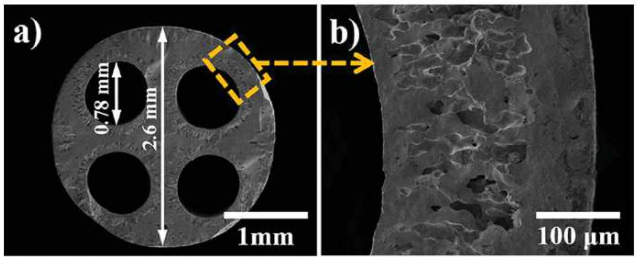

Figure 14. Cross-section (**a**) and wall (**b**) image of the SFN multi-channel hollow fiber membrane used by Zhu et al. [220] to perform POM experiments.

Lastly, dual-phase membranes have shown attractive properties for their application in a POM reactor, especially because of their higher resistance to reducing atmospheres. Yuan et al. [221] proposed an asymmetric planar dual-phase membrane (YSZ-LSCrF) to build a POM membrane reactor. After the sintering procedure, a porous layer of 850 µm and a dense layer of 150 µm were obtained. A maximum flux of 1.1×10^{-6} mol cm^{-2} s^{-1} was obtained at 800 °C during a 50-h test. The analyses performed on the tested sample (SEM and XRD) revealed no changes in the membrane nor the catalyst.

Ruiz-Trejo et al. [222] investigated the performance of a 1 mm-thick dual-phase membrane consisting of $(CGO)_{0.93}$-$(Ag)_{0.07}$. The utilization of this membrane is, however, hampered by the low melting point of Ag, which impedes its application at temperatures above 700 °C. At 700 °C, an oxygen permeation rate of 1.3×10^{-7} mol cm^{-2} s^{-1} was reached in a 50-h long experiment. The characterization analysis of the membrane done after the test showed good tolerance to the POM reducing atmosphere.

Jiang et al. [223] prepared a planar membrane of $SrCo_{0.8}Fe_{0.2}O_{3-\delta}$ doped with 0.5 wt.% of Nb_2O_5 with a porous $Ba_{0.3}Sr_{0.7}Fe_{0.9}Mo_{0.1}O_{3-\delta}$ layer, which protects the system from reducing the POM atmosphere. A stable oxygen flow of 9.7×10^{-6} mol cm^{-2} s^{-1} was achieved in a 1500-h long-term experiment at 850 °C without any remarkable change in the membrane structure.

Apart from the membrane stability, coke deposition, which results from the side reactions, is another factor that may be detrimental for the POM reaction in the membrane reactors. The coke can be deposited onto the Ni-based catalyst and/or result in a mechanical blocking of the reactor, which will influence performance of the membrane and enforce discontinuation operation for clean-up of the reactor. Strategies for extending the lifetime of POM membrane reactors are under study. It was reported that feeding methane/steam mixtures with $CH_4/H_2O \leq 1$ allows us to reduce coke deposition on the Ni-based catalyst [225]. Co-feeding CH_4 and CO_2 also successfully slowed the coke deposition process by the Boudouard reaction between coke and CO_2 [226,227].

Similar to OCM, the main challenge that needs to be solved in order to make the application of oxygen-selective membranes in a POM process feasible is finding a trade-off between a high oxygen permeation flux and a good membrane stability under reducing atmosphere. This achievement would allow a stable oxygen supply during long periods of POM reaction, which enables the substitution of the costly cryogenic air separation unit by a membrane-based process. Based on these requirements, the instability of most of the "standard" perovskite membranes under reacting conditions make them not suitable for this specific application. Similar to OCM, a supported fluorite or a dual-phase membrane seems to be the best option for this application. However, since the yield of this reaction is already high enough, a maximization of the membrane oxygen flux would increase the overall products production. Because of that, special attention should be directed on finding out a membrane with high oxygen flux. In the case of fluorites, a supported-fluorite membrane with a thin dense layer would help increase the oxygen flux.

6.3. Oxidative Dehydrogenation of Ethane

An alternative process for ethylene production is the oxidative dehydrogenation of ethane. Similar to OCM, the reaction is hindered by parallel and consecutive combustion reactions (Equations (10) and (11)), which compete with the desired dehydrogenation (Equation (12)).

$$\boldsymbol{C_2H_6} + \frac{\mathbf{1}}{\mathbf{2}}\,\boldsymbol{O_2} \rightarrow \boldsymbol{C_2H_4} + \boldsymbol{H_2O},\ \Delta H_r = -105\ \text{kJ/mol} \quad (10)$$

$$\boldsymbol{C_2H_6} + \frac{\mathbf{7}}{\mathbf{2}}\,\boldsymbol{O_2} \rightarrow \mathbf{2}\,\boldsymbol{CO_2} + \mathbf{3}\,\boldsymbol{H_2O},\ \Delta H_r = -1428\ \text{kJ/mol} \quad (11)$$

$$\boldsymbol{C_2H_4} + \mathbf{3}\,\boldsymbol{O_2} \rightarrow \mathbf{2}\,\boldsymbol{CO_2} + \mathbf{2}\,\boldsymbol{H_2O},\ \Delta H_r = -1323\ \text{kJ/mol} \quad (12)$$

The process is mildly exothermic, and is performed between 700 and 900 °C and, in most of the cases, as explained below, the membrane is also used to catalyze the reaction.

The integration of membranes in the process has similar advantages as for the OCM process. The desired reaction is favored at low oxygen partial pressures, which increases the C_2H_4 selectivity by distributing the oxygen feeding. Moreover, the heat management becomes easier because of the distribution of the heat released due to the exothermicity of the reactions. Lastly, the distributed feed allows us to operate the system within the overall explosive limits because of the very low local oxygen concentrations. A summary of the membranes used for Oxidative Dehydrogenation of Ethane (ODHE) found in the literature is provided in Table 8.

Table 8. Different membranes tested in literature for the ODHE reaction.

Membrane	Temperature (°C)	Oxygen Flux (mol cm^{-2} s^{-1})	Shape	C_2H_6 Conv.	C_2H_4 Selectivity	C_2H_4 Yield	References
$Ba_{0.5}Sr_{0.5}Co_{0.8}Fe_{0.2}O_{3-\delta}$	800	1.28×10^{-6}	planar	0.84	0.8	0.67	[228]
$BaCo_xFe_yZr_zO_{3-d}$	800	8.56×10^{-7}	hollow fiber	0.90	0.64	0.4	[229]
$Bi_{1.5}Y_{0.3}Sm_{0.2}O_{3-\delta}$	875	6.40×10^{-7}	hollow fiber	0.70	0.8	0.56	[13]
$Ba_{0.5}Sr_{0.5}Co_{0.8}Fe_{0.2}O_{3-\delta}$	775	1.15×10^{-6}	planar	0.85	0.89	0.76	[230]
$Ba_{0.5}Sr_{0.5}Co_{0.8}Fe_{0.2}O_{3-\delta}$	775	7.44×10^{-7}	planar	0.83	0.89	0.74	[230]
$La_{0.5}Ce_{0.1}Sr_{0.4}Co_{0.5}Fe_{0.5}$ $O_{3-\delta}$	850	-	planar	0.86	0.91	0.78	[231]
$Sm_{0.6}Sr_{0.4}Co_{0.5}Fe_{0.5}O_{3-\delta}$	850	-	planar	0.85	0.91	0.77	[231]
$Nd_{0.6}Sr_{0.4}Co_{0.5}Fe_{0.5}O_{3-\delta}$	850	-	planar	0.86	0.89	0.77	[231]
$Ba0.6Sr_{0.4}Fe$ $O_{3-\delta}$	850	-	planar	0.86	0.91	0.78	[231]
$Ba_{0.5}Sr_{0.5}Co_{0.8}Fe_{0.2}O_{3-\delta}$ [a]	850	-	planar	0.89	0.9	0.8	[231]
$Ba_{0.5}Sr_{0.5}Co_{0.8}Fe_{0.2}O_{3-\delta}$	850	-	-	-	-	0.73	[232]

[a] With the addition of graphite platelets.

The first distributed feeding studies were carried out with porous membranes, controlling the oxygen flux fed into the system by changing the pore size of the tubes. In 2002, Wang et al. [228] introduced a dense BSCF membrane to achieve the in situ oxygen-nitrogen separation that was stable after 100 operating hours. At 800 °C and with 90% He dilution, a permeation rate of 1.3×10^{-6} mol cm^{-2} s^{-1} was obtained. The selectivity to C_2H_4 increased, under the same operating conditions, from 53% to 80% when the conventional packed bed reactor was substituted by a porous membrane reactor and reached a 67.4% C_2H_4 yield. Wang et al. [229] also compared the process performance of different BCFZ shapes: a hollow fiber and a disk. The C_2H_4 selectivity at 800 °C and with 90% He dilution was found to be 64% with the hollow fiber, while, in the case of the planar membrane, the value increased up to 79% and reached a C_2H_4 yield of 67%. The difference was attributed to the residence time of the products formed during the reaction, which, in the case of hollow fiber, results in an increase of the importance of the consecutive combustion reactions.

In the same year, Akin et al. [13] also proposed a dense tubular $Bi_{1.5}Y_{0.3}Sm_{0.2}O_{3-\delta}$ membrane to carry out the oxidative dehydrogenation. A permeation flux of 6.4×10^{-7} mol cm^{-2} s^{-1} was achieved at 875 °C, which were stable after 48 operating hours even though Bi reduction was observed. The membrane was proven to be catalytically active, so no extra catalyst was placed in the reactor. A maximum C_2H_4 yield of 56% was reached, with a C_2H_6 conversion of 70% and a C_2H_4 selectivity of 80%.

Rebeilleau-Dassonneville et al. [230] coated a catalytically active layer of V/MgO on top of a BSCF planar membrane to enhance the desired route among the different reactions involved in the ODHE process. At 775 °C, a maximum C_2H_4 yield of 76% was found, while a comparable 74% C_2H_4 yield was reached when Pd nanocluster particles were added. At the same operating conditions, the yield decreased to 50% when a bare BSCF membrane was used.

Applying the concept explained above, Lobera et al. [231] included a catalytic layer on top of a bare BSCF membrane in order to increase its catalytic activity, which resulted in yields above 75%. Their best result was achieved at 850 °C when the surface was modified by adding graphite platelets, which led to the formation of macro-pores. The authors attributed the improvements to the increase in the surface membrane area and the minimization of the consecutive oxidation reactions.

The same author [232] also studied the influence of a reactive diluting agent in the reaction side. The CH_4, which, in this case, was the specie selected as a diluent and limited the consecutive and undesired oligomerization and aromatization reactions, which led to an enhancement of the

C_2H_4 selectivity. Nevertheless, it was noticed that this change also provoked a decrease in the C_2H_6 conversion even though the production of C_2H_4 was found to be higher than in the case in which an inert (Ar) was used as sweep gas. In the analysis performed to the used membranes, it was observed that, even though the permeation was stable during the experiments carried out for several days, some Ba and Sr carbonates appeared on its surface.

Similar to the previous cases, an improved membrane stability together with a high oxygen flux is required to make this configuration suitable for larger scale processes. The criteria to select a proper membrane for this application is very similar to the previous cases. Fluorites and dual-phase membranes are the most suitable options. However, a modification of the standard perovskite could also be an alternative if an extra layer is added to protect the perovskite from the species, which could damage it.

6.4. Other Applications

Similar to ODHE, the membrane reactor concept has also been applied to the oxidative dehydrogenation of other alkanes. For the oxidative dehydrogenation of propane, Wang et al. [233] reached an increase of 29% in the propylene selectivity when the conventional fixed bed was substituted by a BSCF membrane reactor in experiments carried out at 750 °C. Yan et al. [234] also studied the oxidative dehydrogenation of propane using two different membranes including a $La_2Ni_{0.9}V_{0.1}O_{4+\delta}$ and a BSCF membrane. Although the obtained propylene selectivities were around 50%, the propane conversions were always below 10%, which is not yet sufficient for an economically attractive process.

MIEC membranes have also been used to produce pure hydrogen by water splitting. The water dissociation reaction is a thermodynamic equilibrium reaction and, although at operating MIEC membrane temperatures, the equilibrium constant is very low and the reaction can be shifted towards the products by removing the oxygen produced. Balachandran et al. [235] (4.9×10^{-6} mol cm^{-2} s^{-1} using a CGO planar self-supported membrane) and by Li et al. [236] (1×10^{-5} mol cm^{-2} s^{-1} with a $Ba_{0.98}Ce_{0.05}Fe_{0.95}O_{3-\delta}$ membrane) reported the maximum H_2 production reached so far by water splitting. Jiang et al. [237] coupled the water splitting reaction with POM to propose a single unit in which a BCFZ membrane was used to split oxygen from water, while, at the same time, methane was fed in the permeate side, which reacted with the permeated oxygen and produced syngas. The same concept was used by Fang et al. [238]. In this study, the water splitting was combined with POM in a single unit by using a sandwich-like symmetrical dual-phase oxygen membrane in which Ni catalyst particles were coated on the porous parts of the membrane to enhance the water splitting reaction.

Lastly, the methane dehydroaromatization (DMA) is another process whose productivity can be increased by using oxygen membranes. Cao et al. [239] proved that the introduction of a BSCF membrane reactor leads to an improvement in the yield towards the desired aromatic products, especially after some operating time (at 1000 operating minutes, the yield is 3% in the case of the membrane reactor, whereas it is 0.4% when operating with a fixed bed reactor). Compared to the co-feed of methane and oxygen, the authors also noticed that the distributive oxygen feeding results in a decrease in the coke formation, which increases the stability of the catalyst under reaction conditions.

As a general conclusion, the integration of oxygen membranes in conventional chemical processes has shown promising results, which improves, in all the cases, the efficiency of the processes because of the in-situ air separation. Moreover, in some of these processes, an increase in the overall performance of the process has been achieved. On the other side, the oxygen flux and sits stability in long-term experiments needs to be further improved to make these membrane reactor processes economically viable.

6.5. High Temperature Sealing

The sealing of membranes working at a high temperature was demonstrated to be an important issue in the development of high-temperature membrane reactors. Many specific characteristics have to be satisfied simultaneously to fulfill the requirements.

First of all, the material selected for the sealing has to be solid at the operating temperature, which, for most of the processes, is between 750 and 950 °C. In addition, the material of the sealing must not have any chemical interaction with the membrane material to avoid a likely damage of the membrane. Another critical aspect is related with the thermal expansion coefficients of the membrane and sealing materials. A significant difference between both values will lead to the formation of cracks when the heat treatment is applied. Lastly, the sealing technique should be as reproducible as possible to favor its easier implementation at larger scales.

Three different techniques have been extensively applied for the sealing of MIEC oxygen-selective membranes. The first one, used in many membrane reactor works [198,200,202], consists commonly of a specific glass composite applied between membrane and support and can be classified as a non-electronic conductive method (see Figure 15). Different types of glass with some specific modifications depending on the type of oxygen membrane used have been described in the literature [240–242]. As reported by Chen et al. [243], the main drawback of this technique is the likely pollution of the MIEC membrane, which leads to a decrease in the oxygen permeation through the MIEC material in long-term experiments.

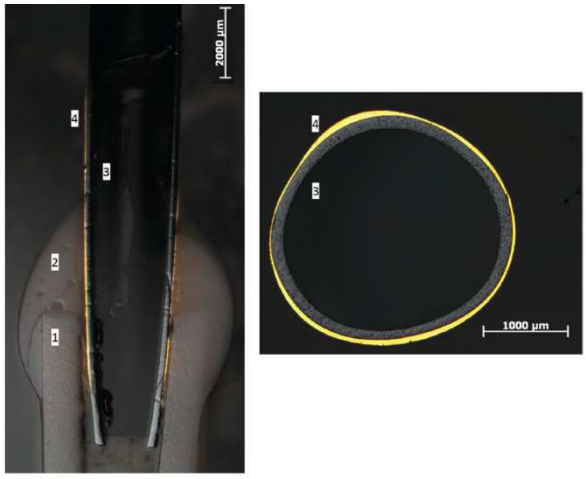

Figure 15. Example of the application of a ceramic sealing into a BSCF membrane [240]. Optical micrographs of the cross sections of perovskite membranes sealed with gold coating + SCHOTT glass sealant 8252. (1) Al_2O_3 tubes, (2) glass seal SCHOTT 8252, (3) membrane wall, and (4) MaTecK gold coating.

The second sealing technique is an electronic conductive sealing, which typically uses a silver alloy and aims to braze the membrane to a metallic tube. The main characteristic of this technique is, as included in the work performed by Chen et al. [243], its capability to enhance the oxygen permeation when an insufficiently high oxygen conductivity membrane is used (see Figure 16). Different Ag-based material compositions coupled with various sintering treatments (performed in different atmospheres) were reported to be successful [244–247].

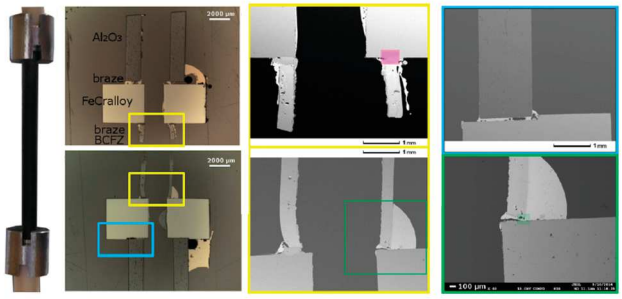

Figure 16. Example of the application of a metallic-ceramic sealing into a BSCF membrane [244].

Lastly, the third option is to place the sealing out of the reaction zone, which reduces the critical conditions required for the high temperature sealing and, consequently, allows the application of a more simple sealing technique, like Teflon rings [248]. The only limitation is related to the strength of the membrane that could be caused because of the temperature gradient occurring between the reaction zone (easily above 800 °C) and the sealing (room temperature). In a membrane reactor, the use of this sealing causes the overdesign of the reactor due to the additional reactor area required to cool the gases and make sure the cold sealing can be applied to the membrane.

In principle, the three types of sealing can be applied to all kind of MIEC membranes. However, there are some limitations. The ceramic (glass-based) sealing can likely react with some of the materials used to prepare MIEC membranes. For instance, the Ba contained in the broadly used BSCF or the MgO support used to make some supported membranes are two examples of materials that react with some of the glass employed for the sealing. In addition, some authors have shown that this sealing could, in some cases, be slightly porous [240]. Because of all these reasons, the materials interaction should be properly addressed if this sealing is selected. A modification of the glass sealing technique by adding an intermediate layer to limit the sealing-membrane reactivity, as shown by Di Felice et al. [240], could be a solution to generalize the application of this sealing.

On the other hand, the metallic-ceramic sealing should have less reactivity problems than the glass-based one, which is especially indicated for fluorite-based membranes because of the enhancement of the membrane material conductivity. Nevertheless, it needs to be considered that the thermal coefficient of the sealing material and of the metallic connector in which the membrane has to be sealed to should be similar to the thermal expansion coefficient of the membrane itself since this material matching is not trivial because of the mixing of ceramic and metallic components.

7. Conclusions and Future Trends

Oxygen is an essential gas for many industrial processes, which is industrially produced by the expensive and energy intensive cryogenic distillation. The development of membrane technology with dense mixed ionic and electronic conducting ceramic membranes (MIEC) could open up the possibility to supply pure oxygen at significantly reduced production costs. In this context, in the last decade, significant efforts have been made to develop new materials to improve the oxygen permeation and stability of MIEC membranes.

Perovskites materials are very unique because of their favorable capacity to transport oxygen ions and electrons, but many perovskite materials show insufficient chemical stability under certain operating conditions (especially in the presence of CO_2 and sulfur compounds). On the other hand, fluorites show a better performance under atmospheres containing CO_2 and sulfur compounds, but their permeation is lower compared to perovskite materials. Combination of two phases (dual-phase) including ceramic-ceramic or ceramic-metal membranes that can lead to a better membrane performance, but good compatibility of the two materials during the sintering and operation process is crucial.

Asymmetric membranes allow us to increase the oxygen flux while maintaining sufficient mechanical strength due to the possibility to deposit a very thin dense layer on top of porous support. However, for the successful fabrication of asymmetric membranes, the layer(s) should attach well with each other, which requires good chemical and thermal compatibility between the selected material of the support and the selective layer during the preparation, sintering, and operation at high temperatures. Recently, papers have been published about asymmetric membranes by focusing on the same or similar materials for both the support and selective layers, and most papers have proven that asymmetric membranes allow reduced bulk diffusion resistance compared with the single layer membranes by reducing the selective layer thickness. For some perovskite membranes, there is a point at which a further decrease of the membrane thickness could not result in higher oxygen permeability because of the limitation of surface kinetics. In addition, activation layers can be applied on top of these membranes to improve the surface exchange speed. For the membranes that operate in

a harsh atmosphere and contains H_2S or CO_2, ceramic oxides with an effective chemical structure are coated on top of the membrane and act as a protective layer of the membrane.

The integration of MIEC membranes in an OCM process can significantly improve the performance of this process because of the integration of air separation inside the reactor and because of improved product yields. The best OCM performance was achieved with a catalytic membrane reactor where the catalyst was coated onto the membrane surface. Similarly, ODHE processes higher product yields and can be reached by integration of oxygen membranes in the reactor. On the other hand, in the POM process, the membranes are only used to avoid the need for a very energy intensive cryogenic air separation unit. In all applications, a careful tuning of the oxygen flux and catalytic reaction rates, and, thus, the membrane and catalyst properties is required, as well as a good compromise need to be found between the membrane mechanical and chemical stability and membrane oxygen permeability with a suitable, gas-tight, and stable sealing, to make membrane reactors a feasible alternative to conventional technologies. Due to their poor stability, "conventional" perovskite membranes do not seem suitable for operating under reacting atmospheres. Although, in most of the cases, the oxygen flux is lower and it has been extensively described that fluorites and/or dual-phase membranes have an improved stability, which is a crucial aspect if long-term tests need to be done. This makes them a promising alternative for its implementation in chemical processes. However, more extensive and larger scale studies are needed to improve and ensure a stable operation of these membranes under long-term reacting tests.

Acknowledgments: This project has received funding from the European Union's Horizon 2020 research and innovation programme under grant agreement No 679933. The present publication reflects only the author's views and the European Union is not liable for any use that may be made of the information contained therein.

Conflicts of Interest: The authors declare no conflict of interest.

Acronyms

BCFZ	$BaCo_{1-x-y}Fe_yZr_xO_{3-\delta}$
BLFZ	$Ba_{1-x}La_xFe_{1-}yZr_yO_{3-\delta}$
BSCF	$Ba_{1-x}Sr_xCo_{1-y}Fe_yO_{3-\delta}$
BSFM	$Ba_{1-x}Sr_xFe_{1-y}Mo_yO_{3-\delta}$
BYS	$Bi_{2-x-y}Y_xSm_yO_{3-\delta}$
CPO	$Ce_{1-x}Pr_xO_{2-\delta}$
CTF	$CaTi_{1-x}Fe_xO_{3-\delta}$
CTO	$Ce_{1-x}Tb_xO_{2-\delta}$
CGO or GDC	$Ce_{1-x}Gd_xO_{2-\delta}$
LBCO	$LaBaCo_2O_{5+\delta}$
LSC or LSCO	$La_{1-x}Sr_xCoO_{3-\delta}$
LSCF	$La_{1-x}Sr_xCo_{1-y}Fe_yO_{3-\delta}$
LSCrF	$La_{1-x}Sr_xCr_{1-y}Fe_yO_{3-\delta}$
LSFN	$La_{1-x}Sr_xFe_{1-x}Ni_xO_{3-\delta}$
LSFO or LSF	$La_{1-x}Sr_xFeO_{3-\delta}$
LSFT	$La_{1-x}Sr_xFe_{1-y}Ta_yO_{3-\delta}$
LSM	$La_{1-x}Sr_xMnO_{3-\delta}$
LSTF	$La_{1-x}Sr_xTi_{1-y}Fe_yO_{3-\delta}$
NFO	$NiFe_2O_4$
PNO	$Pr_2NiO_{4+\delta}$
PNM	$Pr_2Ni_{1-x}Mo_xO_{4+\delta}$
PSFO	$Pr_{1-x}Sr_xFe_2O_{3-\delta}$
SCFO or SCF	$SrCo_{1-x}Fe_xO_{3-\delta}$
SDC	$Ce_{1-x}Sm_xO_{2-\delta}$
SSAF	$Sm_{1-x}Sr_xAl_{1-y}FeyO_3$-$_\delta$
SSF	$Sm_{1-x}Sr_xFeO_{3-\delta}$

YCCC	$Y_{1-x}Ca_xCr_{1-y}Co_yO_3$
YSZ	$(ZrO_2)_{1-x}$-$(Y_2O_3)_x$

Abbreviations

d	Grain size
D_V	Diffusion coefficient of oxygen vacancies
Ea	Activation energy
F	Faraday constant
ΔH_r	Enthalpy of reaction
J_{O2^-}	Oxygen ion permeation
J_{O2}	Oxygen permeation through an MIEC membrane
K	Pre-exponential factor
K_f	Reaction rate constant for the oxygen splitting step
K_r	Reaction rate constant for the oxygen recombination step
L	Membrane thickness
$\frac{\partial \mu_{O_2}}{\partial X}$	Chemical potential gradient
O_O^x	Oxygen ions occupying the lattice
P_{O2}	Oxygen partial pressure
P'_{O2}	Oxygen partial pressure in the retentate
P''_{O2}	Oxygen partial pressure in the permeate
t_{e^-}	Transference number of electrons
$t_{O^{2-}}$	Transference number of oxygen ions
V''_O	Oxygen vacancies (Kröger-Vink notation)

Greek Letters

δ	Oxygen vacancies
$\boldsymbol{\delta_t}$	Total electron and oxygen ions conductivity
$\dot{\varepsilon}$	Creep rate
σ	Stress

References

1. Bose, A.C. (Ed.) *Inorganic Membranes for Energy and Enviromental Applications*; Springer: New York, NY, USA, 2009.
2. Baker, R.W. Future Directions of Membrane Gas Separation Technology. *Ind. Eng. Chem. Res.* **2002**, *41*, 1393–1411. [CrossRef]
3. Diniz, C.; Leo, A.; Liu, S. Development of mixed conducting membranes for clean coal energy delivery. *Int. J. Greenh. Gas Control* **2009**, *3*, 357–367. [CrossRef]
4. Zhang, Z.; Zhou, W.; Chen, Y.; Chen, D.; Chen, J.; Liu, S.; Jin, W.; Shao, Z. Novel Approach for Developing Dual-Phase Ceramic Membranes for Oxygen Separation through Beneficial Phase Reaction. *ACS Appl. Matetr. Interfaces* **2015**, *7*, 22918–22926. [CrossRef] [PubMed]
5. Bhide, B.C.; Stern, S.A. A new evaluation of membrane processes for the oxygen-enrichment of air. II. Effects of economic parameters and membrane properties. *J. Membr. Sci.* **1991**, *62*, 37–58. [CrossRef]
6. Belaissaoui, B.; le Moullec, Y.; Hagi, H.; Favre, E. Energy efficiency of oxygen enriched air production technologies: Cryogeny vs membranes. *Sep. Purif. Technol.* **2014**, *125*, 142–150. [CrossRef]
7. Sunarso, J.; Baumann, S.; Serra, J.M.; Meulenberg, W.A.; Liu, S.; Lin, Y.S.; da Costa, J.C.D. Mixed ionic–electronic conducting (MIEC) ceramic-based membranes for oxygen separation. *J. Membr. Sci.* **2008**, *320*, 13–41. [CrossRef]
8. Bouwmeester, H.J.M. Dense ceramic membranes for methane conversion. *Catal. Today* **2003**, *82*, 141–150. [CrossRef]
9. Gottzmann, C.F.; Prasad, R.; Robinson, E.T.; Schwartz, J.M. Syngas Production Utilizing an Oxygen Transport Membrane. Patent EP1390291A1, 25 February 2004.

10. Christie, G.M.; Lane, J.A. Composite Oxygen Transport Membranes. U.S. Patent 20130156978A1, 20 June 2013.
11. Bouwmeester, H.J.M.; Burggraaf, A.J. Dense ceramic membranes for oxygen separation. *Fundam. Inorg. Membr. Sci. Technol.* **1996**, *4*, 435–528. [CrossRef]
12. Kharton, V.; Yaremchenko, A.; Kovalevsky, A.; Viskup, A.; Naumovich, E.; Kerko, P. Perovskite-type oxides for high-temperature oxygen separation membranes. *J. Membr. Sci.* **1999**, *163*, 307–317. [CrossRef]
13. Akin, F.T.; Lin, Y.S. Selective oxidation of ethane to ethylene in a dense tubular membrane reactor. *J. Membr. Sci.* **2002**, *209*, 457–467. [CrossRef]
14. Godini, H.R.; Trivedi, H.; de Villasante, A.G.; Görke, O.; Jašo, S.; Simon, U.; Berthold, A.; Witt, W.; Wozny, G. Design and demonstration of an experimental membrane reactor set-up for oxidative coupling of methane. *Chem. Eng. Res. Des.* **2013**, *91*, 2671–2681. [CrossRef]
15. Godini, H.R.; Xiao, S.; Kim, M.; Holst, N.; Jašo, S.; Görke, O.; Steinbach, J.; Wozny, G. Experimental and model-based analysis of membrane reactor performance for methane oxidative coupling: Effect of radial heat and mass transfer. *J. Ind. Eng. Chem.* **2014**, *20*, 1993–2002. [CrossRef]
16. Tong, J.; Yang, W.; Cai, R.; Zhu, B.; Lin, L. Novel and ideal zirconium-based dense membrane reactors for partial oxidation of methane to syngas. *Catal. Lett.* **2002**, *78*, 129–137. [CrossRef]
17. Kim, J.; Hwang, G.; Lee, S.; Park, C.; Kim, J.; Kim, Y. Properties of oxygen permeation and partial oxidation of methane in $La_{0.6}Sr_{0.4}CoO_{3-\delta}$(LSC)-$La_{0.7}Sr_{0.3}Ga_{0.6}Fe_{0.4}O_{3-\delta}$ (LSGF) membrane. *J. Membr. Sci.* **2005**, *250*, 11–16. [CrossRef]
18. Takahashi, T.; Esaka, T.; Iwahara, H. Electrical conduction in the sintered oxides of the system Bi_2O_3-BaO. *J. Solid State Chem.* **1976**, *16*, 317–323. [CrossRef]
19. Cales, B.; Baumard, J.F. Oxygen semipermeability and electronic conductivity in calcia-stabilized zirconia. *J. Mater. Sci.* **1982**, *17*, 3243–3248. [CrossRef]
20. de Recherche, C.; Temperatures, H.; Orleans, C. Mixed Conduction and Defect Structure of ZrO-CeO-Y_20_3 Solid Solutions. *J. Electrochem. Soc.* **1984**, *131*, 2407–2413.
21. Yasutake, T.; Zhang, H.M.; Furukawa, S.; Yamazoe, N. Oxygen permeation through perovskite-type oxides. *Chem. Lett.* **1985**, *14*, 1743–1746.
22. Boivin, J.C.; Mairesse, G. Recent Material Developments in Fast Oxide Ion Conductors. *Chem. Mater.* **1998**, *10*, 2870–2888. [CrossRef]
23. Badwal, S.P.S.; Ciacchi, F.T. Ceramic Membrane Technologies for Oxygen Separation. *Adv. Mater.* **2001**, *13*, 993–996. [CrossRef]
24. Yin, X.; Choong, C.; Hong, L. Crafting $La_{0.2}Sr_{0.8}MnO_{3-\delta}$ membrane with dense surface from porous YSZ tube. *J. Solid State Electrochem.* **2006**, *10*, 643–650. [CrossRef]
25. Meng, X.; Ding, W.; Jin, R.; Wang, H.; Gai, Y.; Ji, F.; Ge, Y. Two-step fabrication of $BaCo_{0.7}Fe_{0.2}Nb_{0.1}O_{3-\delta}$ asymmetric oxygen permeable membrane by dip coating. *J. Membr. Sci.* **2014**, *450*, 291–298. [CrossRef]
26. Ramachandran, D.K.; Søgaard, M.; Clemens, F.; Gurauskis, J.; Kaiser, A. Fabrication and performance of a tubular ceria based oxygen transport membrane on a low cost MgO support. *Sep. Purif. Technol.* **2015**, *147*, 422–430. [CrossRef]
27. Chen, A.J.B.C.S.; Kruidhof, H.; Bouwmeester, H.J.M.; Verweij, H. Thickness dependence of oxygen permeation through erbia-stabilized oxide-silver composites. *Solid State Ion.* **1997**, *99*, 215–219. [CrossRef]
28. Teraoka, Y.; Fukuda, T.; Miura, N.; Yamazoe, N. Development of Oxygen Semipermeable Membrane Using Mixed Conductive Perovskite-Type Oxides (Part 2). *J. Ceram. Soc. Jpn.* **1989**, *97*, 533–538. [CrossRef]
29. Mitchell, B.J.; Rogan, R.C.; Richardson, J.W., Jr.; Ma, B.; Balachandran, U. Stability of the cubic perovskite $SrFe_{0.8}Co_{0.2}O_{3-\delta}$. *Solid State Ion.* **2002**, *146*, 313–321. [CrossRef]
30. Sadykov, V.; Zarubina, V.; Pavlova, S.; Krieger, T.; Alikina, G.; Lukashevich, A.; Muzykantov, V.; Sadovskaya, E.; Mezentseva, N.; Zevak, E.; et al. Design of asymmetric multilayer membranes based on mixed ionic-electronic conducting composites supported on Ni-Al foam substrate. *Catal. Today* **2010**, *156*, 173–180. [CrossRef]
31. Dong, X.; Jin, W.; Xu, N.; Li, K. Dense ceramic catalytic membranes and membrane reactors for energy and environmental applications. *Chem. Commun.* **2011**, *47*, 10886–10902. [CrossRef] [PubMed]
32. Deibert, W.; Ivanova, M.E.; Baumann, S.; Guillon, O.; Meulenberg, W.A. Ion-conducting ceramic membrane reactors for high-temperature applications. *J. Membr. Sci.* **2017**, *543*, 79–97. [CrossRef]

33. Liu, Y.; Tan, X.; Li, K. Membrane Processing Mixed Conducting Ceramics for Catalytic Membrane Processing. *Catal. Rev.* **2006**, *48*, 145–198. [CrossRef]
34. Steele, B.C.H. Oxygen ion conductors and their technological applications. *Mater. Sci. Eng. B* **1992**, *13*, 79–87. [CrossRef]
35. Xu, S.J.; Thomson, W.J. Oxygen permeation rates through ion-conducting perovskite membranes. *Chem. Eng. Sci.* **1999**, *54*, 3839–3850. [CrossRef]
36. Wei, Y.; Yang, W.; Caro, J.; Wang, H. Dense ceramic oxygen permeable membranes and catalytic membrane reactors. *Chem. Eng. J.* **2013**, *220*, 185–203. [CrossRef]
37. Jiang, Q.; Faraji, S.; Slade, D.A.; Stagg-williams, S.M. A Review of Mixed Ionic and Electronic Conducting Ceramic Membranes as Oxygen Sources for High-Temperature Reactors. In *Inorganic Polymeric and Composite Membranes: Structure, Function and Other Correlations*, 1st ed.; Elsevier BV.: Amsterdam, The Netherlands, 2011; pp. 235–273. [CrossRef]
38. Repasky, J.M.; Anderson, L.L.; Stein, E.E.; Armstrong, P.A.; Foster, E.P. ITM Oxygen technology: Scale-up toward clean energy applications. In Proceedings of the International Pittsburgh Coal Conference, Pittsburgh, PA, USA, 15–18 October 2012.
39. Kharton, V.; Marques, F.; Atkinson, A. Transport properties of solid oxide electrolyte ceramics: A brief review. *Solid State Ion.* **2004**, *174*, 135–149. [CrossRef]
40. Mogensen, M.; Lindegaard, T.; Hansen, U.R.; Mogensen, G. Physical Properties of Mixed Conductor Solid Oxide Fuel Cell Anodes of Doped CeO_2. *J. Electrochem. Soc.* **1994**, *141*, 2122–2128. [CrossRef]
41. Fagg, D.P.; Shaula, A.L.; Kharton, V.V.; Frade, J.R. High oxygen permeability in fluorite-type $Ce_{0.8}Pr_{0.2}O_{2-\delta}$ via the use of sintering aids. *J. Membr. Sci.* **2007**, *299*, 1–7. [CrossRef]
42. Massey, A.; Schwartz, S. *The CRC Handbook of Solid State Electrochemistry*; CRC: Boca Raton, FL, USA, 1996.
43. Zhu, X.; Yang, W. Critical Factors Affecting Oxygen Permeation Through Dual-phase Membranes. In *Inorganic Polymeric and Composite Membranes: Structure, Function and Other Correlations*, 1st ed.; Elsevier BV.: Amsterdam, The Netherlands, 2011; pp. 275–293. [CrossRef]
44. Fernández-garcía, M. Metal Oxide Nanoparticles. In *Encyclopedia of Inorganic Chemistry*; Wiley: Hoboken, NJ, USA, 2009. [CrossRef]
45. Srinivasan, R.; de Angelis, R.J.; Ice, G.; Davis, B.H. Identification of tetragonal and cubic structures of zirconia using synchrotron x-radiation source. *J. Mater. Res.* **1991**, *6*, 1287–1292. [CrossRef]
46. Nawaz, M.; Gorgishvili, L.; Li, J.; Gorelik, T.; Kolb, U.; Nasdala, L.; Tremel, W. Facile synthesis and characterization of monocrystalline cubic. *Solid State Sci.* **2007**, *9*, 1105–1109. [CrossRef]
47. Hoon, J.; Sook, G.; Yoo, C.; Haeng, J. Contribution of the surface exchange kinetics to the oxygen transport properties in $Gd_{0.1}Ce_{0.9}O_{2-\delta}$-$La_{0.6}Sr_{0.4}Co_{0.2}Fe_{0.8}O_{3-\delta}$ dual-phase membrane. *Solid State Ion.* **2013**, *253*, 64–69. [CrossRef]
48. Peña, M.A.; Fierro, J.L.G. Chemical Structures and Performance of Perovskite Oxides. *Chem. Rev.* **2001**, *101*, 1981–2017. [CrossRef] [PubMed]
49. Cook, R.L.; Sammells, A.F. On the systematic selection of perovskite solid electrolytes for intermediate temperature fuel cells. *Solid State Ion.* **1991**, *45*, 311–321. [CrossRef]
50. Kharton, A.V.K.; Viskup, A.; Yaremchenko, A.A.; Kerko, P.F.; Naumovich, E.N. Ionic transport in $SrCo_{0.85}Ti_{0.1}5O_{3-\delta}$Ceramics at high oxygen pressures. *Mater. Res. Bull.* **2000**, *34*, 1921–1928. [CrossRef]
51. Kharton, V.V.; Shaula, a.L.; Snijkers, F.M.M.; Cooymans, J.F.C.; Luyten, J.J.; Yaremchenko, A.A.; Valente, A.A.; Tsipis, E.V.; Frade, J.R.; Marques, F.M.B.; Rocha, J. Processing, stability and oxygen permeability of Sr(Fe, Al)O_3-based ceramic membranes. *J. Membr. Sci.* **2005**, *252*, 215–225. [CrossRef]
52. Zhu, X.; Cong, Y.; Yang, W. Oxygen permeability and structural stability of $BaCe_{0.15}Fe_{0.8}5O_{3-\delta}$ membranes. *J. Membr. Sci.* **2006**, *283*, 38–44. [CrossRef]
53. Tong, J.; Yang, W.; Zhu, B.; Cai, R. Investigation of ideal zirconium-doped perovskite-type ceramic membrane materials for oxygen separation. *J. Membr. Sci.* **2002**, *203*, 175–189. [CrossRef]
54. Cheng, H.; Yao, W.; Lu, X.; Zhou, Z.; Li, C.; Liu, J. Structural stability and oxygen permeability of $BaCo_{0.7}Fe_{0.2}M_{0.1}O_{3-\delta}$ (M = Ta, Nb, Zr) ceramic membranes for producing hydrogen from coke oven gas Hongwei. *Fuel Process. Technol.* **2015**, *131*, 36–44. [CrossRef]
55. Liu, J.; Cheng, H.; Jiang, B.; Lu, X.; Ding, W. Effects of tantalum content on the structure stability and oxygen permeability of $BaCo_{0.7}Fe_{0.3-x}TaxO_{3-\delta}$ ceramic membrane. *Int. J. Hydrog. Energy* **2013**, *38*, 11090–11096. [CrossRef]

56. Yao, W.; Cheng, H.; Zhao, H.; Lu, X.; Zou, X.; Li, S.; Li, C. Synthesis, oxygen permeability, and structural stability of BaCo0.7Fe0.3-xZrxO$_{3-\delta}$ ceramic membranes. *J. Membr. Sci.* **2016**, *504*, 251–262. [CrossRef]
57. Ganji, E.; Towfighi, J.; Shirazi, L.; Nakhaei, A. Order–disorder transition and phase stability of BaxSr$_{1-x}$Co$_{0.8}$Fe$_{0.2}$O$_{3-\delta}$ oxides. *J. Membr. Sci.* **2011**, *376*, 78–82. [CrossRef]
58. Babakhani, E.G.; Towfighi, J.; Shirazi, L.; Nakhaeipour, A.; Zamaniyan, A.; Shafiei, Z. Structure Stability and Oxygen Permeability of Perovskite-type Oxides of Ba$_{0.5}$Sr$_{0.5}$Co$_{0.8}$Fe$_{0.1}$R$_{0.1}$O$_{3-\delta}$ (R = Al, Mn, Fe, Ce, Cr, Ni, Co). *J. Mater. Sci. Technol.* **2012**, *28*, 177–183. [CrossRef]
59. Niedrig, C.; Taufall, S.; Burriel, M.; Menesklou, W.; Wagner, S.F.; Baumann, S.; Ivers-Tiffée, E. Thermal stability of the cubic phase in Ba$_{0.5}$Sr$_{0.5}$Co$_{0.8}$Fe$_{0.2}$O$_{3-\delta}$ (BSCF)1. *Solid State Ion.* **2011**, *197*, 25–31. [CrossRef]
60. Stevenson, J.W.; Armstrong, I.; Carneim, R.D.; Pederson, L.I.; Weber, W.J. Electrochemical Properties of Mixed Conducting Perovskites La$_{1-x}$MxCo$_{1-y}$FeyO$_{3-\delta}$ (M = Sr,Ba,Ca). *J. Electrochem. Soc.* **1996**, *143*, 2722–2729. [CrossRef]
61. Li, S.; Jin, W.; Huang, P.; Xu, N.; Shi, J.; Hu, M.Z.; Payzant, E.A. Comparison of Oxygen Permeability and Stability of Perovskite Type La$_{0.2}$A$_{0.8}$Co$_{0.2}$Fe$_{0.8}$O$_{3-\delta}$ (A = Sr,Ba,Ca) Membranes. *Solid State Ion.* **1999**, *38*, 2963–2972. [CrossRef]
62. Li, X.; Kerstiens, T.; Markus, T. Oxygen permeability and phase stability of Ba$_{0.5}$Sr$_{0.5}$Co$_{0.8}$Fe$_{0.2}$O$_{3-\delta}$ perovskite at at intermediate temperatures. *J. Membr. Sci.* **2013**, *438*, 83–89. [CrossRef]
63. Baumann, S.; Serra, J.M.; Lobera, M.P.; Escolástico, S.; Schulze-küppers, F.; Meulenberg, W.A. Ultrahigh oxygen permeation flux through supported Ba$_{0.5}$Sr$_{0.5}$Co$_{0.8}$Fe$_{0.2}$O$_{3-\delta}$ membranes. *J. Membr. Sci.* **2011**, *377*, 198–205. [CrossRef]
64. Shubnikova, E.V.; Bragina, O.A.; Nemudry, A.P. Mixed conducting molybdenum doped BSCF materials. *J. Ind. Eng. Chem.* **2018**, *59*, 242–250. [CrossRef]
65. Zhang, X.; Motuzas, J.; Liu, S.; da Costa, J.C.D. Zinc-doped BSCF perovskite membranes for oxygen separation. *Sep. Purif. Technol.* **2017**, *189*, 399–404. [CrossRef]
66. Fan, C.-G.; Huang, X.-X.; Liu, W.; Chen, C.-S. Preparation and Oxygen Permeation for SrCo$_{0.8}$Fe$_{0.2}$O$_{3-\delta}$ Tubular Asymmetric Membrane. *J. Inorg. Mater.* **2008**, *23*, 1221–1224. [CrossRef]
67. Shao, X.; Wang, Z.; Xu, S.; Xie, K.; Hu, X.; Dong, D.; Parkinson, G.; Li, C. Microchannel structure of ceramic membranes for oxygen separation. *J. Eur. Ceram. Soc.* **2016**, *36*, 3193–3199. [CrossRef]
68. Mazanec, T.J.; Cable, T.L.; Frye, J.G. Electrocatalytic cells for chemical reaction. *Solid State Ion.* **1992**, *56*, 111–118. [CrossRef]
69. Chen, C.S.; Boukamp, B.A.; Bouwmeester, H.J.M.; Cao, G.Z.; Kruidhof, H.; Winnubst, A.J.A.; Burggraaf, A.J. Microstructural development, electrical properties and oxygen permeation of zirconia-palladium composites. *Solis State Ion.* **1995**, *76*, 23–28. [CrossRef]
70. Kim, J.; Lin, Y.S. Synthesis and oxygen permeation properties of ceramic-metal dual-phase membranes. *J. Membr. Sci.* **2000**, *167*, 123–133. [CrossRef]
71. Kim, J.; Lin, Y.S. Synthesis and oxygen-permeation properties of thin YSZ/Pd composite membranes. *AIChE J.* **2000**, *46*, 1521–1529. [CrossRef]
72. He, W.; Huang, H.; Gao, J.; Winnubst, L.; Chen, C. Phase-inversion tape casting and oxygen permeation properties of supported ceramic membranes. *J. Membr. Sci.* **2014**, *452*, 294–299. [CrossRef]
73. Han, D.; Sunarso, J.; Tan, X.; Yan, Z.; Liu, L.; Liu, S. Optimizing Oxygen Transport Through La$_{0.6}$Sr$_{0.4}$Co$_{0.2}$Fe$_{0.8}$O$_{3-\delta}$ Hollow Fiber by Microstructure Modification and Ag/Pt Catalyst Deposition. *Energy Fuels* **2012**, *26*, 4728–4734. [CrossRef]
74. Schulze-Küppers, F.; Baumann, S.; Meulenberg, W.A.; Stöver, D.; Buchkremer, H.-P. Manufacturing and performance of advanced supported Ba$_{0.5}$Sr$_{0.5}$Co$_{0.8}$Fe$_{0.2}$O$_{3-\delta}$ (BSCF) oxygen transport membranes. *J. Membr. Sci.* **2013**, *433*, 121–125. [CrossRef]
75. Chena, C.S.; Kruidhof, H.; Verweij, H.; Burggraaf, A.J. Oxygen permeation through oxygen ion oxide-noble metal dual phase composites. *Solid State Ion.* **1996**, *88*, 569–572. [CrossRef]
76. Wu, K.; Xie, S.; Jiang, G.S.; Liu, W.; Chen, C.S. Oxygen permeation through (Bi$_2$O$_3$)$_{0.74}$(SrO)$_{0.26}$-Ag (40%v/o) composite. *J. Membr. Sci.* **2001**, *188*, 189–193. [CrossRef]
77. Capoen, E.; Steil, M.; Nowogrocki, G.; Malys, M.; Pirovano, C.; Lofberg, a.; Bordesrichard, E.; Boivin, J.; Mairesse, G.; Vannier, R. Oxygen permeation in bismuth-based materials. Part I: Sintering and oxygen permeation fluxes. *Solid State Ion.* **2006**, *177*, 483–488. [CrossRef]

78. Balager, M.; Garcia-Fayos, J.; Solis, C.; Serra, J.M. Fast Oxygen Separation Through SO_2- and CO_2-Stable Dual-Phase Membrane Membrane Based on $NiFe_2O_4$–$Ce_{0.8}Tb_{0.2}O_{2-\delta}$. *Chem. Mater.* **2013**, *25*, 4986–4993. [CrossRef]
79. Shaula, A.L.; Kharton, V.V.; Marques, F.M.B.; Kovalevsky, A.V.; Viskup, A.P.; Naumovich, E.N. Oxygen permeability of mixed-conducting composite membranes: Effects of phase interaction. *J. Solid State Electrochem.* **2005**, *10*, 28–40. [CrossRef]
80. Lide, D.R. (Ed.) *CRC Handbook of Chemistry and Physics*; CRC: Boca Raton, FL, USA, 2005.
81. Luo, H.; Jiang, H.; Klande, T.; Cao, Z.; Liang, F.; Wang, H.; Caro, J. Novel Cobalt-Free, Noble Metal-Free Oxygen-Permeable $40Pr_{0.6}Sr_{0.4}FeO_{3-\delta}$-$60Ce_{0.9}Pr_{0.1}O_{2-\delta}$ Dual-phase Membrane. *Cem. Mater.* **2012**, *24*, 2148–2154. [CrossRef]
82. Wang, Z.; Sun, W.; Zhu, Z.; Liu, T.; Liu, W. A novel cobalt-free, CO_2-stable, and reduction-tolerant dual-phase oxygen-permeable membrane. *Appl. Mater. Interfaces* **2013**, *5*, 11038–11043. [CrossRef] [PubMed]
83. Chen, T.; Zhao, H.; Xu, N.; Li, Y.; Lu, X.; Ding, W.; Li, F. Synthesis and oxygen permeation properties of a $Ce_{0.8}Sm_{0.2}O_{2-\delta}$-$LaBaCo_2O_{5+\delta}$ dual-phase composite membrane. *J. Membr. Sci.* **2011**, *370*, 158–165. [CrossRef]
84. Kharton, V.V.; Kovalensky, A.V.; Viskup, A.P.; Figueiredo, F.M.; Yaremchenko, A.A.; Naumovich, E.N. Oxygen permeability and Faradaic efficiency of $Ce_{0.8}Gd_{0.2}O_{2-d}$-$La_{0.7}Sr_{0.3}MnO_{3-d}$ composite. *J. Am. Chem. Soc.* **2001**, *21*, 1763–1767.
85. Shao, X.; Dong, D.; Parkinson, G.; Li, C.-Z. Improvement of oxygen permeation through microchanneled ceramic membranes. *J. Membr. Sci.* **2014**, *454*, 444–450. [CrossRef]
86. Xue, J.; Liao, Q.; Wei, Y.; Li, Z.; Wang, H. A CO_2-tolerance oxygen permeable $60Ce_{0.9}Gd_{0.1}O_{2-\delta}$-$40Ba_{0.5}Sr_{0.5}Co_{0.8}Fe_{0.2}O_{3-\delta}$ dual phase membrane. *J. Membr. Sci.* **2013**, *443*, 124–130. [CrossRef]
87. Joong, K.; Marina, O.A. Highly stable dual-phase $Y_{0.8}Ca_{0.2}Cr_{0.8}Co_{0.2}O_3$-$Sm_{0.2}Ce_{0.8}O_{1.9}$ ceramiccomposite membrane for oxygen separation. *J. Membr. Sci.* **2016**, *499*, 301–306. [CrossRef]
88. Adler, S.B. Chemical Expansivity of Electrochemical Ceramics. *J. Am. Ceram. Soc.* **2001**, *19*, 2117–2119. [CrossRef]
89. Marrocchelli, D.; Bishop, S.R.; Tuller, H.L.; Yildiz, B. Understanding Chemical Expansion in Non-Stoichiometric Oxides: Ceria and Zirconia Case Studies. *Adv. Funct. Mater.* **2012**, *22*, 1958–1965. [CrossRef]
90. Omar, S.; Nino, J.C. Consistency in the chemical expansion of fluorites: A thermal revision of the doped ceria. *Acta Mater.* **2013**, *61*, 5406–5413. [CrossRef]
91. Bishop, S.R.; Duncan, K.L.; Wachsman, E.D. Surface and bulk oxygen non-stoichiometry and bulk chemical expansion in gadolinium-doped cerium oxide. *Acta Mater.* **2009**, *57*, 3596–3605. [CrossRef]
92. Yaremchenko, A.A.; Mikhalev, S.M.; Kravchenko, E.S.; Frade, J.R. Thermochemical expansion of mixed-conducting $(Ba,Sr)Co_{0.8}Fe_{0.2}O_{3-\delta}$ ceramics. *J. Eur. Ceram. Soc.* **2014**, *34*, 703–715. [CrossRef]
93. Mcintosh, S.; Vente, J.F.; Haije, W.G.; Blank, D.H.A.; Bouwmeester, H.J.M. Phase stability and oxygen non-stoichiometry of $SrCo_{0.8}Fe_{0.2}O_{3-\delta}$ measured by in situ neutron diffraction. *Solis State Ion.* **2006**, *177*, 833–842. [CrossRef]
94. Kharton, V.V.; Viskup, A.P.; Kovalevsky, A.V.; Jurado, J.R.; Naumovich, E.N.; Vecher, A.A.; Frade, J.R. Oxygen ionic conductivity of Ti-containing strontium ferrite. *Solis State Ion.* **2000**, *133*, 57–65. [CrossRef]
95. Wang, H.; Tablet, C.; Feldhoff, A.; Caro, J. Investigation of phase structure, sintering, and permeability of perovskite-type $Ba_{0.5}Sr_{0.5}Co_{0.8}Fe_{0.2}O_{3-\delta}$ membranes. *J. Membr. Sci.* **2005**, *262*, 20–26. [CrossRef]
96. Choi, M.-B.; Jeon, S.-Y.; Im, H.-N.; Wachsman, E.D.; Song, S.-J. Oxygen Exchange Kinetics and Ionic Conductivity from Chemical Expansion Relaxation of Mixed Conducting $Ba_{0.5}Sr_{0.5}Co_{0.8}Fe_{0.2}O_{3-\delta}$. *J. Electrochem. Soc.* **2012**, *159*, 23–28. [CrossRef]
97. Bishop, S.R.; Duncan, K.L.; Wachsman, E.D. Thermo-Chemical Expansion in Strontium-Doped Lanthanum Cobalt Iron Oxide. *J. Am. Ceram. Soc.* **2010**, *93*, 4115–4121. [CrossRef]
98. Cheng, J.; Zhang, S.; Meng, B.; Ding, J.; Tan, X. Preparation and the superior oxygen permeability of a new CO_2-resistant Ruddlesden–Popper composite oxide $Pr_2Ni_{0.9}Mo_{0.1}O_{4+\delta}$. *J. Alloy. Compd.* **2018**, *742*, 966–976. [CrossRef]
99. Švarcová, S.; Wiik, K.; Tolchard, J.; Bouwmeester, H.J.M.; Grande, T. Structural instability of cubic perovskite $BaxSr_{1-x}Co_{1-y}FeyO_{3-\delta}$. *Solid State Ion.* **2008**, *178*, 1787–1791. [CrossRef]

100. Pei, S.; Kleefisch, M.S.; Kobylinski, T.P.; Faber, J.; Udovich, C.A.; Zhang-McCoy, V.; Dabrowski, B.; Balachandran, U.; Mieville, R.L.; Poeppel, R.B. Failure mechanisms of ceramic membrane reactors in partial oxidation of methane to synthesis gas. *Catal. Lett.* **1995**, *30*, 201–212. [CrossRef]
101. Balachandran, U.; Dusek, J.T.; Maiya, P.S.; Ma, B.; Mieville, R.L.; Kleefisch, M.S.; Udovich, C.A. Ceramic membrane reactor for converting methane to syngas. *Catal. Today* **1997**, *36*, 265–272. [CrossRef]
102. Prado, F.; Grunbaum, N.; Caneiro, A.; Manthiram, A. Effect of La3+doping on the perovskite-to-brownmillerite transformation in $Sr_{1-x}LaxCo_{0.8}Fe_{0.2}O_{3-\delta}$($0 \leq x \leq 0.4$). *Solid State Ion.* **2004**, *167*, 147–154. [CrossRef]
103. Yang, W.; Wang, H.; Zhu, X.; Lin, L. Development and application of oxygen permeable membrane in selective oxidation of light alkanes. *Top. Catal.* **2005**, *35*, 155–167. [CrossRef]
104. Arikawa, H.; Yamada, T.; Ishihara, T.; Nishiguchi, H.; Takita, Y. Mixed Electronic-Oxide Ionic Conductivity and Oxygen Permeating Property in Ni Doped $LaGaO_3$ Perovskite Oxide. *Chem. Lett.* **1999**, *135*, 1257–1258. [CrossRef]
105. Fang, S.M.; Yoo, C.; Bouwmeester, H.J.M. Performance and stability of niobium-substituted $Ba_{0.5}Sr_{0.5}Co_{0.8}Fe_{0.2}O_{3-\delta}$ membranes. *Solid State Ion.* **2011**, *195*, 1–6. [CrossRef]
106. Meng, X.; Yang, N.; Meng, B.; Tan, X.; Ma, Z.-F.; Liu, S. Zirconium stabilized $Ba_{0.5}Sr_{0.5}(Co_{0.8-x}Zr_x)Fe_{0.2}O_{3-\alpha}$ perovskite hollow fibre membranes for oxygen separation. *Ceram. Int.* **2011**, *37*, 2701–2709. [CrossRef]
107. Qiu, L.; Lee, T.H.; Liu, L.; Yang, Y.L.; Jacobson, A.J. Oxygen permeation studies of $SrCo_{0.8}Fe_{0.2}O_{3-\delta}$. *Solid State Ion.* **1995**, *76*, 321–329. [CrossRef]
108. Takeda, Y.; Kanno, K.; Takada, T.; Takano, M.; Nakayama, N. Phase Relation in the Oxygen Nonstoichiometric System, SrFeOx ($2.5 < x < 3.0$). *J. Solid State Chem.* **1986**, *249*, 237–249.
109. Shao, Z.; Yang, W.; Cong, Y.; Dong, H.; Tong, J.; Xiong, G. Investigation of the permeation behavior and stability of a $Ba_{0.5}Sr_{0.5}Co_{0.8}Fe_{0.2}O_{(3-\delta)}$ oxygen membrane. *J. Membr. Sci.* **2000**, *172*, 177–188. [CrossRef]
110. Shao, Z.; Xiong, G.; Dong, H.; Yang, W.; Lin, L. Synthesis, oxygen permeation study and membrane performance of a $Ba_{0.5}Sr_{0.5}Co_{0.8}Fe_{0.2}O_{3-\delta}$ oxygen-permeable dense ceramic reactor for partial oxidation of methane to syngas. *Sep. Purif. Technol.* **2001**, *25*, 97–116. [CrossRef]
111. Unger, L.S.; Ruhl, R.; Meffert, M.; Niedrig, C.; Menesklou, W.; Wagner, S.F.; Gerthsen, D.; Bouwmeester, H.J.M.; Ivers-Tiffée, E. Yttrium doping of $Ba_{0.5}Sr_{0.5}Co_{0.8}Fe_{0.2}O_{3-\delta}$ part II: Influence on oxygen transport and phase stability. *J. Eur. Ceram. Soc.* **2018**, *38*, 2388–2395. [CrossRef]
112. Ravkina, O.; Klande, T.; Feldhoff, A. Investigation of Zr-doped BSCF perovskite membrane for oxygen separation in the intermediate temperature range. *J. Solid State Chem.* **2013**, *201*, 101–106. [CrossRef]
113. Ravkina, O.; Yaremchenko, A.; Feldhoff, A. Phase separation in BSCF perovskite under elevated oxygen pressures ranging from 1 to 50 bar. *J. Membr. Sci.* **2016**, *520*, 76–88. [CrossRef]
114. Liang, F.; Partovi, K.; Jiang, H.; Luo, H.; Caro, J. B-site La-doped $BaFe_{0.95-x}LaxZr_{0.05}O_{3-\delta}$ perovskite-type membranes for oxygen separation. *J. Mater. Chem. A* **2013**, *1*, 746–751. [CrossRef]
115. Tan, X.; Shi, L.; Hao, G.; Meng, B.; Liu, S. $La_{0.7}Sr_{0.3}FeO_{3-\alpha}$ perovskite hollow fiber membranes for oxygen permeation and methane conversion. *Sep. Purif. Technol.* **2012**, *96*, 89–97. [CrossRef]
116. Lein, H.L.; Wiik, K.; Grande, T. Kinetic demixing and decomposition of oxygen permeable membranes. *Solid State Ion.* **2006**, *177*, 1587–1590. [CrossRef]
117. Zhu, X.; Yang, W. *Mixed Conducting Ceramic Membranes, Green Chemistry and Sustainable Technology*; Springer: Berlin/Heidelberg, Germany, 2017. [CrossRef]
118. Kharton, V.V. *Handbook of Solid Fuel State Electrochemistry: Fundamentals, Methodologies, Applications*; Wiley-VCH: Wernheim, Germany, 2009.
119. Chi, X.; Zhang, J.; Wen, Z.; Liu, Y. Modified Pechini Synthesis of Proton-Conducting $Ba(Ce,Ti)O_3$ and Comparative Studies of the Effects of Acceptors on its Structure, Stability, Sinterability, and Conductivity. *J. Am. Ceram. Soc.* **2014**, *1109*, 1103–1109. [CrossRef]
120. Zhu, Z.; Sun, W.; Yan, L.; Liu, W.; Liu, W. Synthesis and hydrogen permeation of Ni-$Ba(Zr_{0.1}Ce_{0.7}Y_{0.2})O_{3-\delta}$ metal e ceramic asymmetric membranes. *Int. J. Hydrog. Energy* **2011**, *36*, 6337–6342. [CrossRef]
121. Kathiraser, Y.; Wang, Z.; Yang, N.-T.; Zahid, S.; Kawi, S. Oxygen permeation and stability study of $La_{0.6}Sr_{0.4}Co_{0.8}Ga_{0.2}O_{3-\delta}$ (LSCG) hollow fiber membrane with exposure to CO_2, CH_4 and He. *J. Membr. Sci.* **2013**, *427*, 240–249. [CrossRef]
122. Jaiswal, S.K.; Kumar, J. A novel series of $Ba_{0.5}Sr_{0.5}Al_{0.2-x}MgxFe_{0.8}O_{3-\xi}$ ($x \leq 0.2$) membranes for oxygen permeation application. *J. Eur. Ceram. Soc.* **2014**, *34*, 381–390. [CrossRef]

123. Cheng, H.; Luo, L.; Yao, W.; Lu, X.; Zou, X.; Zhou, Z. Novel cobalt-free CO_2-tolerant dual-phase membranes of $Ce_{0.8}Sm_{0.2}O_{2-\delta}$-$Ba_{0.95}La_{0.05}Fe_{1-x}ZrxO_{3-\delta}$ for oxygen separation. *J. Membr. Sci.* **2015**, *492*, 220–229. [CrossRef]
124. Arnold, M.; Wang, H.; Feldhoff, A. Influence of CO_2 on the oxygen permeation performance and the microstructure of perovskite-type $(Ba_{0.5}Sr_{0.5})(Co_{0.8}Fe_{0.2})O_{3-\delta}$ membranes. *J. Membr. Sci.* **2007**, *293*, 44–52. [CrossRef]
125. Efimov, K.; Klande, T.; Juditzki, N.; Feldhoff, A. Ca-containing CO_2-tolerant perovskite materials for oxygen separation. *J. Membr. Sci.* **2012**, *389*, 205–215. [CrossRef]
126. Li, K.; Zhao, H.; Lu, Y.; Ma, Y.; Du, Z.; Zhang, Z. High CO_2 tolerance oxygen permeation membranes $BaFe_{0.95-x}Ca_{0.05}TixO_{3-\delta}$. *J. Membr. Sci.* **2018**, *550*, 302–312. [CrossRef]
127. Waindich, A.; Möbius, A.; Müller, M. Corrosion of $Ba_{1-x}SrxCo_{1-y}FeyO_{3-\delta}$ and $La_{0.3}Ba_{0.7}Co_{0.2}Fe_{0.8}O_{3-\delta}$ materials for oxygen separating membranes under Oxycoal conditions. *J. Membr. Sci.* **2009**, *337*, 182–187. [CrossRef]
128. Zeng, Q.; Zuo, Y.B.; Fan, C.G.; Chen, C.S. CO_2-tolerant oxygen separation membranes targeting CO_2 capture application. *J. Membr. Sci.* **2009**, *335*, 140–144. [CrossRef]
129. Yi, J.; Schroeder, M.; Weirich, T.; Mayer, J. Behavior of $Ba(Co,Fe,Nb)O_{3-\delta}$ Perovskite in CO_2-Containing Atmospheres: Degradation Mechanism and Materials Design. *Chem. Mater.* **2010**, 6246–6253. [CrossRef]
130. Wang, Z.; Kathiraser, Y.; Kawi, S. High performance oxygen permeable membranes with Nb-doped $BaBi_{0.05}Co_{0.95}O_{3-\delta}$ perovskite oxides. *J. Membr. Sci.* **2013**, *431*, 180–186. [CrossRef]
131. Chen, W.; Chen, C.; Winnubst, L. Ta-doped $SrCo_{0.8}Fe_{0.2}O_{3-\delta}$ membranes: Phase stability and oxygen permeation in CO_2 atmosphere. *Solid State Ion.* **2011**, *196*, 30–33. [CrossRef]
132. Yi, J.; Weirich, T.E.; Schroeder, M. CO_2 corrosion and recovery of perovskite-type BaCo1-x-yFexNbyO$_{3-\delta}$ membranes. *J. Membr. Sci.* **2013**, *437*, 49–56. [CrossRef]
133. Popov, M.P.; Bychkov, S.F.; Nemudry, A.P. Modification of mixed conducting $Ba_{0.5}Sr_{0.5}Co_{0.8}Fe_{0.2}$O3–δ by partial substitution of cobalt with tungsten. *Russ. J. Electrochem.* **2016**, *52*, 648–654. [CrossRef]
134. Kharton, V.V.; Viskup, A.P.; Naumovich, E.N.; Lapchuk, N.M. Mixed electronic and ionic conductivity of $LaCo(M)O_3$ (M = Ga, Cr, Fe or Ni). I. Oxygen transport in perovskites $LaCoO_3$-$LaGaO_3$. *Solid State Ion.* **1997**, *104*, 67–78. [CrossRef]
135. Carolan, M.F.; Dyer, P.N.; LaBar, J.M., Sr.; Thorogood, R.M. Process for Restoring Permeance of an Oxygen-Permeable on Transport Membrane Utilized to Recover Oxygen Froman Oxygen-Contaning Gaseous mixture. Patent Application CA002104821A, August 1993.
136. Yi, J.; Feng, S.; Zuo, Y.; Liu, W.; Chen, C. Oxygen permeability and stability of $Sr_{0.95}Co_{0.8}Fe_{0.2}O_{3-\delta}$ in a CO_2-and H_2O-containing atmosphere. *Chem. Mater.* **2005**, *17*, 5856–5861. [CrossRef]
137. Wang, H.; Kölsch, P.; Schiestel, T.; Tablet, C.; Werth, S.; Caro, J. Production of high-purity oxygen by perovskite hollow fiber membranes swept with steam. *J. Membr. Sci.* **2006**, *284*, 5–8. [CrossRef]
138. Cheng, S.; Søgaard, M.; Han, L.; Zhang, W.; Chen, M.; Kaiser, A.; Hendriksen, P.V. A novel CO_2- and SO_2-tolerant dual phase composite membrane for oxygen separation. *Chem. Commun.* **2015**, *51*, 7140–7143. [CrossRef] [PubMed]
139. Khatib, S.J.; Yun, S.; Oyama, S.T. Sulfur resistant Pd and Pd alloy membranes by phosphidation. *J. Membr. Sci.* **2014**, *455*, 283–293. [CrossRef]
140. Gao, J.; Li, L.; Yin, Z.; Zhang, J.; Lu, S.; Tan, X. Poisoning effect of SO_2 on the oxygen permeation behavior of La0.6Sr0.4Co0.2Fe0.8$O_{3-\delta}$ perovskite hollow fiber membranes. *J. Membr. Sci.* **2014**, *455*, 341–348. [CrossRef]
141. Alqaheem, Y.; Thurs, A.; Zhang, G.; Metcalfe, I.S. The impact of sulfur contamination on the performance of $La_{0.6}Sr_{0.4}Co_{0.2}Fe_{0.8}O_{3-\delta}$ oxygen transport membranes. *Solid State Ion.* **2014**, *262*, 262–265. [CrossRef]
142. Wei, Y.; Ravkina, O.; Klande, T.; Wang, H.; Feldhoff, A. Effect of CO_2 and SO_2 on oxygen permeation and microstructure of $(Pr_{0.9}La_{0.1})_2(Ni_{0.74}Cu_{0.21}Ga_{0.05})O_{4+\delta}$ membranes. *J. Membr. Sci.* **2013**, *429*, 147–154. [CrossRef]
143. Wei, Y.; Liao, Q.; Xue, J.; Li, Z.; Wang, H. Influence of SO_2 on the phase structure, oxygen permeation and microstructure of K2NiF4-type hollow fiber membranes. *Chem. Eng. J.* **2013**, *217*, 34–40. [CrossRef]
144. Garcia-Fayos, J.; Balaguer, M.; Baumann, S.; Serra, J.M. Dual-phase membrane based on $LaCo_{0.2}Ni_{0.4}Fe_{0.4}O_{3-x}$-$Ce_{0.8}Gd_{0.2}O_{2-x}$ composition for oxygen permeation under CO_2/SO_2-rich gas environments. *J. Membr. Sci.* **2018**, *548*, 117–124. [CrossRef]

145. Wu, C.; Zhou, J.; Tang, X.; Luo, W.; Zhang, Y.; Ding, W.; Sun, C. The migration behavior of sulfur impurity contained in the dual-phase membrane of $Ce_{0.9}Gd_{0.1}O_{2-\delta}$-$SrCo_{0.8}Fe_{0.1}Nb_{0.1}O_{3-\delta}$ under CO_2 atmosphere. *J. Membr. Sci.* **2016**, *511*, 162–169. [CrossRef]
146. Diethelm, S.; Van, J.; Sfeir, J.; Buffat, P. Correlation between oxygen transport properties and microstructure in $La_{0.5}Sr_{0.5}FeO_{3-\delta}$. *J. Eur. Ceram. Soc.* **2005**, *25*, 2191–2196. [CrossRef]
147. Martynczuk, J.; Arnold, M.; Feldhoff, A. Influence of grain size on the oxygen permeation performance of perovskite-type $(Ba_{0.5}Sr_{0.5})(Fe_{0.8}Zn_{0.2})O_{3-\delta}$ membranes. *J. Membr. Sci.* **2008**, *322*, 375–382. [CrossRef]
148. Li, Q.; Zhu, X.; He, Y.; Cong, Y.; Yang, W. Effects of sintering temperature on properties of dual-phase oxygen permeable membranes. *J. Membr. Sci.* **2011**, *367*, 134–140. [CrossRef]
149. Wagner, C. Diffusion and high temperature oxidation of metals. *At. Mov.* **1951**, *194–199*, 153–173.
150. Phair, J.W.; Badwal, S.P.S.Ã. Materials for separation membranes in hydrogen and oxygen production and future power generation. *Sci. Technol. Adv. Mater.* **2006**, *7*, 792–805. [CrossRef]
151. Pinacci, P.; Louradour, E.; Wimbert, L.; Gindrat, M.; Jarligo, M.O.; Vassen, R.; Comite, a.; Serra, J.M.; Jewulski, J.; Mancuso, L.; Chiesa, P.; et al. Dense Membranes for Oxygen and Hydrogen Separation (DEMOYS): Project Overview and First Results. *Energy Procedia* **2013**, *37*, 1030–1038. [CrossRef]
152. Buchler, O.; Serra, J.; Meulenberg, W.; Sebold, D.; Buchkremer, H. Preparation and properties of thin $La_{1-x}Sr_xCo_{1-y}FeyO_{3-\delta}$ perovskitic membranes supported on tailored ceramic substrates. *Solid State Ion.* **2007**, *178*, 91–99. [CrossRef]
153. Bouchara, A.; Grosso, D.; Durand, D.; Sanchez, C. Controlled formation of highly ordered cubic and hexagonal mesoporous nanocrystalline yttria–zirconia and ceria–zirconia thin films exhibiting high thermal stability. *Angew. Chem.* **2003**, *42*, 347–351.
154. Corma, A.; Atienzar, P.; García, H.; Chane-Ching, J.-Y. Hierarchically mesostructured doped CeO_2 with potential for solar-cell use. *Nat. Mater.* **2004**, *3*, 394–397. [CrossRef] [PubMed]
155. Serra, J.M.; Uhlenbruck, S.; Meulenberg, W.A.; Buchkremer, H.P.; Sto, D. Nano-structuring of solid oxide fuel cells cathodes. *Top. Catal.* **2006**, *40*, 123–131. [CrossRef]
156. Gurauskis, J.; Lohne, Ø.F.; Wiik, K. $La_{0.2}Sr_{0.8}Fe_{0.8}Ta_{0.2}O_{3-\delta}$ based thin film membranes with surface modification for oxygen production. *Solid State Ion.* **2012**, *225*, 703–706. [CrossRef]
157. Cheng, S.; Huang, H.; Ovtar, S.; Simonsen, S.B.; Chen, M.; Zhang, W.; Søgaard, M.; Kaiser, A.; Hendriksen, P.V.; Chen, C. High-Performance Microchanneled Asymmetric $Gd_{0.1}Ce_{0.9}O_{1.95-\delta}$-$La_{0.6}Sr_{0.4}FeO_{3-\delta}$-Based Membranes for Oxygen Separation. *Appl. Mater. Interfaces* **2016**, *3*, 4548–4560. [CrossRef] [PubMed]
158. Kim, J.P.; Park, J.H.; Magnole, E.; Lee, Y. Significant improvement of the oxygen permeation flux of tubular $Ba_{0.5}Sr_{0.5}Co_{0.8}Fe_{0.2}O_{3-\delta}$ membranes covered by a thin $La_{0.6}Sr_{0.4}Ti_{0.3}Fe_{0.7}O_{3-\delta}$ layer. *Mater. Lett.* **2011**, *65*, 2168–2170. [CrossRef]
159. Zhu, X.; Liu, H.; Li, Q.; Cong, Y.; Yang, W. Unsteady-state permeation and surface exchange of dual-phase membranes. *Solid State Ion.* **2011**, *185*, 27–31. [CrossRef]
160. Hayamizu, Y.; Kato, M.; Takamura, H. Effects of surface modification on the oxygen permeation of $Ba_{0.5}Sr_{0.5}Co_{0.8}Fe_{0.2}O_{3-\delta}$ membrane. *J. Membr. Sci.* **2014**, *462*, 147–152. [CrossRef]
161. Serra, J.M.; Meulenberg, W.A. Thin-Film Proton $BaZr_{0.85}Y_{0.15}O_3$ Conducting Electrolytes: Toward an Intermediate-Temperature Solid Oxide Fuel Cell Alternative. *J. Am. Ceram. Soc.* **2007**, *90*, 2082–2089. [CrossRef]
162. Jacobs, M.; Fontaine, M.; Bredesen, R.; Michielsen, B.; Middelkoop, V.; Larring, Y. Surface activation of asymmetric $CaTi_{1-x}FexO_{3-\delta}$ tubular membranes forfor oxygen separation. *J. Membr. Sci.* **2015**, *477*, 58–64. [CrossRef]
163. Liu, T.; Chen, Y.; Fang, S.; Lei, L.; Wang, Y.; Ren, C.; Chen, F. A dual-phase bilayer oxygen permeable membrane with hierarchically porous structure fabricated by freeze-drying tape-casting method. *J. Membr. Sci.* **2016**, *520*, 354–363. [CrossRef]
164. Zhang, K.; Zhang, C.; Zhao, L.; Meng, B.; Liu, J.; Liu, S. Enhanced Oxygen Permeation Behavior of $Ba_{0.5}Sr_{0.5}Co_{0.8}Fe_{0.2}O_{3-\delta}$ Membranes in a CO_2-Containing Atmosphere with a Sm0.2$Ce_{0.8}$O1.9 Functional Functional Shell. *Energy Fuels* **2016**, *30*, 1829–1834. [CrossRef]
165. Kasai, M.; Miyazawa, A.; Suzuki, T.M. Controlled Heating of Palladium Dispersed Porous Alumina Tube and Continuous Oxidation of Ethylene Using Frequency-Variable Single-Mode Microwave Reactor. *Ind. Eng. Chem. Res.* **2014**, *53*, 1073–1078. [CrossRef]

166. Hu, X.; Chen, W.; Huang, Y. Fabrication of Pd/ceramic membranes for hydrogen separation based on low-cost macroporous ceramics with pencil coating. *Int. J. Hydrog. Energy* **2010**, *35*, 7803–7808. [CrossRef]
167. Callister, W.D.; Wiley, J. Thermal Properties. In *Materials Science and Engineering*; John Wiley and Sons: Hoboken, NJ, USA, 2007; pp. 713–729.
168. Ovtar, S.; Gurauskis, J.; Haugen, A.B.; Chatzichristodoulou, C.; Kaiser, A.; Hendriksen, P.V. Oxygen transport properties of tubular $Ce_{0.9}Gd_{0.1}O_{1.95}$-$La_{0.6}Sr_{0.4}FeO_{3-d}$ composite asymmetric oxygen permeation membranes supported on magnesium oxide. *J. Membr. Sci.* **2017**, *523*, 576–587. [CrossRef]
169. Yin, X.; Hong, L.; Liu, Z. Development of oxygen transport membrane $La_{0.2}Sr_{0.8}CoO_{3-\delta}/Ce_{0.8}Gd_{0.2}O_{2-\delta}$ on the tubular CeO_2 support. *Appl. Catal. A Gen.* **2006**, *300*, 75–84. [CrossRef]
170. Fan, E.S.C.; Kesler, O. Deposition of Lanthanum Strontium Cobalt Ferrite (LSCF) Using Suspension Plasma Spraying for Oxygen Transport Membrane Applications. *J. Therm. Spray Technol.* **2015**, *24*, 1081–1092. [CrossRef]
171. Niu, S.; Zhou, K.; Xu, L.; Deng, C.; Liu, M.; Mao, J. A comparative study of $La_{0.6}Sr_{0.4}Co_{0.2}Fe_{0.8}O_{3-\delta}$ oxygen transport membranes deposited on porous metal supports prepared by supersonic air-gas plasma spraying (SAPS) and low pressure plasma spraying-physical vapor deposition (PS-PVD). *Surf. Coat. Technol.* **2016**, *307*, 963–970. [CrossRef]
172. Cao, Z.; Zhu, X.; Li, W.; Xu, B.; Yang, L.; Yang, W. Asymmetric dual-phase membranes prepared via tape-casting and co-lamination for oxygen permeation. *Mater. Lett.* **2015**, *147*, 88–91. [CrossRef]
173. Escribano, J.A.; García-fayos, J.; Serra, J.M. Shaping of 3YSZ porous substrates for oxygen separation membranes. *J. Eur. Ceram. Soc.* **2017**, *37*, 5223–5231. [CrossRef]
174. Zhang, Y.; Yuan, R.; He, Z.; Gao, J.; Chen, C. Phase inversion tape casting and oxygen permeation properties of composite membrane. *Solid State Ion.* **2016**, *288*, 342–346. [CrossRef]
175. Lemes, P.; Motuzas, J.; Machado, R.A.F.; Hotza, D.; Diniz, J.C. Influence of porous structures on O2 flux of BSCF asymmetric membranes. *Sep. Purif. Technol.* **2017**, *175*, 164–169. [CrossRef]
176. Li, Q.; Zhu, X.; Yang, W. Single-step fabrication of asymmetric dual-phase composite membranes for oxygen separation. *J. Membr. Sci.* **2008**, *325*, 11–15. [CrossRef]
177. Liu, Z.; Zhang, G.; Dong, X.; Jiang, W.; Jin, W.; Xu, N. Fabrication of asymmetric tubular mixed-conducting dense membranes by a combined spin-spraying and co-sintering process. *J. Membr. Sci.* **2012**, *415–416*, 313–319. [CrossRef]
178. Fontaine, M.; Smith, J.B.; Larring, Y.; Bredesen, R. On the preparation of asymmetric CaTi0.9Fe0.1$O_{3-\delta}$ membranes by tape-casting and co-sintering process. *J. Membr. Sci.* **2009**, *326*, 310–315. [CrossRef]
179. Yang, C.; Xu, Q.; Liu, C.; Liu, J.; Chen, C.; Liu, W. $Bi_{1.5}Y_{0.3}Sm_{0.2}O_3$-$La_{0.8}Sr_{0.2}MnO_{3-\delta}$ dual-phase composite hollow fiber membrane for oxygen separation. *Mater. Lett.* **2011**, *65*, 3365–3367. [CrossRef]
180. Chang, X.; Zhang, C.; Jin, W.; Xu, N. Match of thermal performances between the membrane and the support for supported dense mixed-conducting membranes. *J. Membr. Sci.* **2006**, *285*, 232–238. [CrossRef]
181. Jin, W.; Li, S.; Huang, P.; Xu, N.; Shi, J. Preparation of an asymmetric perovskite-type membrane and its oxygen permeability. *J. Membr. Sci.* **2001**, *185*, 237–243. [CrossRef]
182. Fang, W.; Gao, J.; Chen, C. $La_{0.8}Sr_{0.2}Cr_{0.5}Fe_{0.5}O_{3-d}$ (LSCF)-$Zr_{0.8}Y_{0.2}O_{2-d}$ (YSZ) based multilayer membrane for CO_2 decomposition. *Ceram. Int.* **2013**, *39*, 7269–7272. [CrossRef]
183. Fang, W.; Zhang, Y.; Gao, J.; Chen, C. Oxygen permeability of asymmetric membrane of functional $La_{0.8}Sr_{0.2}Cr_{0.5}Fe_{0.5}O_{3-\delta}$(LSCrF)-$Zr_{0.8}Y_{0.2}$O-δ(YSZ) supported on porousl porous YSZ. *Ceram. Int.* **2014**, *40*, 799–803. [CrossRef]
184. Yin, X.; Hong, L.; Liu, Z.L. Oxygen permeation through the LSCO-80/CeO_2 asymmetric tubular membrane reactor. *J. Membr. Sci.* **2006**, *268*, 2–12. [CrossRef]
185. Geffroy, P.M.; Bassat, J.M.; Vivet, A.; Fourcade, S.; Chartier, T.; del Gallo, P.; Richet, N. Oxygen semi-permeation, oxygen diffusion and surface exchange coefficient of La(1−x)SrxFe(1−y)Gay$O_{3-\delta}$ perovskite membranes. *J. Membr. Sci.* **2010**, *354*, 6–13. [CrossRef]
186. Trunec, M.; Cihlar, J.; Diethelm, S.; van Herle, J. Tubular $La_{0.7}Ca_{0.3}Fe_{0.8}5Co_{0.15}O_{3-\delta}$ perovskite membranes, Part I: Preparation and properties. *J. Am. Ceram. Soc.* **2006**, *89*, 949–954. [CrossRef]
187. Zhu, X.; Sun, S.; Cong, Y.; Yang, W. Operation of perovskite membrane under vacuum and elevated pressures for high-purity oxygen production. *J. Membr. Sci.* **2009**, *345*, 47–52. [CrossRef]

188. Salehi, M.; Pfaff, E.M.; Junior, R.M.; Bergmann, C.P.; Diethelm, S.; Neururer, C.; Graule, T.; Grobéty, B.; Clemens, F.J. $Ba_{0.5}Sr_{0.5}Co_{0.8}Fe_{0.2}O_{3-\delta}$ (BSCF) feedstock development and optimization for thermoplastic forming of thin planar and tubular oxygen separation membranes. *J. Membr. Sci.* **2013**, *443*, 237–245. [CrossRef]
189. Wu, Z.; Othman, N.H.; Zhang, G.; Liu, Z.; Jin, W.; Li, K. Effects of fabrication processes on oxygen permeation of Nb_2O_5-doped $SrCo_{0.8}Fe_{0.2}O_{3-\delta}$ micro-tubular membranes. *J. Membr. Sci.* **2013**, *442*, 1–7. [CrossRef]
190. Bi, X.; Meng, X.; Liu, P.; Yang, N.; Zhu, Z.; Ran, R.; Liu, S. A novel CO_2-resistant ceramic dual-phase hollow fiber membrane for oxygen separation. *J. Membr. Sci.* **2017**, *522*, 91–99. [CrossRef]
191. Tan, X.; Liu, Y.; Li, K. Preparation of LSCF Ceramic Hollow-Fiber Membranes for Oxygen Production by a Phase-Inversion/Sintering Technique. *Ind. Eng. Chem. Res.* **2005**, *44*, 61–66. [CrossRef]
192. Liu, H.; Tan, X.; Pang, Z.; da Costa, J.C.D.; Lu, G.Q.; Liu, S. Novel dual structured mixed conducting ceramic hollow fibre membranes. *Sep. Purif. Technol.* **2008**, *63*, 243–247. [CrossRef]
193. Huang, H.; Cheng, S.; Gao, J.; Chen, C.; Yi, J. Phase-inversion tape-casting preparation and significant performance enhancement of $Ce_{0.9}Gd_{0.1}O_{1.95}$-$La_{0.6}Sr_{0.4}Co_{0.2}Fe_{0.8}O_{3-\delta}$ dual-phase asymmetric membrane for oxygen separation. *Mater. Lett.* **2014**, *137*, 245–248. [CrossRef]
194. Shao, X.; Dong, D.; Parkinson, G.; Li, C.Z. Thin ceramic membrane with dendritic microchanneled sub structure and high oxygen permeation rate. *J. Membr. Sci.* **2017**, *541*, 653–660. [CrossRef]
195. Liu, T.; Zhao, W.; Wang, Y. Robust Freeze-Cast Bilayer Dual-Phase Oxygen Transport Membrane Targeting Chemical Reactor Application. *ACS Appl. Nano Mater.* **2018**, *1*, 3774–3778. [CrossRef]
196. Stansch, Z.; Mleczko, L.; Baerns, M. Comprehensive kinetics of oxidative coupling of methane over the La_2O_3/CaO catalyst. *Ind. Eng. Chem. Res.* **1997**, *36*, 2568–2579. [CrossRef]
197. Cruellas, A.; Melchiori, T.; Gallucci, F.; Annaland, M.v. Advanced reactor concepts for oxidative coupling of methane. *Catal. Rev.* **2018**, *59*, 234–294. [CrossRef]
198. Tan, X.; Pang, Z.; Gu, Z.; Liu, S. Catalytic perovskite hollow fibre membrane reactors for methane oxidative coupling. *J. Membr. Sci.* **2007**, *302*, 109–114. [CrossRef]
199. Lu, Y.; Dixon, A.G.; Moser, W.R.; Hua, Y.; Balachandran, U. Oxygen-permeable dense membrane reactor for the oxidative coupling of methane. *J. Membr. Sci.* **2000**, *170*, 27–34. [CrossRef]
200. Czuprat, O.; Schiestel, T.; Voss, H. Oxidative Coupling of Methane in a BCFZ Perovskite Hollow Fiber Membrane Reactor. *Ind. Eng. Chem. Res.* **2010**, *49*, 10230–10236. [CrossRef]
201. Wang, H.; Cong, Y.; Yang, W. Oxidative coupling of methane in $Ba_{0.5}Sr_{0.5}Co_{0.8}Fe_{0.2}O_{3-\delta}$ tubular membrane reactors. *Catal. Today* **2005**, *104*, 160–167. [CrossRef]
202. Olivier, L.; Haag, S.; Mirodatos, C.; van Veen, A.C. Oxidative coupling of methane using catalyst modified dense perovskite membrane reactors. *Catal. Today* **2009**, *142*, 34–41. [CrossRef]
203. Akin, F.T.; Lin, Y.S. Controlled Oxidative Coupling of Methane by Ionic Conducting Ceramic Membrane. *Catal. Lett.* **2002**, *78*, 239–242. [CrossRef]
204. Bhatia, S.; Thien, C.Y.; Mohamed, A.R. Oxidative coupling of methane (OCM) in a catalytic membrane reactor and comparison of its performance with other catalytic reactors. *Chem. Eng. J.* **2009**, *148*, 525–532. [CrossRef]
205. Othman, N.H.; Wu, Z.; Li, K. An oxygen permeable membrane microreactor with an in-situ deposited $Bi_{1.5}Y_{0.3}Sm_{0.2}O_{3-\delta}$ catalyst for oxidative coupling of methane. *J. Membr. Sci.* **2015**, *488*, 182–193. [CrossRef]
206. Santamaria, J.; Menéndez, M.; Pena, J.A.; Barahona, J.I. Methane oxidative coupling in fixed bed catalytic reactors with a distributed oxygen feed. A simulation study. *Catal. Today* **1992**, *13*, 353–360. [CrossRef]
207. Coronas, J.; Menéndez, M.; Santamaria, J. Methane oxidative coupling using porous ceramic membrane reactors–II. Reaction studies. *Chem. Eng. Sci.* **1994**, *49*, 2015–2025. [CrossRef]
208. Tiemersma, T.P.; Chaudhari, A.S.; Gallucci, F.; Kuipers, J.A.M.; Annaland, M.V. Integrated autothermal oxidative coupling and steam reforming of methane. Part 2: Development of a packed bed membrane reactor with a dual function catalyst. *Chem. Eng. Sci.* **2012**, *82*, 232–245. [CrossRef]
209. Haag, S.; van Veen, A.C.; Mirodatos, C. Influence of oxygen supply rates on performances of catalytic membrane reactors. *Catal. Today* **2007**, *127*, 157–164. [CrossRef]
210. York, A.P.E.; Xiao, T.; Green, M.L.H. Brief Overview of the Partial Oxidation of Methane to Synthesis Gas. *Top. Catal.* **2003**, *22*, 345–358. [CrossRef]
211. Babakhani, E.G.; Towfighi, J.; Taheri, Z.; Pour, A.N.; Zekordi, M.; Taheri, A. Partial oxidation of methane in $Ba_{0.5}Sr_{0.5}Co_{0.8}Fe_{0.1}Ni_{0.1}O_{3-\delta}$ ceramic membrane reactor. *J. Nat. Gas Chem.* **2012**, *21*, 519–525. [CrossRef]

212. Song, S.; Zhang, P.; Zhang, X.; Han, M. Partial oxidation of methane reaction in $Ba_{0.9}Co_{0.7}Fe_{0.2}Nb_{0.1}O_{3-\delta}$ oxygen permeation membrane with three-layer structure. *Int. J. Hydrog. Energy* **2015**, *40*, 10894–10901. [CrossRef]
213. Gong, Z.; Hong, L. Integration of air separation and partial oxidation of methane in the $L_{a0.4}Ba_{0.6}Fe_{0.8}Zn_{0.2}O_{3-\delta}$ membrane reactor. *J. Membr. Sci.* **2011**, *380*, 81–86. [CrossRef]
214. Song, S.; Zhang, P.; Han, M.; Singhal, S.C. Oxygen permeation and partial oxidation of methane reaction in $Ba_{0.9}Co_{0.7}Fe_{0.2}Nb_{0.1}O_{3-\delta}$ oxygen permeation membrane. *J. Membr. Sci.* **2012**, *415*, 654–662. [CrossRef]
215. Kathiraser, Y.; Kawi, S. $La_{0.6}Sr_{0.4}Co_{0.8}Ga_{0.2}O_{3-\delta}$ (LSCG) hollow fiber membrane reactor: Partial oxidation of methane at medium temperature. *AIChE J.* **2013**, *59*, 3874–3885. [CrossRef]
216. Meng, X.; Bi, X.; Meng, B.; Yang, N.; Tan, X.; Liu, L.; Liu, S. $H_2/CH_4/CO_2$-tolerant properties of $SrCo_{0.8}Fe_{0.1}Ga_{0.1}O_{3-\delta}$ hollow fiber membrane reactors for methane partial oxidation to syngas. *Fuel Process. Technol.* **2017**, *161*, 265–272. [CrossRef]
217. Wang, Z.; Ashok, J.; Pu, Z.; Kawi, S. Low temperature partial oxidation of methane via $BaBi_{0.05}Co_{0.8}Nb_{0.15}O_{3-\delta}$-Ni phyllosilicate catalytic hollow fiber membrane reactor. *Chem. Eng. J.* **2017**, *315*, 315–323. [CrossRef]
218. Liao, Q.; Chen, Y.; Wei, Y.; Zhou, L.; Wang, H. Performance of U-shaped $BaCo_{0.7}Fe_{0.2}Ta_{0.1}O_{3-\delta}$ hollow-fiber membranes reactor with high oxygen permeation for methane conversion. *Chem. Eng. J.* **2014**, *237*, 146–152. [CrossRef]
219. Wei, Y.; Liao, Q.; Li, Z.; Wang, H.; Feldhoff, A.; Caro, J. Partial oxidation of methane in hollow-fiber membrane reactors based on alkaline-earth metal-free CO_2-tolerant oxide. *AIChE J.* **2014**, *60*, 3587–3595. [CrossRef]
220. Zhu, J.; Guo, S.; Liu, G.; Liu, Z.; Zhang, Z.; Jin, W. A robust mixed-conducting multichannel hollow fiber membrane reactor. *AIChE J.* **2015**, *61*, 2592–2599. [CrossRef]
221. Yuan, R.; He, Z.; Zhang, Y.; Wang, W.; Chen, C.; Wu, H.; Zhan, Z. Partial Oxidation of Methane to Syngas in a Packed Bed Catalyst Membrane Reactor. *AIChE J.* **2016**, *62*, 2170–2176. [CrossRef]
222. Ruiz-Trejo, E.; Boldrin, P.; Medley-Hallam, J.L.; Darr, J.; Atkinson, A.; Brandon, N.P. Partial oxidation of methane using silver/gadolinia-doped ceria composite membranes. *Chem. Eng. Sci.* **2015**, *127*, 269–275. [CrossRef]
223. Jiang, W.; Zhang, G.; Liu, Z.; Zhang, K.; Jin, W. A novel porous-dense dual-layer composite membrane reactor with long-term stability. *AIChE J.* **2013**, *59*, 4355–4363. [CrossRef]
224. Balachandran, U.; Dusek, J.T.; Mieville, R.L.; Poeppel, R.B.; Kleefisch, M.S.; Pei, S.; Kobylinski, T.P.; Udovich, C.A.; Bose, A.C. Dense ceramic membranes for partial oxidation of methane to syngas. *Appl. Catal. A Gen.* **1995**, *133*, 19–29. [CrossRef]
225. Caro, J.; Schiestel, T.; Werth, S.; Wang, H.; Kleinert, A.; Kölsch, P. Perovskite hollow fibre membranes in the partial oxidation of methane to synthesis gas in a membrane reactor. *Desalination* **2006**, *199*, 415–417. [CrossRef]
226. Wei, Y.Y.; Huang, L.; Tang, J.; Zhou, L.Y.; Li, Z.; Wang, H.H. Syngas production in a novel perovskite membrane reactor with co-feed of CO_2. *Chin. Chem. Lett.* **2011**, *22*, 1492–1496. [CrossRef]
227. Jansen, L. Aristotle's theory of dispositions from the principle of movement to the unmoved mover, Debating Dispositions: Issues in Metaphysics. *Epistemol. Philos. Mind* **2009**, *202*, 24–46. [CrossRef]
228. Wang, H.; Cong, Y.; Yang, W. Continuous Oxygen Ion Transfer Medium as a Catalyst for High Selective Oxidative Dehydrogenation of Ethane. *Catal. Lett.* **2002**, *84*, 101–106. [CrossRef]
229. Wang, H.; Tablet, C.; Schiestel, T.; Caro, J. Hollow fiber membrane reactors for the oxidative activation of ethane. *Catal. Today* **2006**, *118*, 98–103. [CrossRef]
230. Rebeilleau-Dassonneville, M.; Rosini, S.; van Veen, A.C.; Farrusseng, D.; Mirodatos, C. Oxidative activation of ethane on catalytic modified dense ionic oxygen conducting membranes. *Catal. Today* **2005**, *104*, 131–137. [CrossRef]
231. Lobera, M.P.; Escolástico, S.; Garcia-Fayos, J.; Serra, J.M. Ethylene Production by ODHE in Catalytically Modified $Ba_{0.5}Sr_{0.5}Co_{0.8}Fe_{0.2}O_{3-\delta}$ Membrane Reactors. *ChemSusChem* **2012**, *5*, 1587–1596. [CrossRef] [PubMed]
232. Lobera, M.P.; Escolástico, S.; Serra, J.M. High Ethylene Production through Oxidative Dehydrogenation of Ethane Membrane Reactors Based on Fast Oxygen-Ion Conductors. *ChemCatChem* **2011**, *3*, 1503–1508. [CrossRef]

233. Wang, H.; Cong, Y.; Zhu, X.; Yang, W. Oxidative dehydrogenation of propane in a dense tubular membrane reactor. *React. Kinet. Catal. Lett.* **2003**, *79*, 351–356. [CrossRef]
234. Yan, R.; Liu, W.; Song, C. Oxidative Dehydrogenation of Alkanes using Oxygen-Permeable Membrane Reactor. *Chin. J. Chem. Phys.* **2014**, *27*, 690–696. [CrossRef]
235. Balachandran, U.; Lee, T.H.; Wang, S.; Dorris, S.E. Use of mixed conducting membranes to produce hydrogen by water dissociation. *Int. J. Hydrog. Energy* **2004**, *29*, 291–296. [CrossRef]
236. Li, W.; Cao, Z.; Zhu, X.; Yang, W. High-rate hydrogen separation using an MIEC oxygen permeable membrane reactor. *AIChE J.* **2017**, *63*, 1278–1286. [CrossRef]
237. Jiang, H.; Wang, H.; Werth, S.; Schiestel, T.; Caro, J. Simultaneous Production of Hydrogen and Synthesis Gas by Combining Water Splitting with Partial Oxidation of Methane in a Hollow-Fiber Membrane Reactor. *Angew. Chem. Int. Ed.* **2008**, *47*, 9341–9344. [CrossRef] [PubMed]
238. Fang, W.; Steinbach, F.; Cao, Z.; Zhu, X.; Feldhoff, A. A Highly Efficient Sandwich-Like Symmetrical Dual-Phase Oxygen-Transporting Membrane Reactor for Hydrogen Production by Water Splitting. *Angew. Chem. Int. Ed.* **2016**, *55*, 8648–8651. [CrossRef] [PubMed]
239. Cao, Z.; Jiang, H.; Luo, H.; Baumann, S.; Meulenberg, W.A.; Assmann, J.; Mleczko, L.; Liu, Y.; Caro, J. Natural Gas to Fuels and Chemicals: Improved Methane Aromatization in an Oxygen-Permeable Membrane Reactor. *Angew. Chem. Int. Ed.* **2013**, *52*, 13794–13797. [CrossRef] [PubMed]
240. di Felice, L.; Middelkoop, V.; Anzoletti, V.; Snijkers, F.; Annaland, M.v.; Gallucci, F. New high temperature sealing technique and permeability data for hollow fiber BSCF perovskite membranes. *Chem. Eng. Process. Process Intensif.* **2016**, *107*, 206–219. [CrossRef]
241. Qi, X.; Akin, F.T.; Lin, Y.S. Ceramic–glass composite high temperature seals for dense ionic-conducting ceramic membranes. *J. Membr. Sci.* **2001**, *193*, 185–193. [CrossRef]
242. Vivet, A.; Geffroy, P.M.; Coudert, V.; Fouletier, J.; Richet, N.; Chartier, T. Influence of glass and gold sealants materials on oxygen permeation performances in $La_{0.8}Sr_{0.2}Fe_{0.7}Ga_{0.3}O_{3-\delta}$ perovskite membranes. *J. Membr. Sci.* **2011**, *366*, 132–138. [CrossRef]
243. Chen, Y.; Qian, B.; Hao, Y.; Liu, S.; Tade, M.O.; Shao, Z. Influence of sealing materials on the oxygen permeation fluxes of some typical oxygen ion conducting ceramic membranes. *J. Membr. Sci.* **2014**, *470*, 102–111. [CrossRef]
244. Chen, H.; Li, L.; Kemps, R.; Michielsen, B.; Jacobs, M.; Snijkers, F.; Middelkoop, V. Reactive air brazing for sealing mixed ionic electronic conducting hollow fibre membranes. *Acta Mater.* **2015**, *88*, 74–82. [CrossRef]
245. Deng, X.; Duquette, J.; Petric, A. Silver–Glass Composite for High Temperature Sealing. *Int. J. Appl. Ceram. Technol.* **2007**, *4*, 145–151. [CrossRef]
246. Kiebach, R.; Engelbrecht, K.; Kwok, K.; Molin, S.; Søgaard, M.; Niehoff, P.; Schulze-Küppers, F.; Kriegel, R.; Kluge, J.; Hendriksen, P.V. Joining of ceramic $Ba_{0.5}Sr_{0.5}Co_{0.8}Fe_{0.2}O_3$ membranes for oxygen production to high temperature alloys. *J. Membr. Sci.* **2016**, *506*, 11–21. [CrossRef]
247. Zhang, Y.; Liu, T.; Zhang, J.; Wu, C.; Lu, X.; Ding, W. Induction brazing $BaCo0.7Fe_{0.2}Nb0.1O_{3-\delta}$ membrane tubes to steel supports with Ag-based filler in air. *J. Membr. Sci.* **2017**, *533*, 19–27. [CrossRef]
248. Godini, H.R.; Gili, A.; Görke, O.; Simon, U.; Hou, K.; Wozny, G. Performance Analysis of a Porous Packed Bed Membrane Reactor for Oxidative Coupling of Methane: Structural and Operational Characteristics. *Energy Fuels.* **2014**, *28*, 877–890. [CrossRef]